JAERI-M
87-166

PROGRESS REPORT ON JAERI - ORNL COOPERATIVE NEUTRON SCATTERING RESEARCH APRIL 1, 1985 — MARCH 31, 1987

October 1987

(Ed.) Satoru FUNAHASHI

日本原子力研究所
Japan Atomic Energy Research Institute

JAERI-M レポートは，日本原子力研究所が不定期に公刊している研究報告書です。
入手の問合わせは，日本原子力研究所技術情報部情報資料課（〒319-11茨城県那珂郡東海村）あて，お申しこしください。なお，このほかに財団法人原子力弘済会資料センター（〒319-11 茨城県那珂郡東海村日本原子力研究所内）で複写による実費頒布をおこなっております。

JAERI-M reports are issued irregularly.
Inquiries about availability of the reports should be addressed to Information Division Department of Technical Information, Japan Atomic Energy Research Institute, Tokai-mura, Naka-gun, Ibaraki-ken 319-11, Japan.

編集兼発行　日本原子力研究所
印　　刷　㈱高野高速印刷

JAERI-M 87-166

PROGRESS REPORT ON JAERI - ORNL COOPERATIVE NEUTRON SCATTERING RESEARCH

APRIL 1, 1985 - MARCH 31, 1987

(Ed.) Satoru FUNAHASHI

Department of Physics
Tokai Research Establishment
Japan Atomic Energy Research Institute
Tokai-mura, Naka-gun, Ibaraki-ken

(Received September 22,1987)

Research activities performed by using the Wide Angle Neutron Diffractometer(WAND) installed to the High Flux Isotope Reactor(HFIR) of the Oak Ridge National Laboratory(ORNL) during the period of JFY1985 to 1986 under the US-Japan Cooperative Neutron Scattering Research Program are summarized. JFY1985 was the year of the full-fledged cooperative research. Studies of phase transition kinetics by making use of the rapid temperature change auxiliary equipment and the two-dimensional neutron diffraction studies of single crystals were carried out before the unexpected shutdown of HFIR at November 1986. Two reports related with instrumentation and eleven reports describing the neutron scattering experiments are contained in this volume.

Keywords: Neutron Diffraction, Phase Transition, Time-Resolved Measurement Phase Transition Kinetics, Ordering Kinetics, Diffuse Scattering Phase Stability, Progress Report, Coordinated Research Program

JAERI－M 87－166

原研－オークリッジ国立研　中性子散乱協力研究のプログレス・レポート
（昭和６０年４月１日～昭和６２年３月３１日）

日本原子力研究所東海研究所物理部
（編）舩橋　達

（１９８７年９月２２日受理）

中性子散乱日米科学技術協力により，昭和６０～６１年度の間に，オークリッジ国立研究所に設置した広角中性子回折装置を利用してなされた研究活動をまとめたものである。昭和６０年度はこの協力研究が本格化に入った時期であり，昭和６１年１１月の突然のＨＦＩＲの停止に到るまでの期間に，温度急変用の付属機器を利用した相転移機構の研究，単結晶の２次元回折の研究などが行われた。このレポートには，装置に関する２編の報告と，１１編の中性子散乱実験を収録している。

東海研究所：〒319－11 茨城県那珂郡東海村白方字白根２－４

CONTENTS

目　　次

頁

I. PREFACE

During the past two years since the first issue of this progress report, a number of cooperative experiments were performed using the Wide-Angle Neutron Diffractometer (WAND) before the unexpected shutdown of the High Flux Isotope Reactor (HFIR) in the middle of November 1986 due to embritllement of the pressure vessel. The experiments were carried out with very good cooperation between the scientists of both sides. The WAND machine is becoming familiar to the HFIR users and the usefulness of the machine is recognized more widely.

Three auxiliary equipment systems were made in JAERI and shipped to ORNL. In all cases, their performance was excellent. The rapid temperature change machine has been used frequently for experiments to study phase transition kinetics. It is drawing much attention from the scientists in that field. The high temperature machine and the stress machine have not been used yet because of the HFIR shutdown, though they had been scheduled to be used in late 1986 and early 1987.

Efforts have been made continuously by ORNL experts to upgrade the software of the data acquisition system including data transfer from the WAND computer to the Division computer which was installed after the completion of the WAND machine. Data analysis programs were also developed to use the Division computer and the central computers. Some data processing programs were successfully transferred between JAERI and ORNL.

The characteristics of the curved position sensitive counter has not been changed greatly in the past two years.

The first progress report issued in 1985 contained almost equal space for instrumentation and for research done with the WAND machine. The present second issue concentrates on the research projects done in about two years, many of which were carried out utilizing the rapid temperature change equipment. Some other projects made use of another capability of the WAND machine to measure two-dimensional diffraction patterns using single crystal samples. Several short unscheduled experiments were performed in addition to the experiments described in this report.

We hope for the early and safe restart of HFIR operation in order to resume our cooperative experiments utilizing the WAND machine. We expect the experimental activities to be resumed immediately after the restart and the collaboration between ORNL and JAERI to grow steadily.

The editors would like to express their sincere thanks to all people, including those who have moved to new positions, who have contributed to this ORNL-JAERI collaboration program.

R.M.Moon
Solid State Division
Oak Ridge National Laboratory

S.Funahashi
Department of Physics
Japan Atomic Energy Research Institute

September 1987

In publishing this progress report as a volume of JAERI-M report, the editors express their deep apprecation to the following;

The American Institute of Physics for the permission to reproduce the paper published in the "Review of Scientific Instruments" as article 2 in section II and the paper published in the "Journal of Applied Physics" as article 3 in section III.

The North-Holland Physics Publishing for the permission to reproduce the paper published in the "Physica" as article 1 in Section III;

II. INSTRUMENT

1. CURRENT STATUS OF THE WIDE ANGLE NEUTRON DIFFRACTOMETER FACILITY

Y.Morii, S.Funahashi, and H.R.Child

The Wide Angle Neutron Diffractometer (WAND) has been used very efficiently and satisfactorily for a number of experiments in the last two years. In this period, a lot of effort has been made to upgrade the facility. Some of these improvements are described here.

The most important change in the operation is archiving experimental data both on hard disks of the PDP11/44 at the High Flux Isotope Reactor (HFIR), and in addition, on magnetic tapes on the Data General Eclipse MV/10000 which was recently installed at the Solid State Division (SSD), rather than only on hard disks. This latter process is of great advantage, not only for the safety in storage of the data, but also the analysis of large data sets by more complex programs. All of the 37 data files, totaling 300 M Bytes in capacity, have been transferred through a data communication line between HFIR and SSD. The biggest file has 8.7 M Bytes of data.

The band width of the address channel of the time digitizing CAMAC module (TDC) was increased in cooperation with M. K. Kopp and his associates. About 1900 channels are used out of 2048 channels of a memory region so that the angle resolution is improved to about 0.067 degrees per channel.

The angle resolution of the detecter itself was measured using a cadmium mask with slits which is placed in front of the detecter window. The measured Full Width at Half Maximum (FWHM) of the neutron intensity peak from the slit

is shown in Fig.1 and shows that the intrinsic resolution of the detector is about 0.7 degrees over a relatively wide range of two theta angle.

The Rietveld program[1] has been transplanted from Japan to the ORNL Solid State Division and used for the profile analysis of various powder diffraction patterns. The scattering data from a standard powder sample, Al_2O_3, is analyzed and displayed in Fig.2 showing that a quite good fitting with a fitting indicator, W.P. factor, of 8.7 % which is comparable to that of conventional triple axis spectrometers with a standard (about 30 minutes) collimation.

In the process of the fitting, we found that two theta angle can be expressed by a fourth order polynomial function of the channel address number of the TDC to adequate accuracy.

One of the authors (H.R.C.) has developed both black/white and color plotting programs to draw contour maps of the scattering intensities for a wide range of reciprocal planes of single crystals. A contour map of scattering intensity on the [hk0] reciprocal plane of a $Cu_{69.2}Al_{25.4}Ni_{5.4}$ crystal is drawn in Fig.3 which clearly shows Bragg peaks and diffuse streaks along [110] directions. A part of the contour map can be zoomed in for an extensive study. A perspective drawing to visualize the scattering intensity of the zoomed area has also been developed.[2]

The black/white contour and perspective drawing program accompanied by some other programs for data analysis have been transplanted from ORNL to JAERI and are working well with the WAND data which a Japanese researcher (S.F.) brought back with him on a magnetic tape.[3]

A very high temperature furnace has been shipped from JAERI to ORNL and assembled at SSD. The infra-red light, which is focused by the gold plated

curved mirror, enables us to heat spacimens up to 2000 K. Some experiments on the phase transition of the ZrO_2 ceramics and high melting temperature materials are scheduled. The stress modulation machine and a special hoist, which is designed to avoid any disturbances of the WAND while the stress machine is in use, have been tuned up for the study of stress induced martensitic phase transition of MnCu and MnNi alloys. Neither of these auxiliary equipments described above could be used, unfortunately, for the scheduled experiments due to the shut down of the HFIR.

A Japanese personal computor, NEC-9800Vm2, has been installed in an office at SSD and used as a terminal of the DG computer for various data analysis as well as a terminal of the PDP11/44 for monitoring the ongoing experiment and transferring the data to the DG. The NEC machine has also been used for computer communication between ORNL and JAERI. A graphic terminal and a hard copier will be obtained for the preparation room at the HFIR to allow secondary users to analyze their data at the same time that a primary user runs his experiment.

REFERENCES

1. F.Izumi, "A Software Package for the Rietveld Analysis of X-ray and Neutron Diffraction Patterns", KEK Report, National Laboratory for High Energy Physics, Tsukuba, Japan.
2. Y.Morii, M.Iizumi, S.Funahashi, and H.R.Child, Proc. of Int. Conf. of Martensitic Transformation (1986) 150, JIM.
   S.Funahashi, Y.Morii, and H.R.Child, J.A.P. **61** (1986) 4114.
3. S.Funahashi, Y.Morii, and H.R.Child, "Magnetic Diffraction in Cr_2Te_3, $CsNiBr_3$ and Beta-Manganese" in this report.

FIGURE CAPTIONS

Fig.1 Full Width at Half Maximum, FWHM, of the peaks of a neutron beam which comes through narrow slits in a cadmium mask which is placed in front of the WAND detector.

Fig.2 Rietveld profile analysis of a diffraction pattern of Al_2O_3 powder obtained with WAND. A fitting indicator, W.P. factor, of 8.7% is evaluated.

Fig.3 A color contour map of neutron scattering intensity on the [hk0] reciprocal plane of a $Cu_{69.2}Al_{25.4}Ni_{5.4}$ crystal is shown. The frame, graduations, and characters are traced and accented manually after computing grawing.

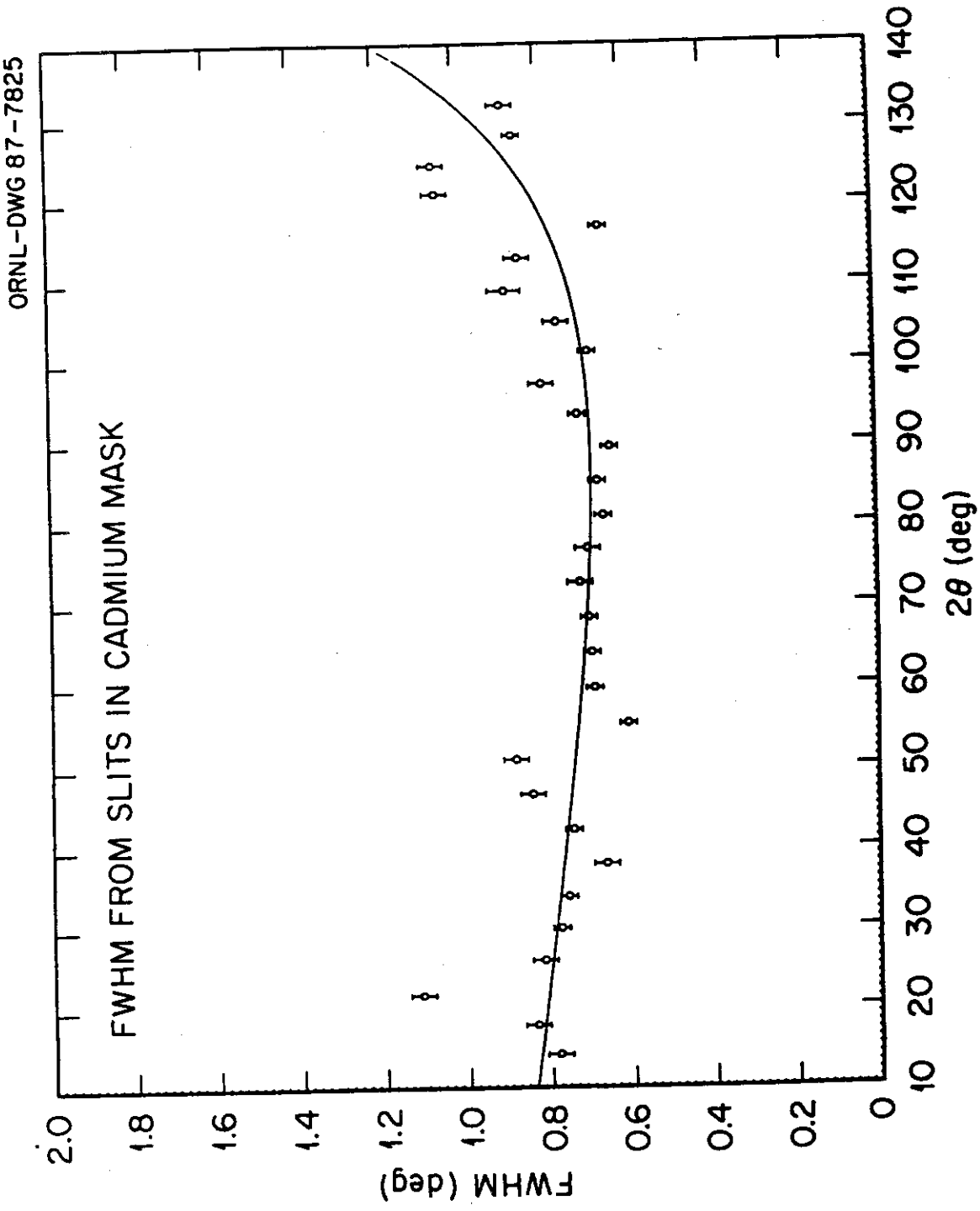
ORNL-DWG 87-7825
FWHM FROM SLITS IN CADMIUM MASK
FWHM (deg)
2θ (deg)
2.0
1.8
1.6
1.4
1.2
1.0
0.8
0.6
0.4
0.2
0
10
20
30
40
50
60
70
80
90
100
110
120
130
140

Fig.1

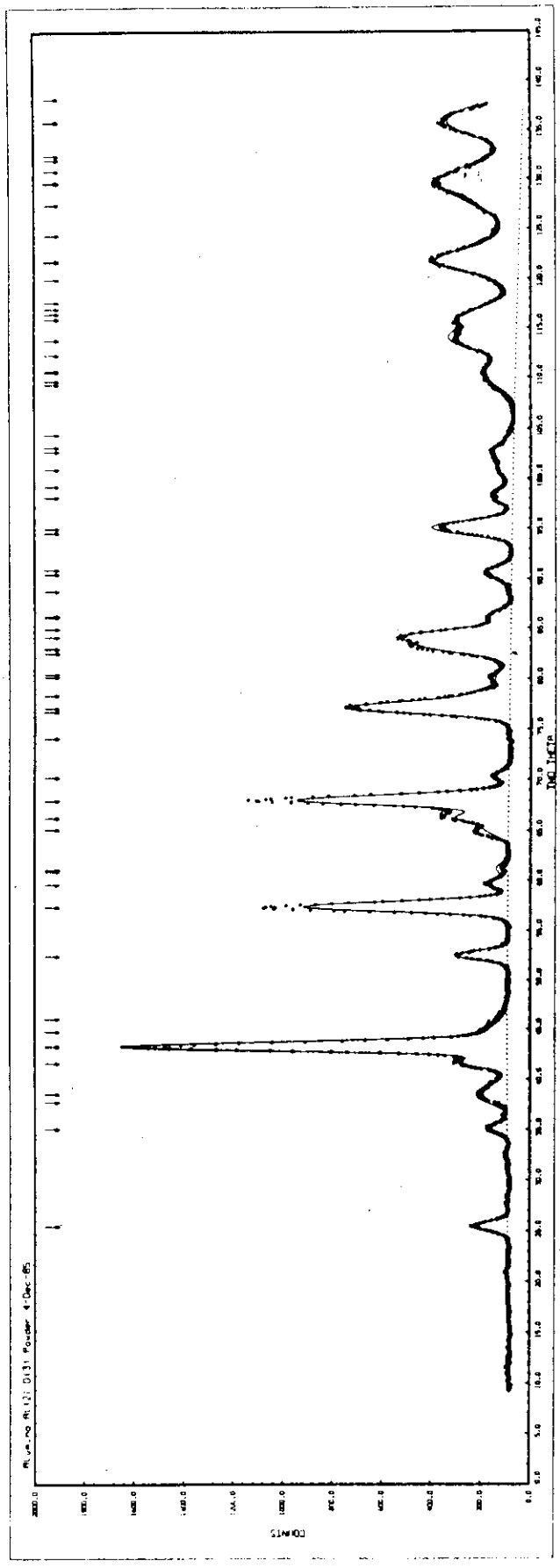

Fig.2

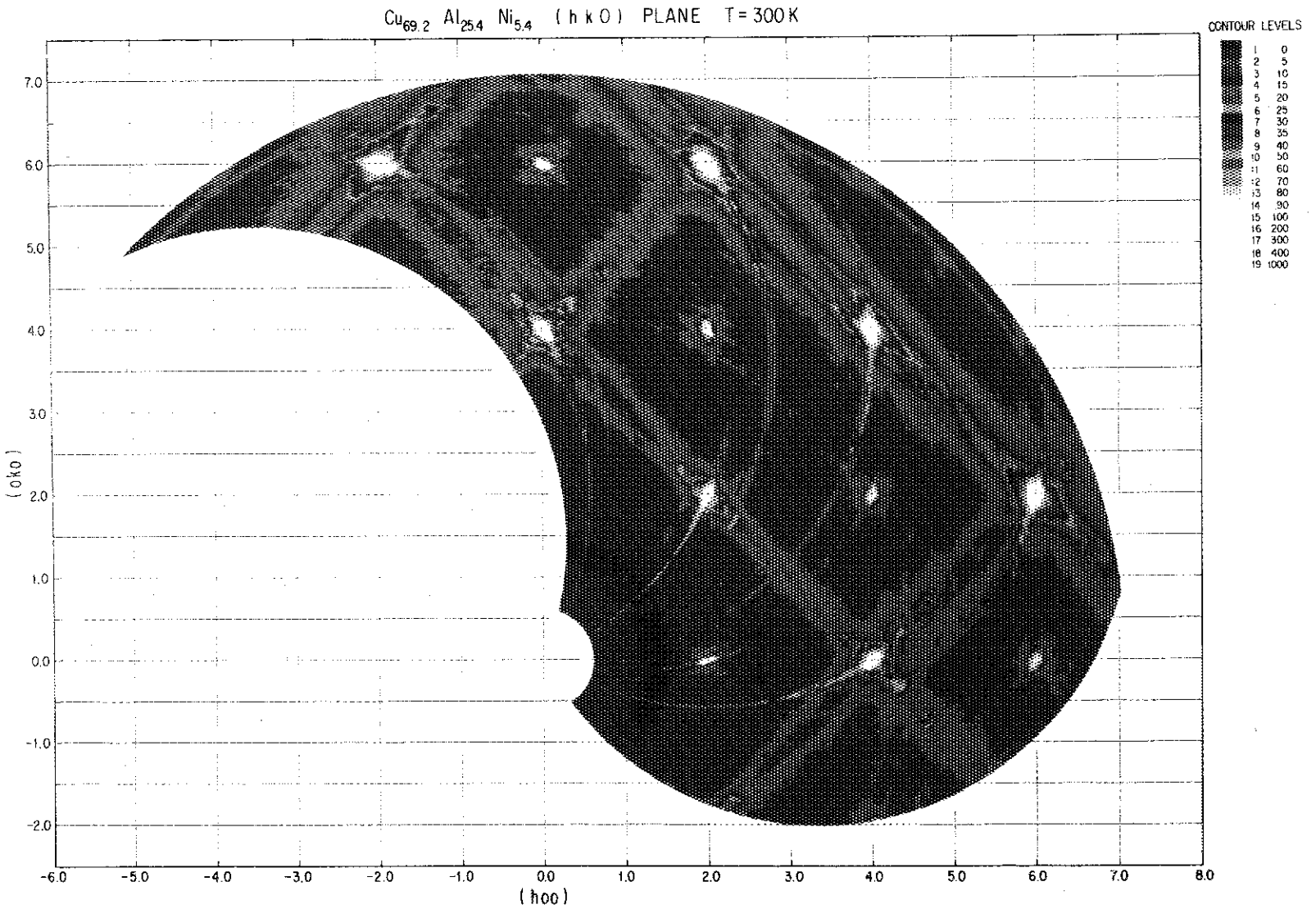
Cu69.2 Al25.4 Ni5.4 (h k 0) PLANE T = 300 K
CONTOUR LEVELS
1 0
2 5
3 10
4 15
5 20
6 25
7 30
8 35
9 40
10 50
11 60
12 70
13 80
14 90
15 100
16 200
17 300
18 400
19 1000
7.0
6.0
5.0
4.0
3.0
2.0
1.0
0.0
-1.0
-2.0
(0 k 0)
-6.0
-5.0
-4.0
-3.0
-2.0
-1.0
0.0
1.0
2.0
3.0
4.0
5.0
6.0
7.0
8.0
(h 0 0)

Figure 3

Reproduced from The Review of Scientific Instruments, vol.57,1409-1412(1986) by permission of The American Institute of Physics.

2. Furnace for rapid change of temperature for neutron diffraction

S. Katano, H. Motohashi, and M. Iizumi

Department of Physics, Japan Atomic Energy Research Institute, Tokai, Ibaraki 319-11, Japan

(Received 2 December 1985; accepted for publication 28 March 1986)

A new furnace for neutron diffraction experiments is capable of heating and cooling a sample very rapidly. The rapid heating is done by two circular infrared lamps placed over and under a sample, whose radiation is roughly focused on the sample by a reflector. The rapid cooling is done by high-pressure gas blows against the sample from two circular nozzles which are also placed over and under the sample. This system enables us to obtain the heating rate of over 1000°C/min and cooling rate of − 500°C/min for an alloy of 10 mm diameter and 30-mm length. The performance is sufficient to carry out some kinetics measurements in real-time neutron diffraction by the use of a position-sensitive detector. This kind of experiment is demonstrated by the observation of the relaxation process of order–disorder transitions in CuZn and Ni_3Mn alloys.

INTRODUCTION

Recently the study of time-dependent phenomena has received great attention.[1] As neutron diffraction is one of the most powerful techniques to study these phenomena from microscopic viewpoints, some real-time experiments at the steady-state reactor have been done by the use of a multidetector.[2] In the high flux isotope reactor (HFIR) of Oak Ridge National Laboratory, a new curved one-dimensional position sensitive detector was installed for this kind of experiment.[3] In the case of pulsed neutron source, a potential for enhanced time-resolution capabilities has been discussed.[4]

In some alloy systems, such phenomena take place at high temperatures with a time constant from the order of a second to that of a day. To investigate these time-dependent phenomena, it is necessary to change the temperature of a sample as rapidly as possible over a wide temperature range. However, conventional furnaces usually take several minutes to change it over 100°. Therefore, we designed and fabricated a new type of furnace which utilizes infrared lamps whose images are roughly focused on a sample for the rapid heating[5] and gas blows against the sample for the rapid cooling. This system enables us to change the temperature of the sample within 10 s over 100°. This performance is enough to investigate time-dependent phenomena of some alloy systems. Of course, as this furnace can freely control the rate of heating and that of cooling, it has various applications to other neutron diffraction experiments.

I. DESIGN AND CONSTRUCTION

A schematic drawing of the furnace is shown in Fig. 1. A sample (A) is mounted on a holder made of transparent quartz (B). These are set in a quartz tube (C) of diameter 80 mm whose inside can be evacuated. The heating elements are four semicircular infrared lamps of maximum power 8 kW (4×2 kW). As shown in the insert of this figure, the four lamps form two circular heaters (D). One of them is placed over the sample and the other is under it to avoid additional scattering from heating elements. To get the high heating rate and wide uniformity of the temperature, images of the lamps are roughly focused on the sample by a reflector (E). This reflector was made of aluminum alloy 2 mm in thickness whose inside surface was coated with gold. For the rapid cooling, the high-pressure gas is blown against the sample from many small holes of two circular nozzles of quartz (F). Similar to the case of the lamps, one of these nozzles is over the sample and the other is under it. Due to this simple structure of the furnace, the neutron beam can go through this furnace with rather slight scattering. The gas blow is controlled by electromagnetic valves (G). The temperature of the sample was measured by two chromel–alumel thermocouples; one of them was spot welded on the surface of the sample and the other was fixed in a hole which was made near the center in the diametrical direction of it. The temperature of the sample, the rate of the temperature change, and the operation of gas valves are controlled by a programmable temperature controller.

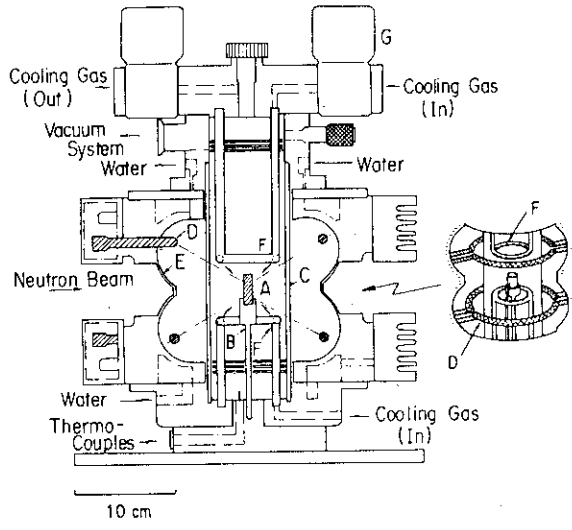

FIG. 1 Vertical section of the furnace: A—sample; B—holder; C—quartz tube; D—infrared lamp; E—reflector; F—nozzle for gas blow; G—electromagnetic valve for high-pressure gas. The insert shows the arrangement of lamps and nozzles around the sample.

 0034-6748/86/071409-04$01.30

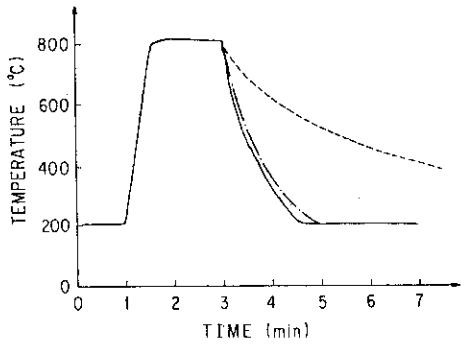

FIG. 2 Time dependence of the temperature when the rapid temperature change between 200 and 800°C was done. A stainless-steel rod 10 mm in diameter and 30 mm in length was used. The solid line shows the temperature measured on the surface of the sample and the dash–dotted line does that near the center in the diametrical direction of it. The dashed line indicates a result of the cooling without gas blow.

II. RESULTS

A. Temperature change of a sample

The result of a test intended to get the rate of 1000°C/min between 200 and 800°C is shown in Fig. 2. The sample was a stainless-steel rod 10 mm in diameter and 30 mm in length. To control the temperature, the thermocouple welded on the surface of the sample was connected with the temperature controller. In this figure, the solid line shows the time dependence of the temperature on the surface and the dash–dotted line indicates that near the center. The heating up to 800°C was done by putting nearly full power on the heaters, and the cooling was done by cutting the power and simultaneously blowing the high-pressure gas of about 5 kg/cm^2 against the sample. The result shows that the heating rate of 1000°C/min can be easily obtained. The difference of the temperature between the surface and the inside was not discernible. In cooling, the obtained rate was about −800°C/min at the beginning, −550°C/min around 600°C, and −300°C/min around 400°C. In this case the temperature difference between the surface and the inside was noticed. For reference, the result of the cooling without the gas blow is shown by the dashed line.

Figure 3 shows the result of repetition of rapid changes of the temperature. The case of the temperature change between 400 and 600°C is shown in 3(a) and that between 495 and 500°C is in 3(b). In the latter case, a continuous gas blow at about 1 kg/cm^2 was needed to get good stability of the temperature. In both cases, the rapid temperature change was satisfactorily obtained.

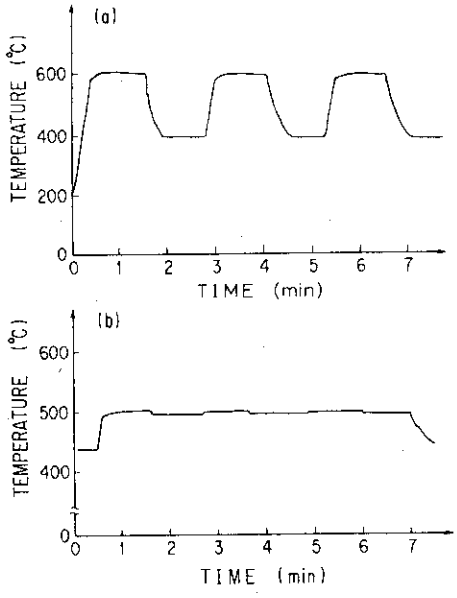

FIG. 3 Time dependence of the temperature when the rapid temperature change was repeated: (a) between 400 and 600°C and (b) between 495 and 500°C.

B. Neutron diffraction experiments

The experiments were done using this furnace on the wide-angle neutron diffractometer (WAND)[3] which had been installed in HFIR of Oak Ridge National Laboratory. Since the WAND utilizes the curved one-dimensional position-sensitive detector which covers 130°, we are able to obtain a diffraction pattern all at once; hence real-time experiment of time-dependent phenomena is one of the most interesting research subjects. The maximum time resolution of the data-acquisition system is 10 ms.

We investigated the relaxation process of order–disorder transition in CuZn and Ni_3Mn alloys: the decay of the superlattice peak in the ordered state and the growth of the short range order (SRO) in the disordered state. In the following experiments, samples of 5 mm diameter and 30 mm length were used. In the case of CuZn alloy, the transition is of second order, thus the time constant is expected to be quite short. However, an experiment by electrical resistivity indicated that the time constant of growth of SRO above 5° of the transition temperature is over 1 h.[6] If the time constant is of this order of magnitude, it may be very easy to observe the relaxation process by the use of our furnace. Figure 4 (a) shows the decay of the (111) superlattice peak after the temperature was increased from 450 to 465°C. (The transition temperature is around 470°C.) For reference the diffraction patterns at 450 and 460°C at the equilibrium state are also shown. The insert shows the temperature change of the sample. Although the temperature reached to the desired temperature in a few seconds, afterwards it oscillated a little. The time-resolved measurements with 10-s steps were done until 5 min. In order to get good counting statistics such a measurement was repeated 120 times and each time data for 10 s was accumulated. The integrated intensity of these peaks is shown as a function of time in Fig. 4(b). From these figures it is clear that the superlattice peak and its intensity reach the equilibrium within 10 s, that is, the time constant is very short. The growth of SRO was investigated by the change of the temperature from 550 to 475°C. This result also shows that the time constant is quite short. Thus, our result is rather different from that of the electrical resistivity measurement mentioned above. At present we cannot explain this difference. However, the result obtained here seems to be

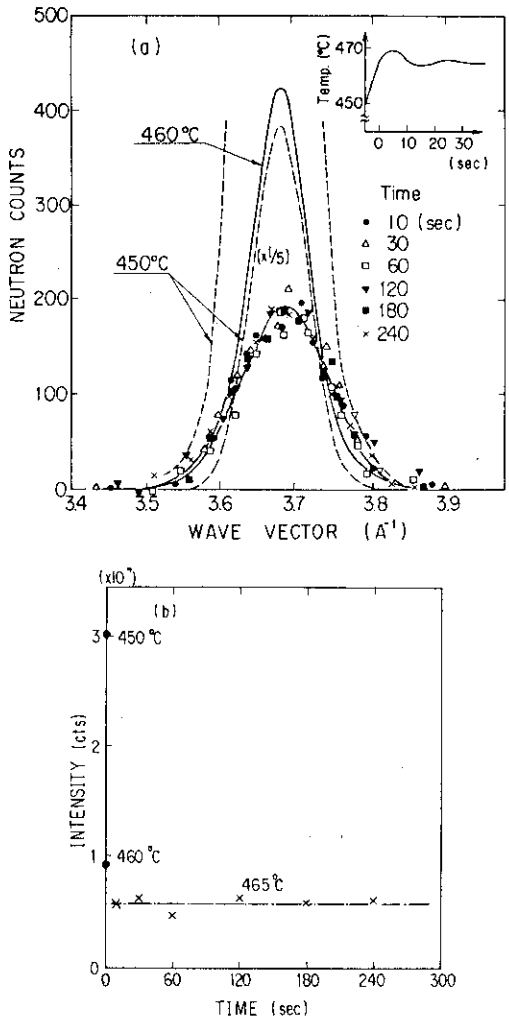

FIG. 4 (a) Time dependence of the superlattice peak of CuZn when temperature was changed from 450 to 465°C. The insert shows the temperature of a sample 5 mm in diameter and 30 mm in length as a function of time. (b) Integrated intensity of the superlattice peak as a function of time.

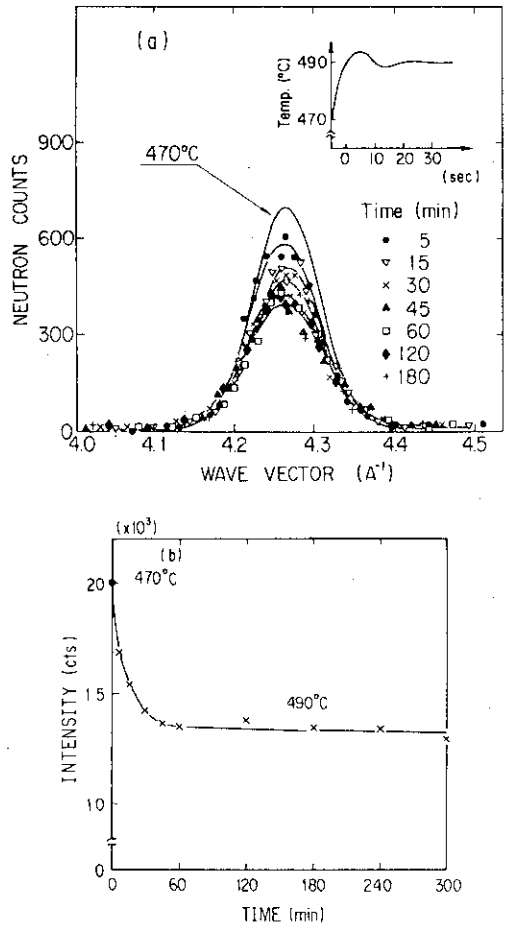

FIG. 5 (a) Time dependence of the superlattice peak of Ni_3Mn when temperature was increased from 470 to 490°C. The insert shows the temperature of a sample 5 mm in diameter and 30 mm in length as a function of time. (b) Integrated intensity of the superlattice peak as a function of time.

reasonable if we refer to the neutron diffraction study on SRO of this alloy.[7] In that study SRO peak at various temperatures were clearly observed in a series of a quick scan of the total time of 90 min. This suggests that the peak may reach its equilibrium in a short time.

The decay of the (211) peak of Ni_3Mn is shown in Figs. 5(a) and 5(b). The temperature was increased from 470 to 490°C. (The transition temperature is around 510°C.) It is known that the transition of this alloy is the first order and the time constant is fairly long.[8,9] Thus the time-resolved measurements with 10-min steps were done until 12 h. It is clearly seen in these figures that the superlattice peak decays with time. The obtained time constant is about 30 min. This result is consistent with the previous reports, although the value is somewhat shorter than theirs. The growth of SRO was also investigated by the change of temperature from 600 to 515°C. Although the counting statistics was not enough because of the weak intensity with broadened distribution, the result indicates that the time constant is over 10 min.

As shown in these demonstrations, the rapid temperature change can be stably accomplished by this system. The temperature of a sample can be changed within a second for the change over 10°. Although a small oscillation of the temperature was seen after the rapid change, this should be reduced by the use of a higher performance temperature controller. Then, it is possible to investigate time-dependent phenomena with the time constant of the order of a second.

Using this system, the ordering kinetics in Ni_3Mn was also investigated in detail. This result will be published elsewhere.

ACKNOWLEDGMENTS

The authors are greatly indebted to M. Ichihashi and his colleagues of R. H. Department, Shinku Riko Ltd., Hakusan-cho, Yokohama, Japan for making this furnace. This

work was partly carried out at Oak Ridge National Laboratory under the U.S.–Japan Cooperative Program in Neutron Scattering.

[1]J. D. Gunton, M. San Miguel, and P. S. Sahni, in *Phase Transitions and Critical Phenomena*, edited by C. Domb and J. L. Lebowitz (Academic, London, 1983), Vol. 8.
[2]For example, C. Rieckel, and R. Schollhorn, Mater. Res. Bull. **11**, 369 (1976).
[3]M. Iizumi, S. Funahashi, S. Katano, R. M. Moon, R. M. Nicklow, H. R. Child, and M. K. Kopp, Hahn-Meitner-Institute Report HMI-B411, 1984, and Japan Atomic Energy Research Institute Report JAERI-M 85-112, 1985, edited by M. Iizumi.
[4]J. Faber, Rev. Phys. Appl. **19**, 643 (1984).
[5]As the focused heating by light is very efficient, it has been applied to some neutron diffraction experiments. Recently this heating method was used to investigate the interaction of light with materials. [A. Stockli and A. Furrer, Rev. Phys. Appl. **19**, 751 (1984).]
[6]I. Hatta and M. Shibuya, J. Phys. Soc. Jpn. **45**, 487 (1978).
[7]C. B. Walker and D. T. Keating, Phys. Rev. **130**, 1726 (1963).
[8]M. R. Collins and H. C. Teh, Phys. Rev. Lett. **30**, 781 (1973).
[9]N. Wakabayashi, Phys. Rev. B (to be published).

III. RESEARCH

Reproduced from The Physica, vol.136B(1986)36-41 by permission of The North-Holland Physics Publishing.

Physica 136B (1986) 36–41
North-Holland, Amsterdam

1. REAL-TIME NEUTRON DIFFRACTION STUDIES OF PHASE TRANSITION KINETICS

Masashi IIZUMI
Department of Physics, Japan Atomic Energy Research Institute, Tokai, Ibaraki 319-11, Japan

Invited paper

A neutron diffractometer with the function of measuring the change of diffraction patterns in real-time is described. The kinetics of the first-order phase transitions occurring after a temperature jump across the transition temperature was observed by using the diffractometer. The structural change between white and grey tin, the continuous ordering in Ni_3Mn are shown as examples. Observation of the kinetics of slow chemical reaction is illustrated by the hydration process of the portland cement.

1. Introduction

The development of curved one-dimensional position-sensitive detectors (PSDs) with wide angle coverage enables one to obtain a complete neutron diffraction pattern simultaneously in a short period of measuring time. Advantageous combination of high flux neutron beam and the state-of-the-art PSD system has made the measuring time so short that fairly rapid changes of neutron diffraction patterns can be observed in real-time [1]. Nowadays the shortest measuring period in one-shot phenomena has been reduced down to about 1 min. One can study kinetic processes such as chemical reactions and first-order phase transitions as long as the characteristic time scale of the change is a few minutes or longer.

When a physical system is brought to a metastable state by an abrupt change of a thermodynamic variable, say temperature, of the system across a first-order phase transition boundary, the system starts to transform to an equilibrium state. This problem, though studied for a long time from a point of view of practical importance in metallurgy and other fields, draws a renewed interest in the statistical physics of non-equilibrium state.

Generally the approach of metastable states to equilibrium takes place through build-up and growth of heterophase fluctuations. In the real-time diffraction the relevant observables are (1) the intensity of diffraction peaks corresponding to the new (equilibrium) phase, (2) their widths, and, more precisely, (3) their line shapes, all as functions of time. They give direct information about (1) the volume fraction of the new phase, (2) average size of the regions of the new phase formed heterogeneously within the metastable phase, and (3) the space-correlation between the heterogeneous regions. These are invaluable to study the time evolution of the heterophase fluctuations in metastable state.

In this paper the real-time diffraction function of the new neutron diffractometer at the HFIR in Oak Ridge National Laboratory is introduced and some examples obtained by the instrument are presented.

2. Diffractometer with real-time function

The new diffractometer [2] installed at the HFIR has the function of real-time measurement of neutron diffraction pattern. The detector is a curved one-dimensional position-sensitive proportional counter with an effective radius of 75 cm, covering a 130° angular range. The position analysis is performed by a distributed LC delay-line cathode. The encoded time difference determines the address of the histogramming memory in which the neutron events are accumu-

lated. Automatic time slicing for the real-time measurements can be done by adding a constant offset time to the digitized time difference for each successive slice.

The real-time measurements are performed synchronously with the change of external condition applied to a sample. There are two types of real-time measurements: one-shot and periodic. The one-shot measurements are done for the phenomena which cannot be repeated easily. The study of the transition kinetics of the first-order transition is an example. The feasibility of this kind of measurements is determined by the shortest time period in which one diffraction pattern is acquired. In the most favorable case of measuring strong powder-diffraction peaks the shortest record was a few seconds but in the case of measuring the time evolution of diffraction peaks in accordance with a phase transition the shortest practical time slice was one minute. The second type of real-time measurements, periodic measurements, are employed in cases where the change is reversible according to a periodic external condition. The electric field induced incommensurate-to-commensurate phase transitions in ferroelectrics in one of the examples of this type.

3. Reconstructive phase transition in tin [3]

The reconstructive phase transition is a kind of structural phase transition where the primary coordination (first-nearest-neighbor) bonds are broken and reformed. Since the reconstructive phase transitions give rise to large discontinuities in the physical properties, the energy barrier involved in this type of phase transitions is generally high. Therefore the transitions may proceed according to the so-called nucleation and growth mechanism.

We carried out a few measurements of the kinetics of this type of phase transitions. here only the results on a transition between alpha and beta phases in tin (Sn) are briefly given.

At room temperature tin (Sn) is metallic and is called white tin, or beta phase tin. The white tin transforms to gray tin, or alpha phase tin below about 260 K. The gray tin is semiconducting and has a diamond structure, while the white tin has a special tetragonal structure found only in this element.

The beta-to-alpha transition is fairly slow, taking from 1 to 12 hours, depending on temperature. The reverse transition from the alpha to the beta phase occurs above about 290 K and the change becomes very rapid as the temperature increases. Extensive measurements were carrried out on both the alpha-to-beta and beta-to-alpha transitions.

Fine-powder samples of alpha or beta phase were prepared from white tin grains (99.999% purchased from Mitsubishi Metal Co.) by repeated temperature cycles between 230 K and 330 K.

The Displex system was used to change the sample temperature on the diffractometer. In case of the beta-to-alpha transition the sample was kept at 320 K for at least 30 minutes before temperature changes. In the case of the alpha-to-beta transition the sample is kept at 230 K for at least two hours before heating up.

The time increment in the time-slicing measurement was chosen within the range of 1 to 30 min in accordance with the speed of the kinetics. Use of unequal time slices was convenient to record the whole course of change in the limited number of time slices.

A typical change of the diffraction patterns during the transient is illustrated in fig. 1 which shows a limited part of the whole diffraction patterns for only a few selected time slices.

A diffraction pattern at time t, $f(s;t)$ is a superposition of that in pure alpha phase, $f_a(s)$, and that in pure beta phase, $f_b(s)$:

$$f(s;t) = x(t)f_a(s) + [1 - x(t)]f_b(s)\,, \qquad (1)$$

where s indicates the scattering angle or the channel in the recorded data and $x(t)$ indicates the fraction of existing alpha phase. The entire diffraction patterns were used to determine the fractions of existing alpha and beta phases in the respective time slice.

Fig. 2 summarizes the results for the beta-to-alpha transition. In this figure the obtained $x(t)$'s

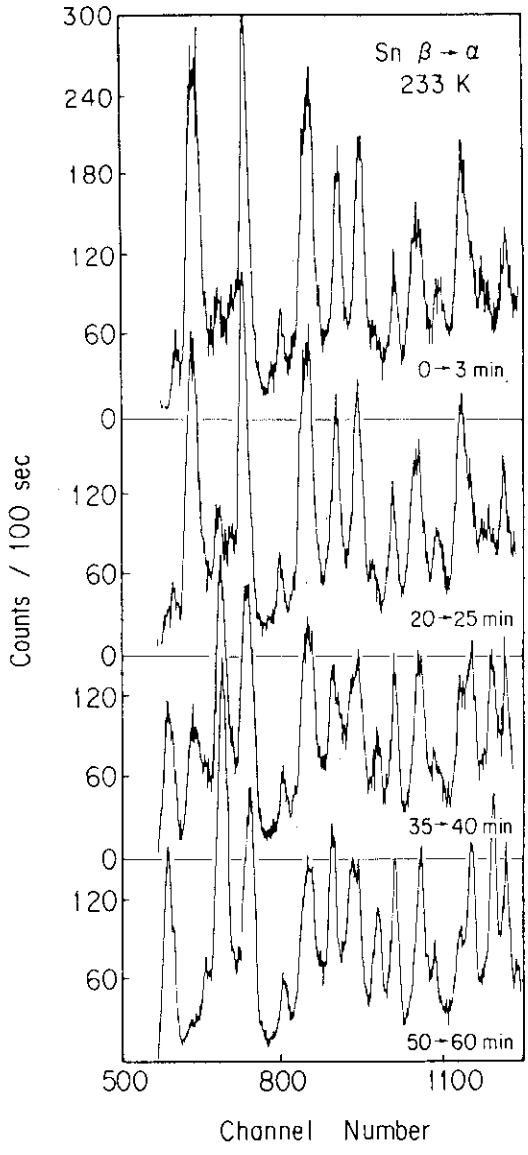

Fig. 1 Change of the diffraction pattern of tin during transformation from the beta-to-alpha phase. The temperature was changed abruptly at $t = 0$ from 320 K to 233 K.

are shown as functions of time t for various final temperatures. The $x(t)$ curves follow typical nucleation-and-growth kinetics; they have fairly long incubation periods during which the metastable phase does not show any change and then the new phase starts to appear first gradually, then becomes quite rapid and finally becomes

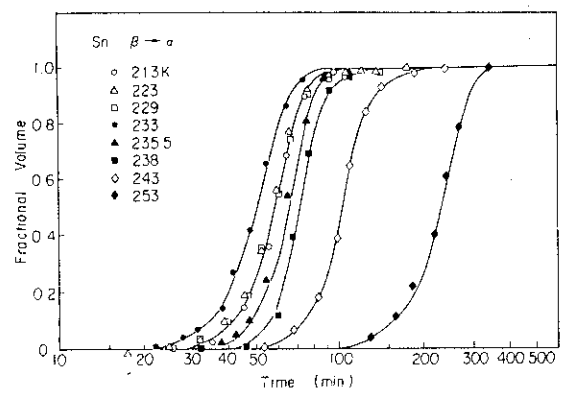

Fig. 2 Measured change of the fractional volume with time for the beta-to-alpha phase transition in tin for various choices of the final temperatures.

sluggish. The change is most rapid at the final temperature around 233 K and becomes slow at temperatures either higher or lower than this value. Similar results were obtained for the alpha-to-beta transitions.

The volume fraction transformed at time t is known to be expressed generally by the so-called Avrami or Johnson–Mehl equation (hereafter this equation will be abbreviated as AJM equation):

$$x(t) = 1 - \exp[-(t/\tau_0)^n] , \qquad (2)$$

where the relaxation time τ_0 depends both on the nucleation rate and the growth speed. The exponent $n = 4$ was originally proposed by Avrami for the case where the nuclei are formed homogeneously and the nucleation rate is constant in time and the further growth takes place isotropically with a constant velocity. Actual experimental situations are different from the ideal case assumed by Avrami. It is, however, known that most of the situations can be covered by the choice of exponent values deviating from 4. It is therefore convenient to make the exponent as well as the relaxation time as fitting parameters to the experimentally observed x vs. t relations and see what sort of values we obtain as the result of least-square fitting.

The results of the fitting of the measured time-dependence of the transformed fraction to the AJM-type equation given by (2) are summarized in fig. 3, where both the alpha-to-beta and

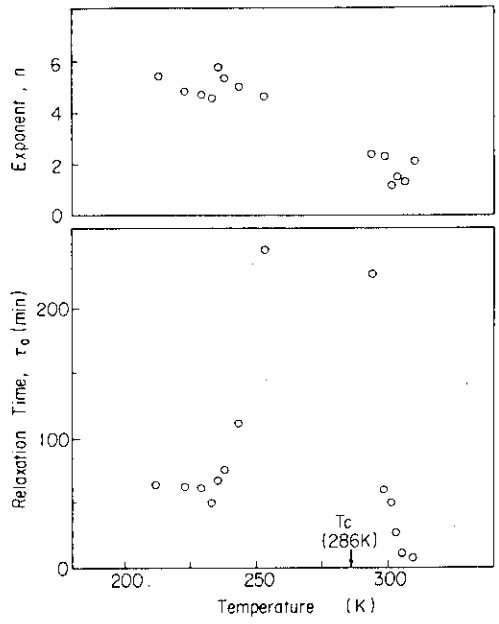

Fig. 3 Relaxation times and exponents obtained by the fitting shown as functions of the final temperatures.

reverse transitions are indicated. The relaxation time shows the slowing-down behavior as the temperature approaches the transition temperature from both sides. The characteristic exponent of the kinetics is about 5 in the beta-to-alpha transition and about 2 for alpha-to-beta. In case of the linear growth rate the exponent larger than 4 means that the nucleation rate increases with time, that is, it takes a long time to attain the equilibrium distribution of nuclei. This seems to be the case in the beta-to-alpha transition. The exponent below three cannot be explained by the isotropic growth. The exponent 2 just corresponds to the case of two-dimensional growth from the nuclei generated instantaneously at grain edges. The obtained value of the exponent suggests that this is the case for the alpha-to-beta transition.

As the form of eq. (2) suggests, the AJM-type equation automatically satisfies the scaling with respect to time, if the time is scaled by the relaxation time, $\tau = t/\tau_0$. In the case of beta-to-alpha transition the scaling property applies almost perfectly with $n = 5$, as is shown in fig. 4.

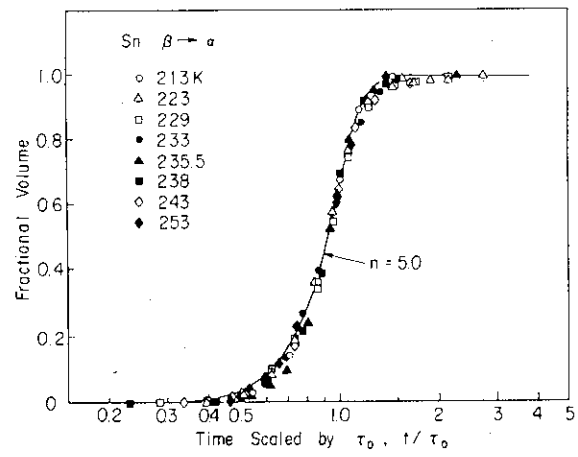

Fig. 4 Scaling behavior of the fractional volume with respect to time. Various symbols indicate different final temperatures in the beta-to-alpha phase transition.

Similar but less perfect scaling was found with $n = 2.3$ in the alpha-to-beta transition.

We tried to reveal the information concerning the size of the transformed region at the early stage of the transition. Some signs of the widened peaks were noticed but the poor statistics and the large instrumental width prevented us from obtaining reliable information with respect to the particle sizes.

4. Continuous ordering in Ni_3Mn [4]

The ordering process in Ni_3Mn is favorable for neutron diffraction because the order–disorder process is only visible by neutrons and the time scale of the ordering process is fairly long. Measurements by Collins and Teh [5] and by Wakabayashi [6] were done by using conventional neutron diffractometers. Therefore their observations were restricted to the later stage of ordering process. It was our intention to reveal the initial stage of the process by means of the fast real-time function of the new diffractometer. A furnace designed specially to change the sample temperature rapidly was also indispensable in observing the fast initial stage.

Fig. 5 shows the time change of the 211 superlattice reflection after the temperature is abruptly changed from 600°C to 470°C across the transition

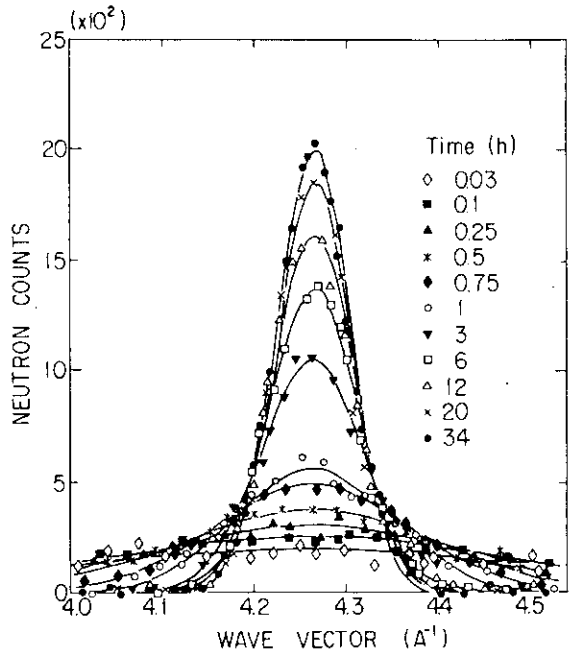

Fig. 5 Time change of the 211 superlattice peak of Ni_2Mn.

temperature (about 510°C). The temperature of the sample reached the final temperature in about 15 s. The early stage (up to 30 min) was observed by the 1 min time-slice. In order to get sufficient counting-statistics the identical measurements were repeated 30 times with the data being accumulated on the same memory area. For the later stage the time slicing with 6 min interval was repeated 5 times. Fig. 5 clearly indicates that the superlattice peak starts from a very broad peak shape and then becomes sharper with time. The

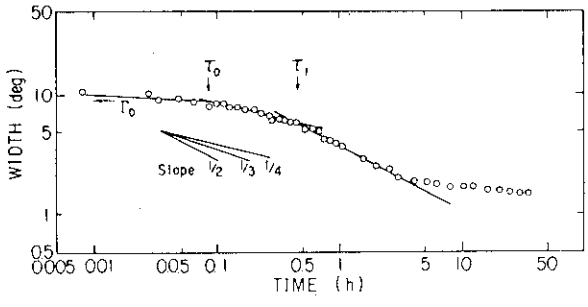

Fig. 6 Change of the width of the 211 sublattice peak with time.

change of the widths of observed peaks is indicated in fig. 6. At the initial stage ($t < \tau_0$) the widths remain almost constant and then they gradually start to decrease and at the later stage ($t > \tau_1$) the widths decrease with the 1/2 power law as was already pointed out for the ordering process. The detailed analysis of the widths as well as the intensity change under various temperature conditions are now in progress.

5. Hydration of portland cement [6]

Kinetics of the chemical reaction of commercial portland cement with heavy water was studied by the real-time neutron diffraction method. The cement is a mixture of various kinds of silicate, aluminate and other compounds. The hydration process of the mixture is very complicated. The rate of reaction with heavy water is different from one component to another with characteristic time constants ranging from a few minutes to several days. Some slow changes even take periods of years to complete. Moreover these reactions interfere with each other; one reaction proceeds under the strong influence of other components which also change their contents from time to time.

The kinetics of hydration of each main component of cement has been studied by Christensen using D1B in ILL [7]. It is the intention of the present authors to see how the real-time neutron diffraction technique works in analyzing a complicated reaction process taking place in commercial cement consisting of mixed compounds.

The mixture of cement powder and heavy water was prepared and transferred rapidly to the sample container made of vanadium. The ratio of cement to heavy water was 100 to 40 in weight which is equivalent to the water cement ratio of 0.36 in case of light water. The equivalence is with respect to the numbers of molecules participating the reaction.

Two kinds of real-time measurements have been performed; to observe the initial stage of hydration and to observe the later stage. In the first category the fastest measurement was done

by the 1.5 min preparation and transfer stage and the time slices of 1 min each. Some predominant peaks are visible and their time-change is discernible even for that short time slice but the better counting statistics is desirable in order to obtain quantitative information on the rapid change of minor components.

The slower change of the diffraction pattern is obtained by measuring for 15 min in every 3 hours up to 5.5 days. The decay of the peaks corresponding to the component compounds and the evolution of the hydration products, such as C_3AD_6 and $Ca(OD)_2$, were clearly observed. Although the time change of the main components can be deduced from a rather simple analysis, more detailed results including the time evolution of minor components can only be obtained by a more sophisticated analysis of the Rietveld type.

Acknowledgement

The present paper is a summary of a part of the JAERI-ORNL joint research done under the US-Japan Cooperation Program on Neutron Scattering. The author would like to thank all the participants of the joint research, S. Funahashi, S. Katano and Y. Morii of JAERI and R.M. Moon, R.M. Nicklow and H.R. Child of ORNL.

References

[1] C. Riekel, in: Position-Sensitive Detection of Thermal Neutrons, P. Covert and J.B. Forsyth, eds. (Academic Press, London, 1983).
[2] M. Iizumi, S. Funahashi, S. Katano, R.M. Moon, R.M. Nicklow, H.R. Child and M.K. Kopp, HMI-B411 (1984) p. 243. Also to be submitted to Nucl. Instr. & Meth.
[3] M. Iizumi, S. Katano, H.R. Child and R.M. Nicklow, unpublished.
[4] S. Katano, M. Iizumi, H.R. Child and R.M. Nicklow, unpublished.
[5] M.R. Collins and H.C. Teh, Phys. Rev. Lett. 30 (1973) 781.
[6] N. Wakabayashi, unpublished.
[7] M. Iizumi, Y. Morii, K. Doi, M. Sawaide and N. Ishikawa, unpublished.
[8] A.N. Christensen, HMI-B411 (1984) p. 58.

2. Dynamical Scaling in the kinetics of Ordering in Ni_3Mn Alloy

S. Katano, M. Iizumi,
H. R. Child and R. M. Nicklow

Abstract

A time resolved neutron diffraction experiment of Ni_3Mn alloy reveals the whole process of the ordering kinetics. The result indicates a crossover of the growth exponent, which can be attributed to the transition from the coalescence process of the ordered regions to the migration process of the domain walls. The obtained scaling function is compared with the result of theories and computer simulations.

The study of the kinetics of the first-order phase transitions has recently received considerable attention as a problem of the far-from equilibrium phenomena. These studies are classified into two categories; the transition in which the order parameter is conserved as in phase separation and that in which the order parameter is not conserved as in order-disorder transition. For both cases, ideas of self-similar growth and dynamical scaling have been ascertained by many works, in particular computer simulations.[1] This universality is expressed as follows. The non-equilibrium structure factor behaves according to

$$S(q,t) = R^d(t)F(qR(t)), \qquad (1)$$

where d is the dimensionality, q is the wave vector and F is a scaling function. The characteristic length R(t) follows a power law as

$$R(t) = t^a, \qquad (2)$$

where a is a universal exponent.

In the case of non-conserved order parameter, many studies by computer simulations have succeeded to verify this idea,[2-6] however, experimental works have been done less extensively.[7-9] The scaling behavior has not been studied in detail except a recent work on Cu_3Au alloy by Noda, Nishihara and Yamada.[10]

In order to investigate the scaling property in the ordering

kinetics further, we choose Ni_3Mn alloy for the following reasons. (1) The time constant is fairly long, and this is advantageous to study the initial stage of the ordering process. (2) Ni and Mn atoms have similar size, so the elastic strain involved in the transition should be small. This is good for a comparison with theories or simulations. (3) The neutron cross sections are favorable for measurements because of the negative scattering length of Mn.

Owing to these reasons, neutron diffraction studies on this alloy have been done by Collins and Teh[8] and recently by Wakabayashi.[9] However, since they used a conventional furnace and diffractometer, it took over 30 min to change the temperature and to have the first diffraction pattern. Therefore, their studies were restricted to the later stage of the process. In the present work, we used a new-type neutron diffractometer, the WAND (the Wide-angle Neutron Diffractometer) installed at the High Flux Isotope Reactor at the Oak Ridge National Laboratory, which has a capability of doing time resolved experiments[11] and a special furnace which can change the temperature very rapidly.[12] As a result, we could investigate the whole process of the kinetics from the very initial to the final stage.

The polycrystalline Ni_3Mn alloy was prepared by melting of 99.99% pure Ni and Mn in an argon-arc furnace. The ingot was melted several times to homogenize. Since the loss of weight was small, the nominal concentration (25.1 at% Mn) was adopted. The sample in the cylindrical form with dimensions of 6 mm diameter and 40 mm length was placed in the furnace. This sample was

heated to 600°C and kept at this temperature for 30 min to achieve the disordered state, and then, the temperature was abruptly changed to 470°C across the transition temperature around 510°C. The temperature of the sample reached the final temperature in about 15 s. To observe the initial stage up to 30 min, time resolved measurement for 1 min was done. For sufficient counting statistics, the identical measurements were repeated 30 times and each of data was accumulated on the memory of the data acquisition system. For the later stage, time resolved measurements for 6 min were repeated 5 times.

The time evolution of the 211 superlattice diffraction pattern is shown in Fig. 1 against the wave vector. The data of this figure were obtained by a smoothing of the raw data by the least square fit. As seen in the figure, a peak over a wide wave vector is observed even at the very initial stage. With time the width becomes narrow (i.e. the size of the ordered region R(t) grows), and the background level decreases. Fig. 2 shows the integrated intensity as a function of time. This indicates that the intensity is also of some (non zero) value at the initial stage, then rapidly increases and saturates. The broad peak at the very initial time indicates that fairly small ordered regions are formed in the sample. However, other regions are still disordered, which is suggested by the high background level and the small integrated intensity at this stage. The increase of the intensity at the later stage shows that such ordered regions increases with time and the ordering becomes complete.

In order to compare the experimental result with the power

law (2), the second moment q_2,

$$q_2(t) = \Sigma_q q^2 S(q,t) / \Sigma_q S(q,t), \qquad (3)$$

which corresponds to the square of the peak width, was calculated. In the calculation, the pure profile of the diffraction pattern, which was obtained by the deconvolution of the pattern shown in Fig. 1 using the 220 fundamental reflection, was used as S(q,t). The result is shown in Fig. 3 on the double logarithmic scale. As is clearly seen, $q_2^{1/2}$ decreases gradually and its entire time evolution cannot be expressed by a single power law. The result indicates that the ordered region grows slowly at the initial stage, then its growth becomes faster and finally saturates. The final stage is a mixture of four kinds of ordered domains, as shown by the electron microscopy.[13] Our experiment indicates that the size of these domains at the final stage is an order of one hundred Å.

As mentioned before, the entire data cannot be expressed by a single power. However, by choosing appropriate data points at the later stage, the data can be fitted by a straight line. The slope shown in the figure is -1/2, which is coincides with the prediction by Allen and Cahn in the process of the migration of the ordered domains driven by the curvature of domain walls.[14] This exponent was verified by many works of simulations and also experiments. For the former time we can fit the data to the straight line with the slope of -1/4. Hence, the exponent clearly indicates a crossover, which was observed also in the

phase separation of Fe-Cr alloys.[15,16] Therefore this kind of crossover is considered to be universal in the growth of the clusters. Theoretically, Furukawa predicted universal exponents for the case of non-conserved order parameter. In his theory, the exponent of the coalescence process is -1/3 for bulk diffusion and -1/4 for the surface diffusion.[17] Our result suggests 1/4 rather than 1/3. Therefore, the surface diffusion may take place easily compared to the bulk diffusion. Thus, it is considered that the ordering process changes from the stage of the formation of the ordered regions to that of the slow growth by coalescence of clusters, then to that of the fast growth by the migration of the domain walls and comes to an end.

The present result is very similar to that of Cu_3Au by Hashimoto et al.; that is, the initial stage also shows rather slow growth. They, however, interpreted that their result indicates the formation of very small ordered regions (about 25 Å) at the moment of the transition(i.e. t=0). Our detailed experiment indicates that small ordered regions (about 10 Å) at the initial stage actually grow with time according to a power law. However, the result of Cu_3Au by Noda et al. is considerably different from these. They observed a very fast growth in the early stage. The reason of such a difference is not clear at the present.

In order to extend the comparison with the scaling theory, we have calculated the normalized scaling function $\tilde{F}$.

$$\tilde{F}[q/(q_2(t))^{1/2}] = (q_2(t))^{3/2}\,\tilde{S}(q,t), \quad (4)$$

where the normalized structure factor $\tilde{S}(q,t)$ is defined as

$$\tilde{S}(q,t) = S(q,t) / \Sigma_q \, q^2 \, S(q,t)\delta q. \qquad (5)$$

The plot of $\tilde{F}(x)$, where $x = q/q_2^{1/2}$, for different times are shown in Fig. 4. It is found that the scaling is well satisfied after a very short time. The scaling function becomes a little sharper at the late stage. However, the change is not drastic, compared to that observed in phase separation of Fe-Cr alloy.[15]

In the case of non-conserved order parameter, the scaling function $\tilde{F}(x)$ was calculated by Ohta et al. on the basis of the motion of domain walls by the Allen and Cahn's mechanism.[18] Experimentally, Noda et al. proposed the squared Lorentzian curve for the fit to the experimental result of Cu_3Au alloy. Both of these curves have asymptotically x^{-2} dependence at small x and x^{-4} dependence at large x. Certainly our result show these x dependence at each x region. However, there are some problems for a more precise comparison between those curves; for example, an ambiguity in the scales of the vertical and horizontal axis. Hence, we had to change the scales of these axis appropriately. In Fig. 4 the dotted curve is the result of Ohta et al., and the solid curve is that of the squared Lorentzian. Note that $\tilde{F}(0)$ is put equal and $\tilde{F}(x) \simeq 1 - x^{-2}/a + O(x^{-4})$ at small x for each curve, where a is a constant. The experimental result seems to indicate a small deviation from the theory of Ohta et al. Rather, the squared Lorentzian represents the experimental result well. A similar situation is observed in the comparison between

the theory of Ohta et al. and renormalization theory or computer simulations in the two-dimensional case.[19,20] As pointed by Noda et al., the squared Lorentzian was firstly proposed by Debye, Anderson and Brumberger for small-angle scattering by an inhomogeneous solid.[21] Although the form of the scaling function can be expressed well by this curve, it is not clear that the idea of random-distributed clusters in their theory can be applicable to the case of the growth of ordered domains.

In conclusion, the whole process of the ordering kinetics in Ni_3Mn alloy have been investigated by time resolved neutron diffraction. The result are explained by the recent scaling concept. A crossover of the growth law is observed similarly to the case of phase separation. This indicates that such a crossover is universal in the growth of the order. The scaling function can be expressed by the squared Lorentzian, and is consistent with the result of the recent renormalization theory and computer simulations. The detailed temperature dependence of the ordering kinetics of this alloy have been investigated. The results will be published elsewhere.

References

[1] J. D. Gunton, M. San Miguel, and P. S. Sahni, in Phase Transitions and Critical Phenomena, edited by C. Domb and J. L. Lebowitz (Academic, New York, 1984), vol. 8.

[2] M. K. Phani, J. L. Lebowitz, M. H. Kalos, and O. Penrose, Phys. Rev. Lett. 45, 366 (1980).

[3] P. S. Shani, G. Dee, J. D. Gunton, M. Phani, J. L. Lebowitz, and M. Kalos, Phys. Rev. B 24, 410 (1981).

[4] P. S. Shani, D. J. Srolvitz, G. S. Grest, M. P. Anderson, and S. A. Safran, Phys. Rev. B 28, 2705 (1983).

[5] K. Kaski, M. C. Yalabik, J. D. Gunton, and P. S. Sahni, Phys. Rev. B 28, 5263 (1983).

[6] A. Sadiq and K. Binder, J. Stat. Phys. 35, 517 (1984).

[7] T. Hashimoto, K. Nishihara, and Y. Takeuchi, J. Phys. Soc. Jpn 45, 1127 (1978).

[8] M. R. Collins and H. C. Teh, Phys. Rev. Lett. 17, 781 (1973).

[9] N. Wakabayashi, Phys. Rev. B 33, 6441 (1986).

[10] Y. Noda, S. Nishihara, and Y. Yamada, J. Phys. Soc. Jpn. 53, 4241 (1984).

[11] Japan Atomic Energy Research Institute Report, edited by M. Iizumi, JAERI-M, 85-112 (1985).

[12] S. Katano, H. Motohashi, and M. Iizumi, Rev. Sci. Instrum. 57, 1409 (1986).

[13] F. Reynaud, Phys. Stat. Sol. (a) 72, 11 (1982).

[14] S. M. Allen and J. W. Cahn, Acta. Metall. 27, 1085 (1979).

[15] S. Katano, and M. Iizumi, Phys. Rev. Lett. 52, 835 (1984).

[16] S. Spooner, in Kinetics of Aggregation and Gelation, edited

by F. Family and D. P. Landau (North-Holland, Amsterdam, 1984).

[17] H. Furukawa, Phys. Lett. 97A, 346 (1983).

[18] T. Ohta, D. Jasnow, and K. Kawasaki, Phys. Rev. Lett. 49, 1223 (1982).

[19] F. C. Zhang, O.T. Valls, and G. F. Mazenko, Phys. Rev. B 31, 1579 (1985).

[20] H. Furukawa, Adv. PHys. 6, 703 (1985).

[21] P. Debye, H. R. Anderson Jr., and H. Brumberger, J. Appl. Phys. 28, 679 (1957).

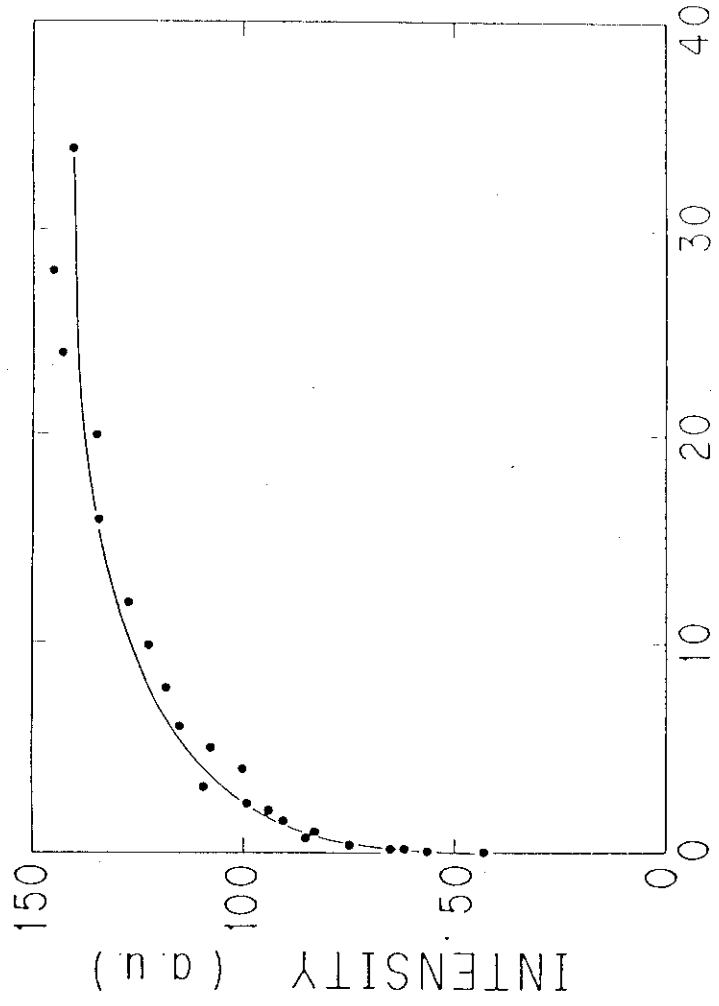

Fig. 2 Time dependence of integrated intensity.

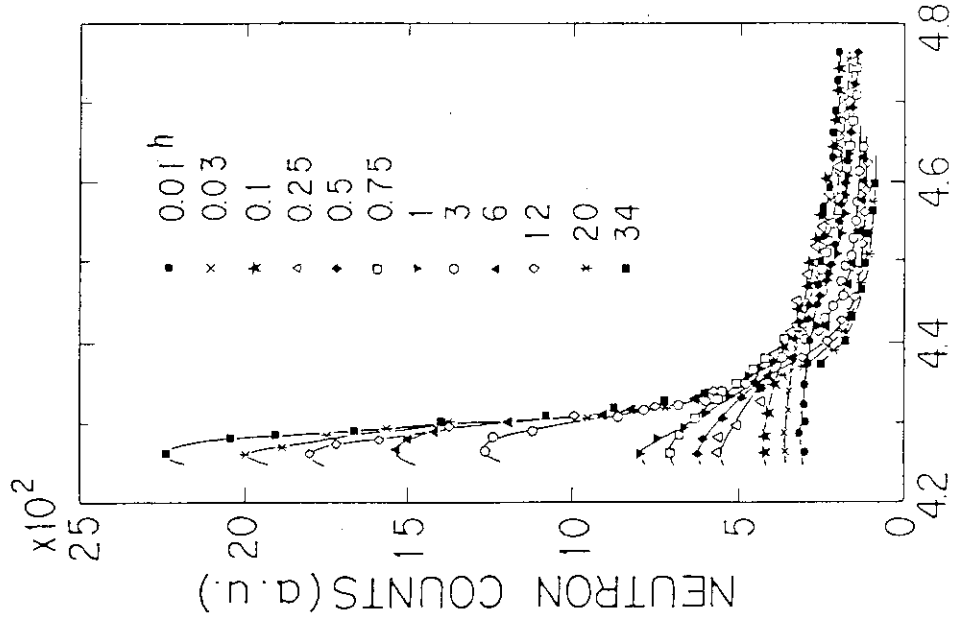

Fig. 1 Time evolution of the 211 superlattice diffraction pattern (arbitrary units) of Ni_3Mn annealed at 470°C for times up to 34 h.

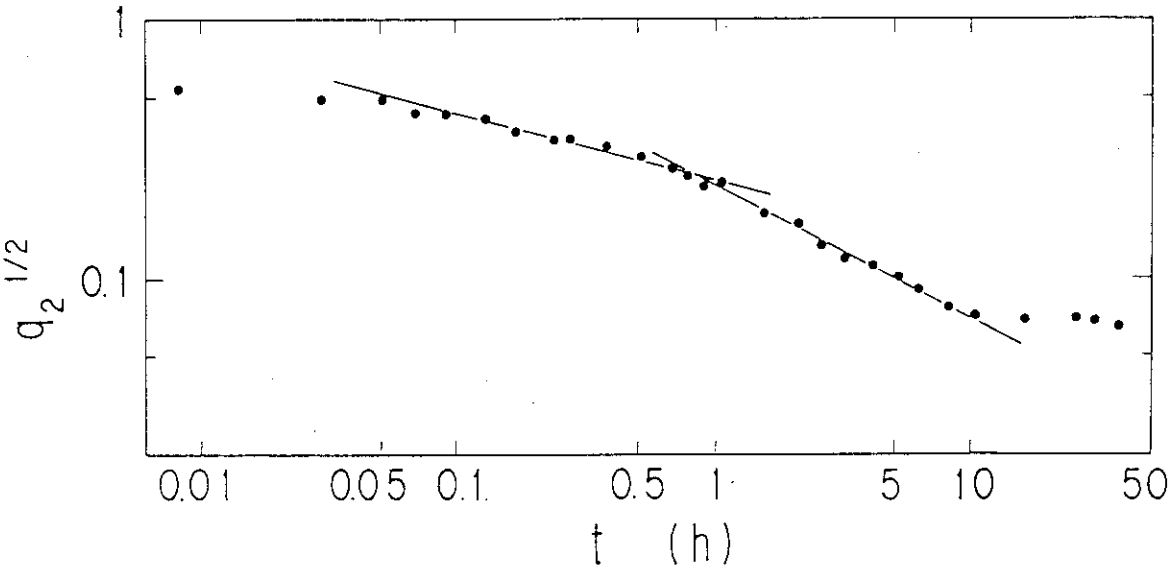

Fig. 3 Time dependence of $q_2(t)^{1/2}$. The solid lines show the exponent a=-1/4 at the early stage and -1/2 at the late one.

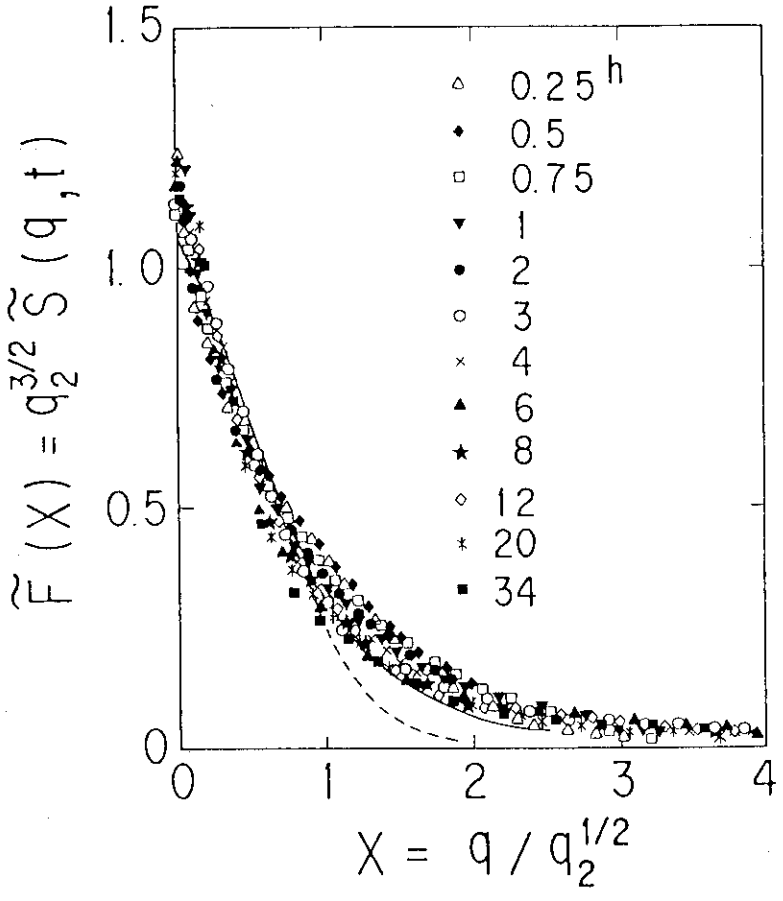

Fig. 4 The scaling function of the normalized structure factor. The dashed line represents the result of the theory by Ohta et al., and the solid line is the squared Lorentzian. The unit of horizontal and vertical axis of these lines are appropriately changed.

Reproduced from The Journal of Applied Physics, vol.61,4114-4116(1987) by permission of The American Institute of Physics.

3. Two-dimensional neutron diffraction of YFe_2O_4 and $CoCr_2O_4$

S. Funahashi and Y. Morii
Department of Physics, Japan Atomic Energy Research, Institute, Tokai-mura, Ibaraki-ken 319-11, Japan
H. R. Child
Solid State Division, Oak Ridge National Laboratory, Oak Ridge, Tennessee 37831

A new wide-angle neutron diffraction instrument has been used to study $CoCr_2O_4$ and YFe_2O_4. The instrument is capable of measuring the scattered intensity over a wide region of reciprocal space in a short time, and this feature was used to measure the magnetic diffraction pattern of these materials at temperatures below the magnetic ordering temperature.

I. INTRODUCTION

Recent development of large one-dimensional position-sensitive neutron detectors has opened a new area of neutron diffractometry.[1,2] The wide-angle neutron diffractometer (WAND) which has been installed at the high flux isotope reactor (HFIR) at Oak Ridge National Laboratory, is equipped with a curved position-sensitive detector covering 130° of scattering angle. Owing both to the high intensity of the incident neutron beam from HFIR and to the wide angular range covered by the detector, WAND has the capability of collecting diffraction patterns of polycrystalline samples very quickly. Time-dependent phenomena of a polycrystalline sample can be measured with this machine very efficiently. For single-crystal samples, a two-dimensional diffraction pattern covering a wide range can be observed in a short time by step scanning of the sample orientation. Diffuse scattering accompanying crystallographic transitions, for example, can be observed in the two-dimensional patterns. The diffractometer table of WAND is designed to be tilted to make it possible for the user to choose any diffraction plane which is parallel to that of the flat setting. The present paper presents a brief summary of some recent work on this new machine.

One of the most useful fields of wide-angle neutron diffractometry is magnetic neutron diffraction. One-dimensional diffraction rods reflecting two-dimensional magnetic ordering, two-dimensional planes reflecting one-dimensional ordering, and magnetic diffuse scattering, for example, can be measured very effectively. It is possible also to search for unknown satellites efficiently in incommensurate structure cases. In this paper, we report typical applications of WAND for a two-dimensional magnetic ordering in YFe_2O_4 and an incommensurate magnetic structure in $CoCr_2O_4$.

II. TWO-DIMENSIONAL MAGNETIC DIFFUSE SCATTERING—YFe_2O_4

Rare-earth iron oxides of the form RFe_2O_4 have a basically hexagonal layered crystal structure and show a strongly two-dimensional magnetic character.[3,4] Crystallographically, all iron atoms occupy 18*h* sites in the hexagonal $R\bar{3}m$ structure, but electronically, divalent and trivalent irons coexist on the equivalent sites. Like magnetite, strong electron exchange interactions exist between iron atoms in the same layer. Consequently, magnetic ordering depends on the stoichiometry, namely on the oxygen content. Nearly perfect two-dimensional magnetic ordering develops in oxygen-deficient YFe_2O_4, while a three-dimensional ordering occurs in stoichiometric YFe_2O_4.

With conventional neutron diffractometers, a one-dimensional diffraction rod in reciprocal space associated with two-dimensional magnetic ordering would be measured point by point along the rod. However, a curved position-sensitive one-dimensional detector measures the diffraction intensity along an arc in a certain plane in reciprocal space in a single measurement. When the sample is turned about an axis perpendicular to the plane defined by the counter, the counter arc scans the plane. Figure 1 shows diffraction intensity contour maps of an oxygen-deficient YFe_2O_4 in a portion of the reciprocal [110]-[001] plane measured with WAND at 9 and 295 K. Development of (1/3 1/3 *l*) and (2/3 2/3 *l*) diffraction rods at low temperature is visible. The resolution for our machine is poor along the arc ($\sim 0.7°$) due to counter characteristics, while it is much better perpendicular to the arc ($< 0.2°$) because of the fine collimation and large monochromator takeoff angle ($2\theta_M = 52.5°$). Two circular intensity maxima which are centered on the origin are (200) and (220) intensities of the aluminum sample container. Although a fan-shaped five-degree moving collimator is installed in WAND to reduce background coming from scattering by any materials in the main neutron beam, and it effectively reduces the background by air scattering, it cannot be made so fine as to remove the scattering from the sample container without too much loss in intensity. Tails are seen for some strong nuclear Bragg peaks (110), (009), (00 12), and (1 1 12) toward low angle (i.e., toward the origin) along the counter arc. They are due to counter characteristics for high counting rates. Weak diffraction points at (1/2 1/2 0), (1/2 1/2 9/2), (1/2 1/2 6), and (1/2 1/2 12) are due to a slight half-wavelength contamination which passed through the graphite filter. Since the diffraction intensity is collected in equal steps of

 0021-8979/87/084114-03$02.40

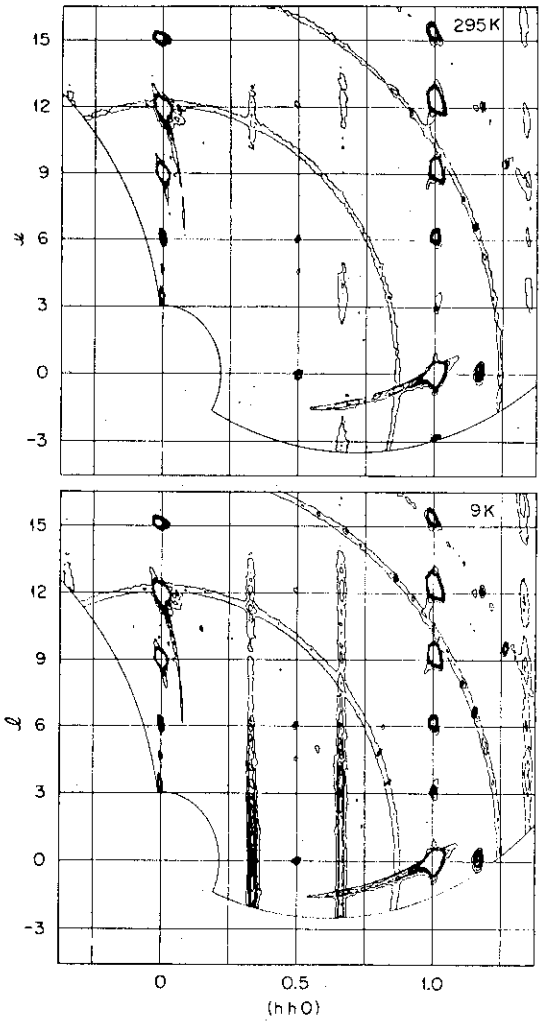

FIG. 1 Intensity contour plot of a portion of the [110]–[001] reciprocal plane of a YFe_2O_4 crystal at (a) 295 K and (b) 9 K.

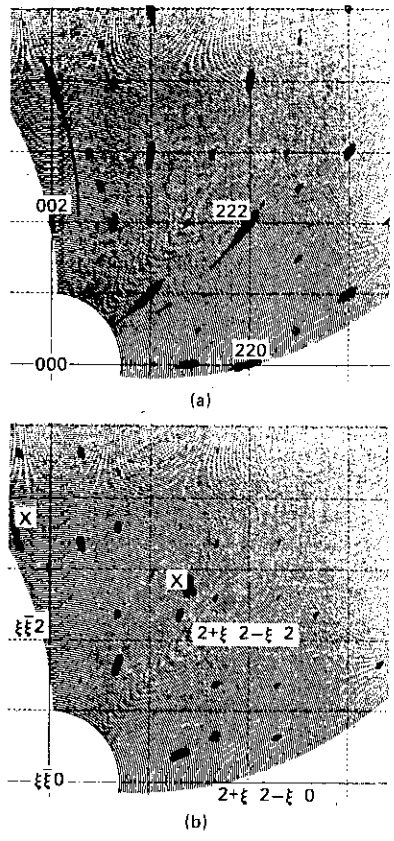

FIG. 2 Two-dimensional diffraction pattern observed with WAND for the [110]–[001] plane at 20 K with (a) tilt $\eta = 0°$, i.e., in this plane, and (b) tilted at $\eta = 4.7°$ to show the plane τ cos 60° containing a second set of magnetic satellites.

the sample orientation angle (ω) and the scattering angle (2θ), the measured points are not distributed in equal steps in reciprocal space. Therefore, for further data processing, some kind of two-dimensional interpolation is needed in general. The intensity, for example, along the (1/3 1/3 l) line for $-1 \leqslant l \leqslant 30$ shows broad scattering at low l at 9 K indicating two-dimensional magnetic ordering. Intensity along any line can be obtained by on-line programs in the same way.

III. MAGNETIC SATELLITE REFLECTIONS—$CoCr_2O_4$

Cobalt chromite, $CoCr_2O_4$, is one of the typical helimagnets.[5,6] The crystal structure is cubic spinel. Divalent cobalt ions on 8a sites and two magnetically different trivalent chromium ions on 16d sites make a triple cone structure at low temperature with a propagation vector τ parallel to the [110] axis. Figure 2(a) shows a two-dimensional diffraction pattern observed with WAND for the [110]–[001] plane at 20 K. Besides the strong fundamental reflections, which include a ferromagnetic contribution located on the reciprocal lattice points, incommensurate satellite reflections are observed at τ away from certain fundamental reflections, where $\tau = \pm\delta$ [110] with $\delta = 0.63$. As mentioned by Menyuk *et al.*,[6] not all of the fundamental reflections have observable satellites due to the antiferromagnetic (or ferrimagnetic) character of the complex spiral structure. Weak reflections at the center of the lattice are half-wavelength reflections. Since the crystal is cubic and the propagation vector is parallel to the [110] axis, there are 12 satellite reflections associated with each fundamental reflection corresponding to the crystallographically equivalent propagation vectors. Figure 2(a) shows only two of them corresponding to $\tau = \pm\delta$ [110], ten other reflections being out of the [110]–[001] plane. Those ten reflections can be classified into two groups. The first group is defined with $\tau = \pm\delta$ [1$\bar{1}$0] and the second group with $\tau = \pm\delta$ [101], $\pm\delta$ [10$\bar{1}$], $\pm\delta$ [0$\bar{1}$1], and $\pm\delta$ [0$\bar{1}\bar{1}$]. The propagation vectors $\tau = \pm\delta$ [1$\bar{1}$0] of the first group are perpendicular to the [110]–[001] plane, while the other eight propagation vectors are tilted from the perpendicular direction by 60°. Those satellites of propagation vectors with plus signs in the above notation are located above the [110]–[001] plane while those of minus signs are below that plane. Four satel-

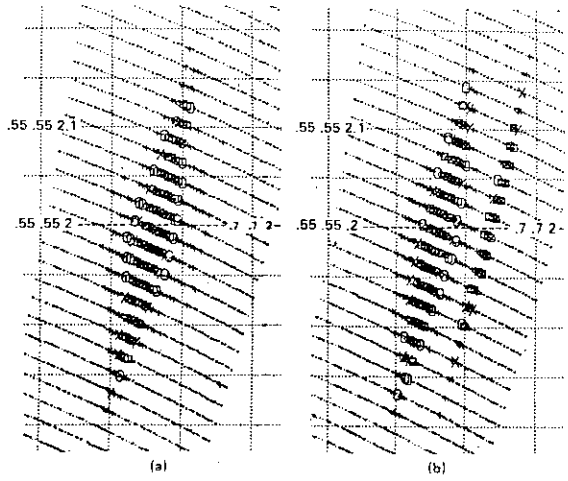

FIG. 3 A detailed map of the region near [002] + δ[110] at (a) 12.7 K and (b) 12.2 K showing the presence of a second magnetic satellite at the lower temperature.

lites of the second group having the same sign are lying in the same plane parallel to the [110]–[001] plane. The distance between the [110]–[001] plane and those satellites are $|\tau| \times \cos 60° = 0.0533 \times 2\pi$ Å^{-1}. The curved position-sensitive detector of WAND is mounted on a table which can be inclined about a horizontal axis perpendicular to the incoming neutron beam. The sample goniometer is sitting on the same table on which the counter is mounted. Consequently, measurements in the reciprocal planes which are parallel to the plane at the flat position can be done in the so-called flat cone configuration. The distance between the reciprocal planes of the flat setting and the inclined one is given by $(2\pi/\lambda)\sin\eta$, where η is the inclination angle of the table and λ is the neutron wavelength. In order to make the sets of the four plus sign satellites of the second group described above fall on the same measuring plane, the table was inclined an angle $\eta = 4.7°$. Figure 2(b) shows the result measured at this inclination angle at 14 K. Only the satellite reflections with $\tau = \delta$ [101], δ [$1\bar{0}1$], δ[$\bar{0}11$], and δ [$\bar{0}\bar{1}1$] are observed as expected.

Figure 3(a) shows a detailed map of the satellite at [002] + δ[110] measured at 12.7 K. It is evident the satellite appears to be elongated along the counter arc due to the anisotropic resolution described earlier. The peak position corresponds to $\delta = 0.63$, in agreement with the propagation vector found by Menyuk *et al.*[6] At lower temperatures another satellite appears, as shown in Fig. 3(b) for 12.1 K. Two satellites are clearly seen with the second one having $\delta = 0.67$ in agreement with that reported by Plumier.[7] This result suggests than an incommensurate to commensurate transition occurs at about 12.5 K. The anomaly which has been found near 11 K in the magnetic resonance behavior[8] is attributed to the transition found here. It is obvious that this second transition may be very sensitive to oxygen content, hence strongly sample dependent. Also, since both satellites are present, the transition is not complete in this crystal and shows a temperature hysteresis effect when studied in detail.

IV. SUMMARY

The present experiments show that the wide-angle neutron diffractometer is very efficient in measuring both low-dimensional magnetic ordering and incommensurate magnetic diffraction because it can measure a wide range of reciprocal space quickly. The well-collimated incident beam makes it possible to resolve close, sharp peaks except for the case when they are located on nearly the same counter arc because the position resolution of the counter is rather poor. Of course, the machine is also very useful for obtaining polycrystalline patterns rapidly.

Further, it is possible to measure three-dimensional diffraction by repeating the ω scans and changing the inclination angle η. Unless the scattering is very weak, one measurement can be done in about 1 min. Thus, one scan needs about 10^3 min if we cover 100° of ω angle with 0.1° steps. Therefore, ten two-dimensional scans, each covering one quadrant in a reciprocal plane at different inclination angles, can be carried out in a few days. In this case we would accumulate diffraction intensity at about 10 million points covering a large region of three-dimensional reciprocal space.

ACKNOWLEDGMENTS

This research was carried out at the Oak Ridge National Laboratory under the U.S.–Japan Cooperative Program in Neutron Scattering and sponsored in part by the U.S. Department of Energy under Contract No. DE-AC05-840R21400 with Martin Marietta Energy Systems, Inc.

[1] M. Iizumi, Physica **136B**, 36 (1986).
[2] M. Iizumi, S. Funahashi, S. Katano, R. M. Moon, R. M. Nicklow, H. R. Child, and M. K. Kopp, Hahn-Meitner Institute Report, HM1-B411 (1984).
[3] J. Akimitsu, Y. Inada, S. Siratori, I. Shindo, and N. Kimizuka, Solid State Commun. **32**, 1065 (1979).
[4] S. Funahashi, J. Akimitsu, K. Siratori, N. Kimizuka, M. Tanaka, and H. Fujishita, J. Phys. Soc. Jpn. **53**, 2688 (1984).
[5] D. H. Lyons, T. A. Kaplan, K. Dwight, and N. Menyuk, Phys. Rev. **126**, 540 (1962).
[6] N. Menyuk, K. Dwight, and A. Wold, J. Phys. **25**, 528 (1964).
[7] R. Plumier, J. Appl. Phys. **39**, 635 (1968).
[8] S. Funahashi, K. Siratori, and Y. Tomono, J. Phys. Soc. Jpn. **29**, 1179 (1970).

Proceedings of The International Conference on
Martensitic Transformations (1986) pp. 150-153
The Japan Institute of Metals

4. DIFFUSE NEUTRON SCATTERING IN β_1-PHASE Cu-Al-Ni ALLOY

Y. Morii, M. Iizumi, S. Funahashi, and H. R. Child*

Diffuse Neutron scattering patterns of a β_1-phase Cu-Al-Ni sample have been studied in detail by the Wide-Angle Neutron Diffractometer (WAND) which was installed recently at the Oak Ridge National Laboratory. Strong diffuse streaks along <110> directions in addition to the main Bragg peaks are observed in the (00ℓ) reciprocal planes (ℓ = 0 and 2). The diffuse streaks are related to the anomalously low energies of the [110]TA_1 phonon (e//[1$\bar{1}$0]) leading to the martensitic phase transition of the alloy. It is also emphasized that the WAND is a powerful machine to study satellite peaks of an alloy over a wide range of reciprocal space in a relatively short time.

I. Introduction

Cu-Al-Ni alloy with composition near Cu_3Al is of great interest because of its shape memory effects [1], high damping properties, and potential capability as laser memory media [2]. These phenomena are explained basically by the martensitic phase transition. Although the nucleation problems of the martensitic transformation are not well understood, many authors believe that the inherent mechanical instability of the β-phase alloys including Cu-Al-Ni is closely related to the nucleation [3, 4, 5]. From this point of view, some of the authors (Y. M. and M. I.) reported that the [110]TA_1 phonon (e//[1$\bar{1}$0]) of a β_1-$Cu_{69.2}Al_{25.4}Ni_{5.4}$ crystal has quite low energies ($E \lesssim 5$meV) with an anomalous dip in the dispersion curve [6]. It was also reported that temperature dependent elastic peaks on the [110] axis are attributable to 2H and 18R martensites of the alloy. Therefore, we have carried out an extensive survey of the elastic scattering of the crystal and examined the scattering patterns in various reciprocal planes.

II. Experimental

The single crystal β_1-$Cu_{69.2}Al_{25.4}Ni_{5.4}$ (in at.%) used in this work is the same crystal used in the previous work [6]. The crystal transforms into the martensite phase (2H type martensite) at lower temperatures. The transition temperatures Ms, Mf, As, and Af are 256, 248, 274, and 289 K, respectively.

Neutron scattering experiments were carried out on the Wide-Angle Neutron Diffractometer (WAND) [7] which was installed recently at the High Flux Isotope Reactor at the Oak Ridge National Laboratory. The WAND is a one-dimensional position sensitive neutron detector which covers a 2θ angle range from 10 to 140 degrees simultaneously. A beryllium monochrometer was used to get an incident neutron beam with wavelength of 1.537 Å. A pyrolitic graphite filter was placed in the incident beam to suppress the second order contamination of the beam.

Physics Division, Japan Atomic Energy Research Institute, Tokai, Ibaraki 319-11, Japan.
*Solid State Division, Oak Ridge National Laboratory, Oak Ridge, Tennessee 37831, U.S.A.

The WAND detector and sample crystal are capable of being tilted simultaneously about an axis perpendicular to the incident beam so that the scattering in reciprocal planes perpendicular to the rotation axis of the crystal can be measured. This is the procedure referred to as "flat-cone geometry."

III. Results and Discussion

Two-dimensional neutron diffraction patterns obtained by the WAND at room temperature are shown in Fig. 1(a) for h k 0, and 1(b) for h k 2 reciprocal planes. Each fan-shaped pattern consists of 651 ω-scans (every 0.2 degree crystal rotation). Darker points represent stronger diffraction intensities. Diffuse streaks in <110> directions are observed in addition to strong Bragg peaks which show the Fe_3Al structure of the ordered phase of β_1-Cu-Al-Ni.

The diffuse streaks are only on the lines for which

$$|h| + |k| + |\ell| = 4n \quad n = 1, 2, \ldots \quad (1)$$

for $\ell = 0$ and 2.

Since diffuse streaks are observed in the planes of $\ell = 0$ and 2, but no streaks are observed in the plane for $\ell = 1$, one can say that the diffuse streaks are rod shape along the lines (1) which include fundamental Bragg peaks but not the superlattice peaks.

A typical intensity distribution on the [110] axis is characterized by a strong diffuse tail of the Bragg peak which is identical to our previous measurement [6], and M. A. Dvorack and Hayden Chen's x-ray work on a similar Cu-Al-Ni system [8]. The width of the streaks is larger for the lines for larger n in Eq. (1).

The diffuse streaks are interpreted as phonon diffuse scattering in electron diffraction [9] and x-ray diffraction [8] experiments. The present results basically support this interpretation.

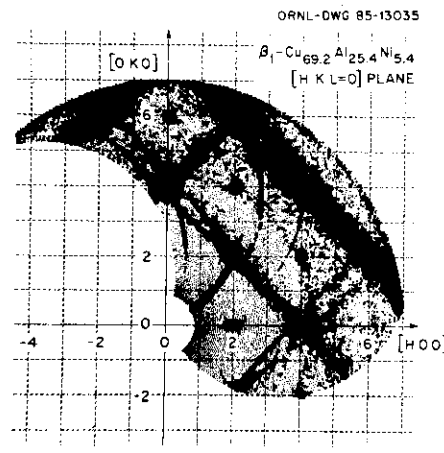

Fig. 1 (a)

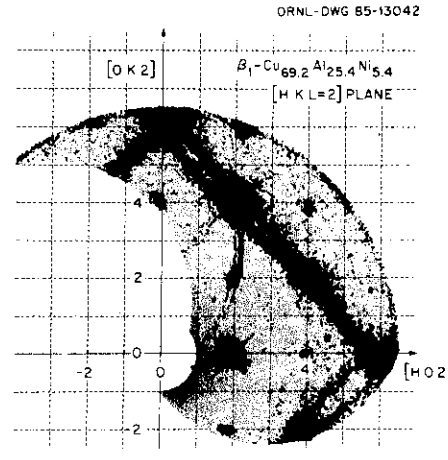

Fig. 1 (b)

Fig. 1 Thermal phonon diffuse streaks of β_1-$Cu_{69.2}Al_{25.4}Ni_{5.4}$ are shown along <110> directions in the [00ℓ] reciprocal planes with $\ell = 0$ and 2 in the Fig. (a) and (b).

One of the interesting features of the streaks revealed in this work is the structure of the streaks. Since the diffuse scattering intensity from the phonon is proportional to the inverse of the square of the phonon energy, the intensity on the [110] axis should be strongest. In contradiction to this expectation, one can see the splitting of the streaks between (2,2,0) and (-2,6,0), (4,4,0) and (0,8,0), and (2,-2,0) and (6,2,0) in Fig. 1(a), and also between (3,3,2) and (0,6,2), and (4,-2,2) and (6,0,2) in Fig. 1(b). It is in progress to carefully measure the phonon energy for the double streaks to get a better understanding of this splitting.

Several curved high intensity streaks which are curved toward the origin from the high intensity Bragg peaks are not real neutron counts but an instrumental effect due to the extremely high count rate at the Bragg angles.

In addition to the diffuse streaks, a satellite peak at (2.315, 1.685, 0) is shown in both a contour map (Fig. 2) and a perspective map (Fig. 3). This satellite is attributable to 18 R martensite of the alloy as reported in the previous work [6].

These mapping techniques help us measure the intensity over a wide range of reciprocal space of the alloy in a relatively short time in order to characterize the structure of the diffuse scattering and to locate incommensurate Bragg peaks.

Acknowledgements

This research was carried out at ORNL under the U.S.-Japan Cooperative Program on Neutron Scatterng, and sponsored in part by the Division of Material Sciences, U.S. Department of Energy, under contract DE-AC05-840R21400, with Martin Marietta Energy Systems, Incorporated.

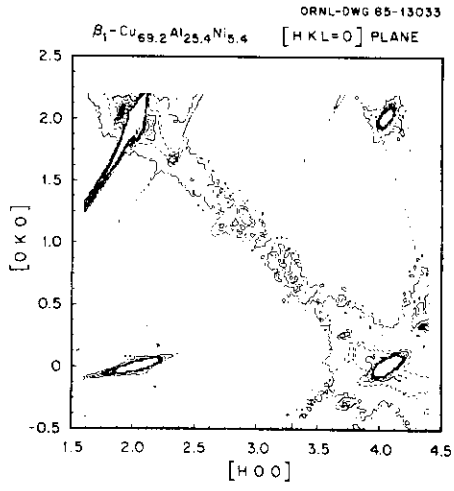

Fig. 2 Contour map of the diffuse streak from the (2, 2, 0) to (4, 0, 0) Bragg peak of β_1-$Cn_{69.2}Al_{25.4}Ni_{5.4}$.

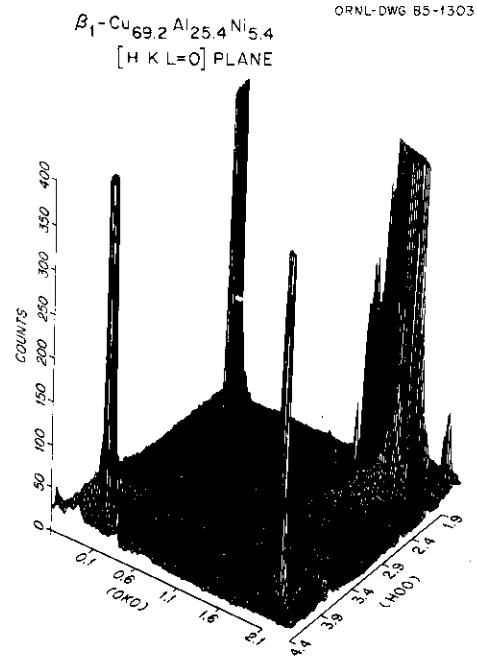

Fig. 3. An elastic peak at (2.315, 1.685, 0) and the diffuse streak from the (2, 2, 0) to (4, 0, 0) Bragg peak are displayed in this perspective map of the elastic scattering intensities.

References

[1] K. Otsuka and K. Shimizu, Scripta. Metall., **4**(1970), 469.
[2] T. Minemura, H. Andoh, and I. Ikuta, J. Mater. Sci., to be submitted.
[3] L. Delaey, P. F. Gobin, G. Guenin, and J. Warlimont, Proc. of ICOMAT 79, Cambridge (1979), 400.
[4] N. Nakanishi, Prog. in Mater. Sci., **24**(1979), 143.
[5] G. Guenin, D. Rios Jara, M. Morin, L. Delaey, R. Pynn, and R. F. Gobin, J. de Physique, **C4**(1982), C4-597.
[6] Y. Morii and M. Iizumi, J. Phy. Soc. Jpn., **54**(1985), 2948.
[7] M. Iizumi, S. Funahashi, S. Katano, R. M. Moon, R. M. Nicklow, H. R. Child, and M. K. Kopp, **HMI-B411** (1984), 243. Also to be submitted to Nucl. Instr. & Meth.
[8] M. A. Dvorack and H. Chen, Scripta Metallurgica, **17**(1983), 131.
[9] K. Otsuka, C. M. Wayman, and H. Kubo, Metall. Trans., **A9**(1978), 1075.

5. Real-time Neutron Diffraction Study of Crystallization Kinetics in Amorphous $Fe_{78}B_{13}Si_9$ Alloy

S. Katano, Y. Morii, M. Iizumi,
H. R. Child and R. M. Nicklow

Abstract

The transformation from the as-quenched amorphous to the crystalline state in $Fe_{78}B_{13}Si_9$ alloy has been investigated using a new-type neutron diffractometer. The time resolved diffraction patterns clearly show that this alloy crystallizes into FeSi alloy and Fe_2B in that order. The time evolution of these crystalline phases can be analyzed by the Kolmogorov-Johnson-Mehl-Avrami equation with the exponent of about 2.5 over a wide temperature range. This suggests that the crystallization occurs by the diffusion-controlled growth with a constant nucleation rate. The scaling behavior in the crystallization kinetics is also discussed.

1. Introduction

In order to investigate the thermal stability and crystallization behavior of amorphous metals and alloys, many kinetics studies have been done using various techniques such as differential scanning calorimetry, Mössbauer effect, transmission electron microscopy and, recently, magnetization measurements.[1-6] However, there have been very few systematic experiments by diffraction, though this technique is one of the most direct methods to study the structural change of materials. The main reason may be that a conventional diffractometer is incapable of doing real-time experiments; that is, it takes several hours to get a diffraction pattern over a wide angle. Recently, however, new-types of diffractometers with multidetectors or one-dimensional position-sensitive detector became available to observe the structural change in real-time. The neutron diffraction experiment is favorable in this type of observation because the environmental control around a sample is considerably easy owing to the high penetrability of neutrons. At the Institut Laue-Langevin the crystallization process was investigated using the diffractometer D1B in the condition of increasing the temperature at a constant rate.[7] In the present work we used the WAND (the Wide-Angle Neutron Diffractometer) installed at the High Flux Isotope Reactor at the Oak Ridge National Laboratory to study the crystallization kinetics at constant temperatures. Since this diffractometer consists of a curved one-dimensional position-sensitive detector which covers a

130° angle, we are able to study the kinetics of phase transition by time resolved technique. [8] Using this diffractometer, the crystallization kinetics could be investigated directly and quantitatively. From the obtained results several interesting aspects of crystallization in the amorphous alloy will be discussed.

2. Experimental

Amorphous $Fe_{78}B_{13}Si_9$ (METGLAS 2605S-2) in the form of a ribbon 2.54 cm wide and 25 μm thick was obtained from the Allied Chemical Corporation. The ribbon was cut into sheets in the dimension of 1 cm wide and 5.5 cm long. A bundle of about 120 sheets were inserted in a holder made of quartz with the inner dimension of about 1 cm x 0.3 cm wide and 1.5 cm high. This sample was set in a furnace which can precisely control the heating-rate up to 1000°C/min by the use of infrared lamps. [9] In order to protect the surface of the sample from a damage by heat-radiation, the sample was wrapped by an Al-foil and heated up at a moderate rate of 50°C/min. This heating rate was, however, fast enough in the temperature-range of the present study. The time evolution of diffraction patterns at 450, 465, 480, 500 and 520°C was studied using the WAND after the temperature had reached these temperatures. The minimum time division for the measurements was 2 min at the highest temperature.

3. Results and Discussion

Fig. 1 (a) and (b) show the time evolution of the diffraction patterns annealed at 450°C. As shown in the insert of (a), the obtained pattern is a superposition of the amorphous and the crystalline state. Therefore, in order to see small changes at the early stage, the difference between patterns at various times and that of the amorphous state was plotted. Up to 3 h, a change over a very wide angle can be seen around the first broad peak of the amorphous state (about 570 channel). Although such a change should be attributed to either the beginning of crystallization or the structure relaxation in the amorphous state, it is hard in this study to clarify which is proper. At 6 h, the change over a wide angle becomes a sharp peak, but any other change in the pattern is still not clear. After 24 h passed, several peaks can be seen at about 570, 890, 1150 and 1390 channels, which are identified to be the diffraction peaks of FeSi alloy. After 36 h, peaks at about 660, 750, 1110 and 1320 channels become clear; these are the peaks of Fe_2B. (Note that the peak at about 570 channel is a superposition of the peaks of FeSi and Fe_2B.) After that those peaks continue to grow up to 100 h, and reaches the equilibrium values. At this time the sample has completed the transformation to the crystalline state, as shown in the insert. The change of the width for the peaks of FeSi and Fe_2B was not clearly visible; the width is fairly narrow already when the intensity becomes strong enough to identify the width. The well-known compound Fe_3B, which is

observed in the crystallization of amorphous $Fe_{80}B_{20}$ and other alloys, does not appear in the diffraction patterns. These features of the transformation are basically the same at other temperatures except the scale of time.

In order to discuss the kinetics quantitatively the time-dependent fraction of the crystalline state x(t) was calculated by comparing the peak intensity at each time with that of the final equilibrium state. In the present experiment the the time evolution of FeSi and Fe_2B can be investigated separately. For this purpose the peak intensity at about 890 channel (the 200 reflection of FeSi) and 750 channel (the 202 and 130 reflections of Fe_2B) were used. The result of the strongest peak at about 570 channel was not shown here, since this peak is a superposition of the 110 reflection of FeSi and the 121 reflection of Fe_2B and, moreover, its behavior at the initial stage earlier than 6 h is complicated and is beyond the scope of the present investigation as stated before . The obtained fraction x(t) can be analyzed in terms of the Kolmogorov-Johnson-Mehl-Avrami equation

$$x(t) = 1 - \exp[-(t/\tau)^n], \qquad (1)$$

where τ is a temperature dependent constant and considered to be a characteristic time in crystallization, and n is related to the mechanism of the nucleation-growth process. According to this equation a log-log plot of $\ln(1-x)^{-1}$ versus time follows a straight line as is shown in Fig. 2, and the obtained values n

and τ are listed in Table 1. The exponent n is 2.5 $\pm$ 0.2 for FeSi and 2.7 $\pm$ 0.2 for Fe_2B, except at 520°C where the exponents for both components are about 2. Although the exponent for Fe_2B is a little larger than that for FeSi, these values can be regarded as 2.5 within experimental errors. The value of about 2.5, which is consistent with the previous result for $Fe_{78}B_{12}Si_{10}$ alloy by calorimetry method [2], indicates that the crystallization occurs by the diffusion-controlled isotropic growth with a constant nucleation rate. [10] On the other hand the exponent of about 2 at 520°C means a decrease of the nucleation rate with time. The reason is probably that the nucleation is much promoted at the early stage owing to the high temperature but thereafter the rate decreases relatively.

In the nucleation-growth theory it is well known that the size of the new phase formed by the diffusion-controlled growth increases according to the parabolic $t^{1/2}$ law. However, a change of the line width, which is inversely proportional to the average size of the new phase, was not observed clearly as mentioned earlier. This result may be related to the number and dimension of the newly developed crystalline phase at the early stage. A transmission electron microscopy (TEM) experiment shows that at the early stage of the transition the number of the crystalline phase is small but its radius is already a order of several hundred Å. [11] Hence by the time when the intensity becomes strong enough to be observed, the dimension is already beyond the minimum size which can be determined by the resolution of the detector.

As shown before, the exponents n takes almost the same value irrespective of the temperature; that is, the crystallization kinetics follows the same mechanism over a wide temperature range. Therefore, the curves of the fraction for various temperatures display a single form when time is scaled by the characteristic time τ. This is a straightforward consequence of eq. (1) with the temperature-independent exponent. The result for FeSi is shown in Fig. 3. In the case of Fe_2B, the same behavior is observed. Quite recently, a study by magnetization measurements for $Fe_{83}B_{12}Si_5$ alloy also succeeded to show a similar result. [6] In the experiment, however, one had to assume that the changes of the magnetization are simply linear to the volume fraction of the crystalline FeSi, and the temperature range was rather narrow ($361 \leq T \leq 393^{\circ}C$). Compared to this study, our neutron diffraction experiment gives direct information about the structure change and, moreover, shows that the scaling behavior holds good over a much wider temperature range.

These results are examples of the scaling behavior which has been recently investigated concerning to the transition from the non-equilibrium state to the equilibrium one. In the present case this idea means that the growth patterns of the new phase at various temperatures are very much similar to one another if time is scaled by τ for the respective temperatures. However, the time evolution of the shape and the width of the diffraction pattern could not be observed, as mentioned before. Therefore, the scaling behavior of the structure factor S(q,t), which is one

of the main results of the scaling theory for the first-order phase transition [12], could not be examined.

The characteristic time τ can be analyzed by the Arrhenius law,

$$1/\tau = 1/\tau_0 \exp(-E_a/k_BT), \qquad (2)$$

where τ_0 is a time constant, and E_a is an activation energy which has contributions from both nucleation and growth mechanisms. The plot of the ln $(1/\tau)$ versus $1/k_BT$ is shown in Fig. 4 for both cases of FeSi and Fe_2B. From this figure the activation energy is obtained to be 3.9 $\pm$ 0.1 eV for FeSi and 4.0 $\pm$ 0.1 eV for Fe_2B, which are also consistent with the experiment by calorimetry method. [2] The observed differences in the kinetics for both crystalline states are generated by such a small difference in the activation energy. The frequency $1/\tau_0$ is the order of 10^{21} /s for both FeSi and Fe_2B, which is considerably high compared with the Debye frequency (the order of 10^{14} /s). However, it may not make sense to compare τ_0 directly with the one which appears in the simple diffusion process, since the kinetics observed here is a complicated combination of nucleation and growth mechanisms.

In conclusion, the crystallization kinetics in $Fe_{78}B_{13}Si_9$ alloy could be investigated by time resolved neutron diffraction technique. The fit of the experimental results to the Kolmogorov-Johnson-Mehl-Avrami equation indicates that the crystallization of this alloy takes place by the diffusion-

controlled growth with a constant nucleation rate over a wide temperature range. This assures the scaling behavior in the crystallization kinetics.

References

1) A. L. Greer: Acta Metall. 30 (1982) 171.

2) V. R. V. Ramanan and G. E. Fish: J. Appl. Phys. 53 (1982) 2273.

3) A. S. Schaafsma, H. Snijders, F. van der Woude, J. W. Drijver and S. Radelaar: Phys. Rev. B20 (1979) 4423.

4) Hang Nam Ok and A. H. Morrish: Phys. Rev. B22 (1980) 3471.

5) C. F. Chang and J. Marti: J. Mat. Sci. 18 (1983) 2297.

6) Y. Wolfus, Y. Yeshurun, I. Felner and J. Wolny: Solid State Commun. 61 (1987) 519.

7) P. Mongin: Institut Laue-Langevin, Annual Report (1984).

8) Japan Atomic Energy Research Institute Report, JAERI-M (1985) 85-112.

9) S. Katano, H. Motohashi and M. Iizumi: Rev. Sci. Instrum. 57 (1986) 1409.

10) J. W. Christian: The Theory of Transformation in Metals and Alloys(Pergamon Press, New York, 1975).

11) M. von Heimendahl and G. Maussner: J. Mat. Sci. 14 (1979) 1238.

12) H. Furukawa: Adv. Phys. 34 (1985) 703.

Table I Kinetic parameters n(the exponent) and τ (the characteristic time) [eq. (1)] for FeSi and Fe_2B at various temperatures.

	T(°C)	n	τ (h)
FeSi	450	2.3	58.3
	465	2.5	26.2
	480	2.6	8.2
	500	2.4	1.2
	520	1.9	0.3
Fe_2B	450	2.7	68.8
	465	2.6	31.2
	480	2.8	9.0
	500	2.7	1.4
	520	2.0	0.3

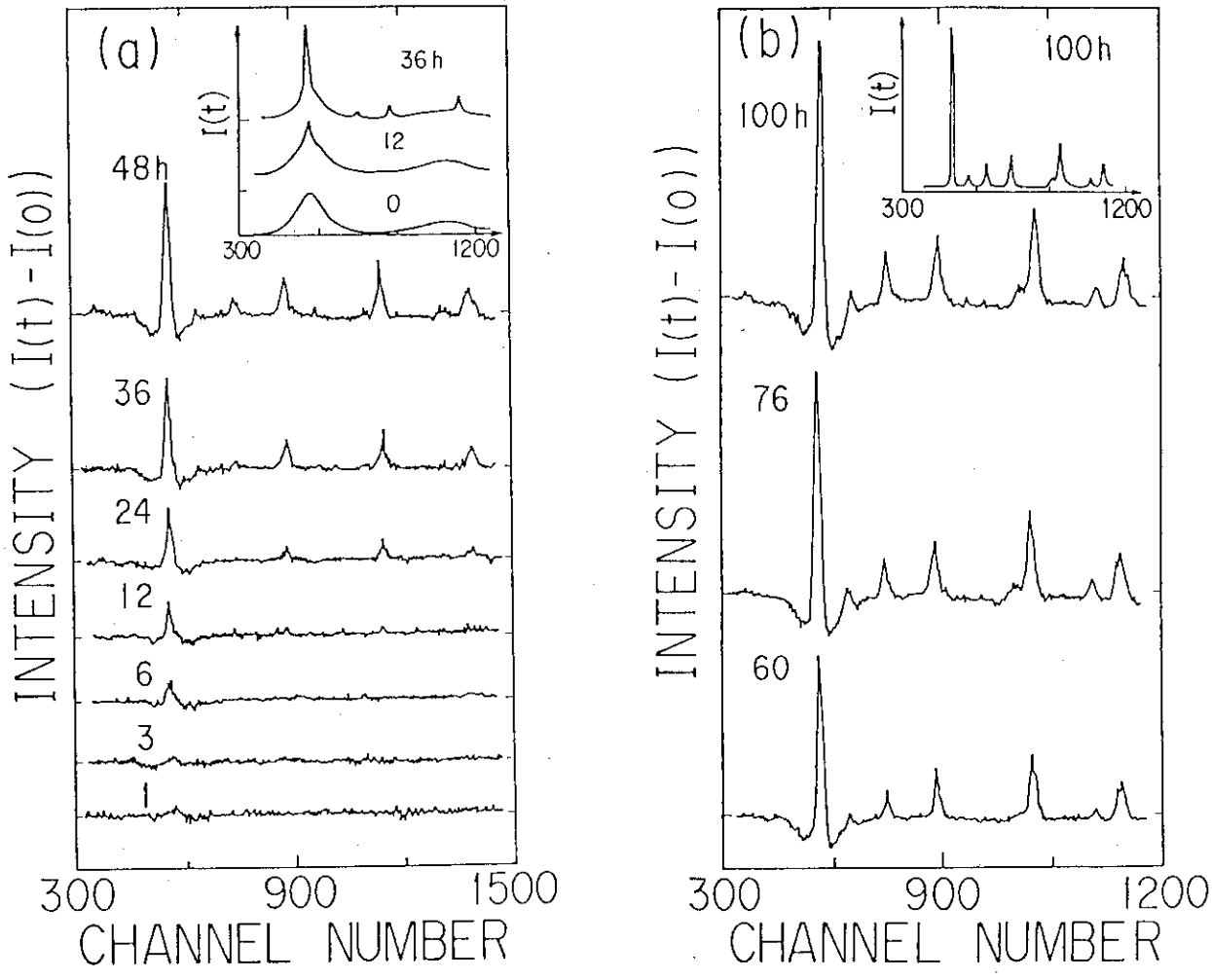

Fig. 1 Time evolution of the diffraction pattern annealed at 450°C. In order to clarify small changes in the diffraction pattern, the difference between the diffraction patterns at various time and that of the amorphous state is plotted. The insert indicates the measured pattern, which shows a superposition of the amorphous and crystalline state.

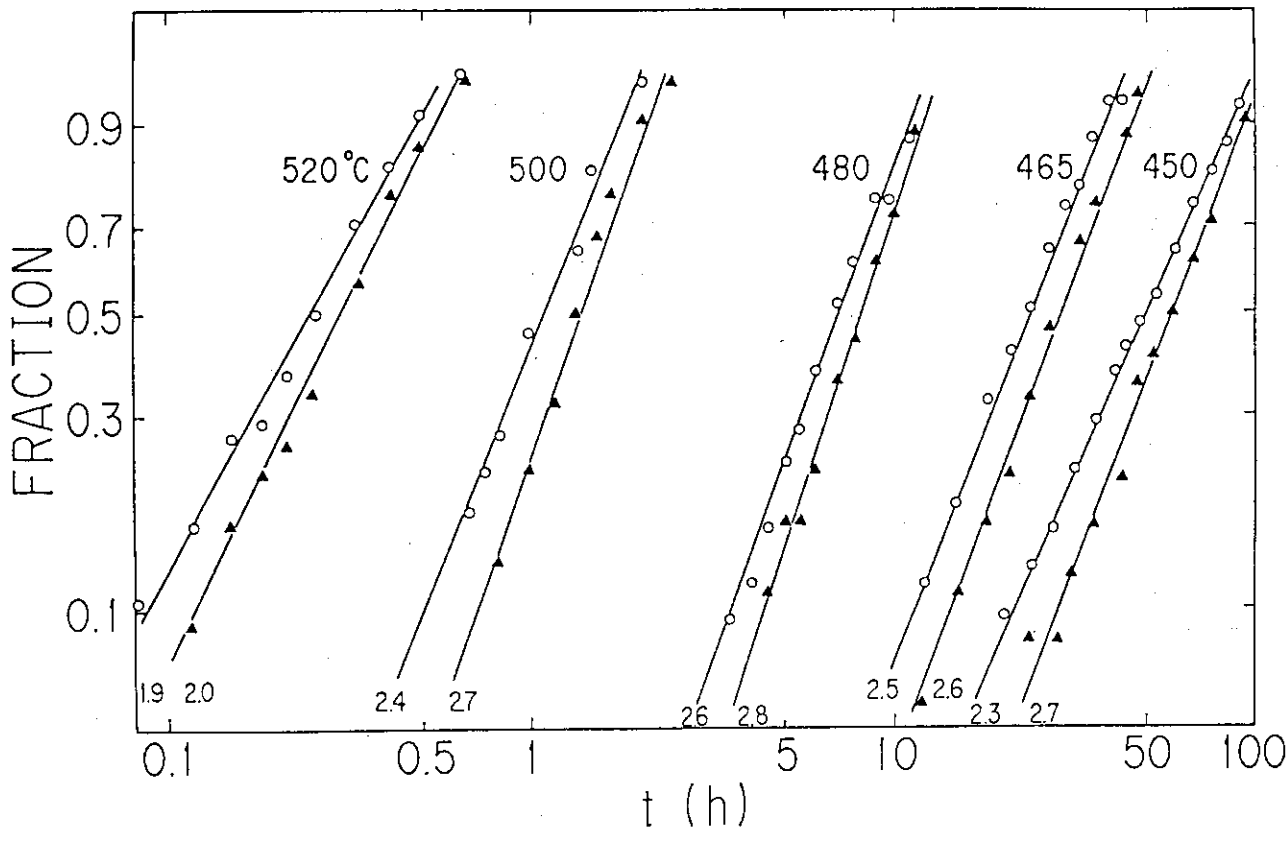

Fig. 2 Fraction of the crystalline state x plotted as $\ln(1-x)^{-1}$ vs time on log-log scale for FeSi(○) and Fe_2B(▲). Values of the exponent n in the Kolmogorov-Jonnson-Mehl-Avrami equation are also indicated.

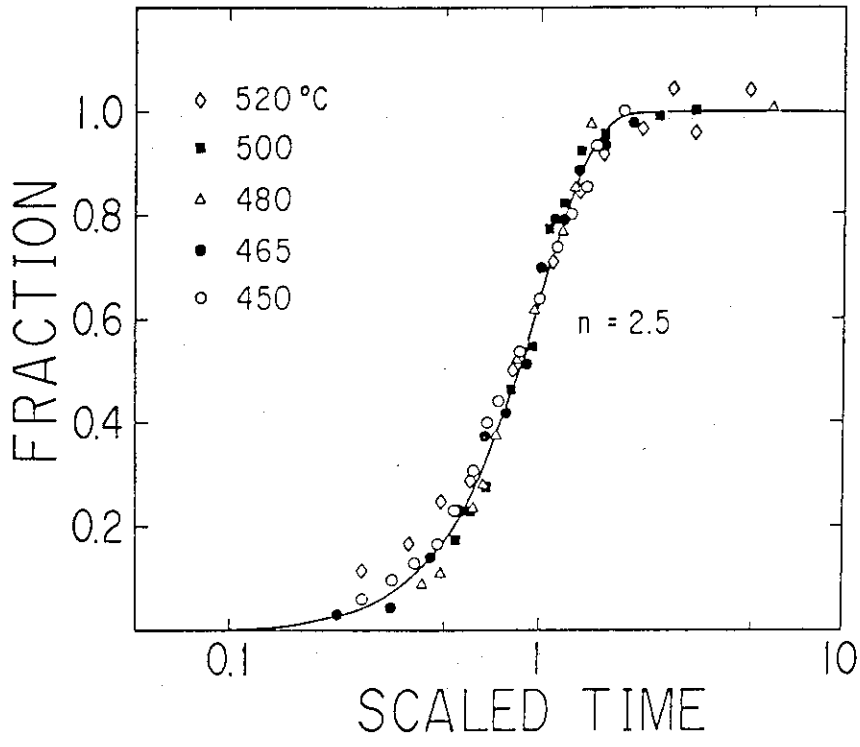

Fig. 3 Scaling behavior of the fraction of the crystalline FeSi with respect to the scaled time t/τ. The solid curve is the Kolmogorov-Johnson-Mehl-Avrami curve for the exponent of 2.5.

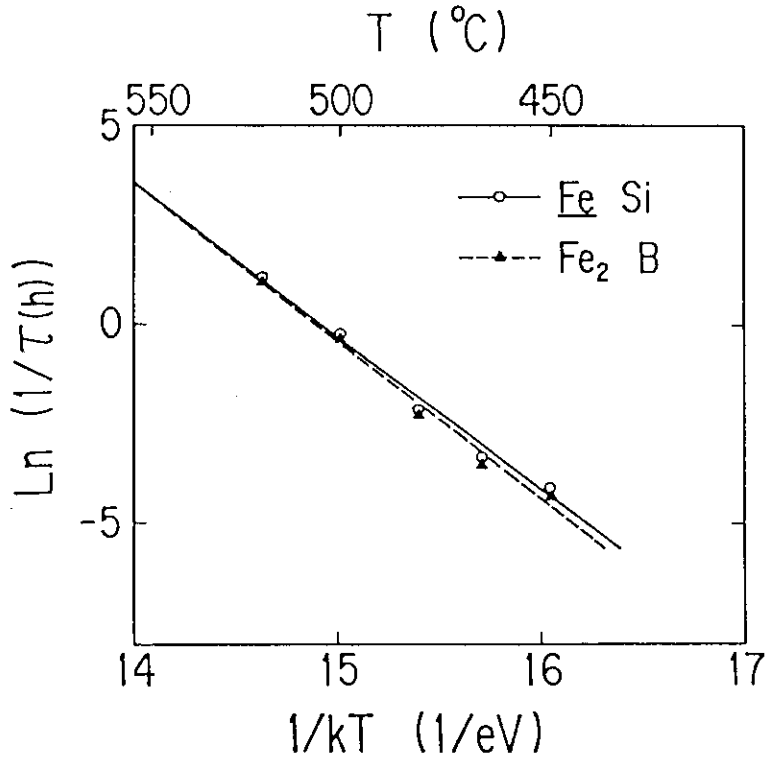

Fig. 4 Arrhenius plot of the characteristic time vs temperature for FeSi(o) and Fe_2B(▲).

6. Crystallization Kinetics in Amorphous $Fe_{80}P_{14}Si_6$ Alloy

S. Katano, Y. Morii, M. Iizumi,
H. R. Child and R. M. Nicklow

Abstract

The transformation from the as-quenched amorphous to the crystalline state in $Fe_{80}P_{14}Si_6$ alloy has been investigated at 395, 410, 430 and 450°C on the isothermal condition. The time resolved diffraction patterns at the lower temperatures show that this alloy crystallizes into FeSi alloy and Fe_3P in that order. On the other hand, the patterns at the higher temperatures show the existence of a different phase at the initial stage of the transformation though its structure could not been identified. The time evolution of these crystalline phases can be analyzed by the Kolmogorov-Johnson-Mehl-Avrami equation with the exponent of about 1.5.

Previously we investigated the crystallization kinetics of amorphous $Fe_{78}B_{13}Si_9$ alloy. In this report, we describe the result of amorphous $Fe_{80}P_{14}Si_6$. The kinetics of this alloy is considerably different from that of $Fe_{78}B_{13}Si_9$.

Amorphous $Fe_{80}P_{14}Si_6$ in the form of a ribbon 3 mm wide and about 30 μm thick was obtained by melt spinning method. The ribbon was cut into sheets in the dimension of 3 mm wide and 55 mm long. A bundle of about 100 sheets were inserted in a holder made of quartz with the inner dimension of about 3 mm x 3 mm wide and 15 mm high. This sample was set in a furnace which can precisely control the heating-rate up to 1000°C/min by the use of infrared lamps. In order to protect the surface of the sample from a damage by heat-radiation, the sample was wrapped by an Al-foil and heated up at a moderate rate of 50°C/min. This heating rate was, however, fast enough in the temperature-range of the present study. The time evolution of diffraction patterns at 395, 410, 430 and 450°C was studied using the WAND (the Wide-Angle Neutron Diffractometer) after the temperature had reached these temperatures.

Fig. 1 shows the time evolution of the diffraction patterns annealed at 395°C. As shown in the insert, the obtained pattern is a superposition of the amorphous and the crystalline state. Therefore, in order to see small changes at the early stage, the difference between patterns at various times and that of the amorphous state was plotted. Up to 3 h, a change over a very wide angle can be seen around the first broad peak of the

amorphous state (about 570 channel). Although such a change should be attributed to either the beginning of crystallization or the structure relaxation in the amorphous state, it is hard in this study to clarify which is proper. At 6 h, the change over a wide angle becomes a sharp peak at about 570 channel. Moreover, peaks at about 890, 1150 channels can be seen. These are identified to be the diffraction peaks of FeSi alloy. After 24 h, peaks at about 500, 640, 670, 1020 channels become clear; these are the peaks of Fe_3P. (Note that the peak at about 570 channel is a superposition of the peaks of FeSi and Fe_3P.) After that, those peaks continue to grow up to 48 h, and reach the equilibrium values. At this time the sample has completed the transformation to the crystalline state, as shown in the insert. The change of the width for the peaks of FeSi and Fe_3P was not clearly visible; the width is fairly narrow already when the intensity becomes strong enough to identify the width.

The result at 450°C is shown in Fig. 2. Several sharp peaks are seen already after 2 min. However, these peaks are different from those observed in the experiment at 395 C. Although we tried to identify these peaks, the structure of this crystal could not been decided. At 10 min, the peaks of FeSi appear and those of Fe_3P become clear. As is clearly seen in the peaks around 1100 channels of the data between 10 and 30 min, the peak of first crystalline state becomes weak, while that of FeSi becomes strong.

In order to discuss the kinetics quantitatively, the time-dependent fraction of the crystalline state x(t) was

calculated by comparing the peak intensity at each time with that of the final equilibrium state. The result of the FeSi peak at about 1150 channel is shown in Fig. 3. The fraction x(t) can be analyzed by the Kolmogorov-Johnson-Mehl-Avrami equation

$$x(t) = 1 - \exp[-(t/\tau)^n], \qquad (1)$$

where τ is a temperature dependent constant and considered to be a characteristic time in crystallization, and n is related to the mechanism of the nucleation-growth process. The exponent n is obtained to be about 1.5. If the growth of this phase is caused by the isotropic diffusion similar in the case of $Fe_{78}B_{13}Si_9$, the nucleation rate is nearly 0. Nucleation in this alloy may be considerably fast, and may almost finish at the time of the sample preparation.

The characteristic time τ can be analyzed by the Arrhenius law,

$$1/\tau = 1/\tau_0 \exp(-E_a/k_BT), \qquad (2)$$

where τ_0 is a time constant, and E_a is an activation energy. According to this equation, the activation energy for the crystalline FeSi is obtained to be 3.4 ± 0.2 eV.

We would like to thank Professor Y. Hamaguchi for providing us the sample.

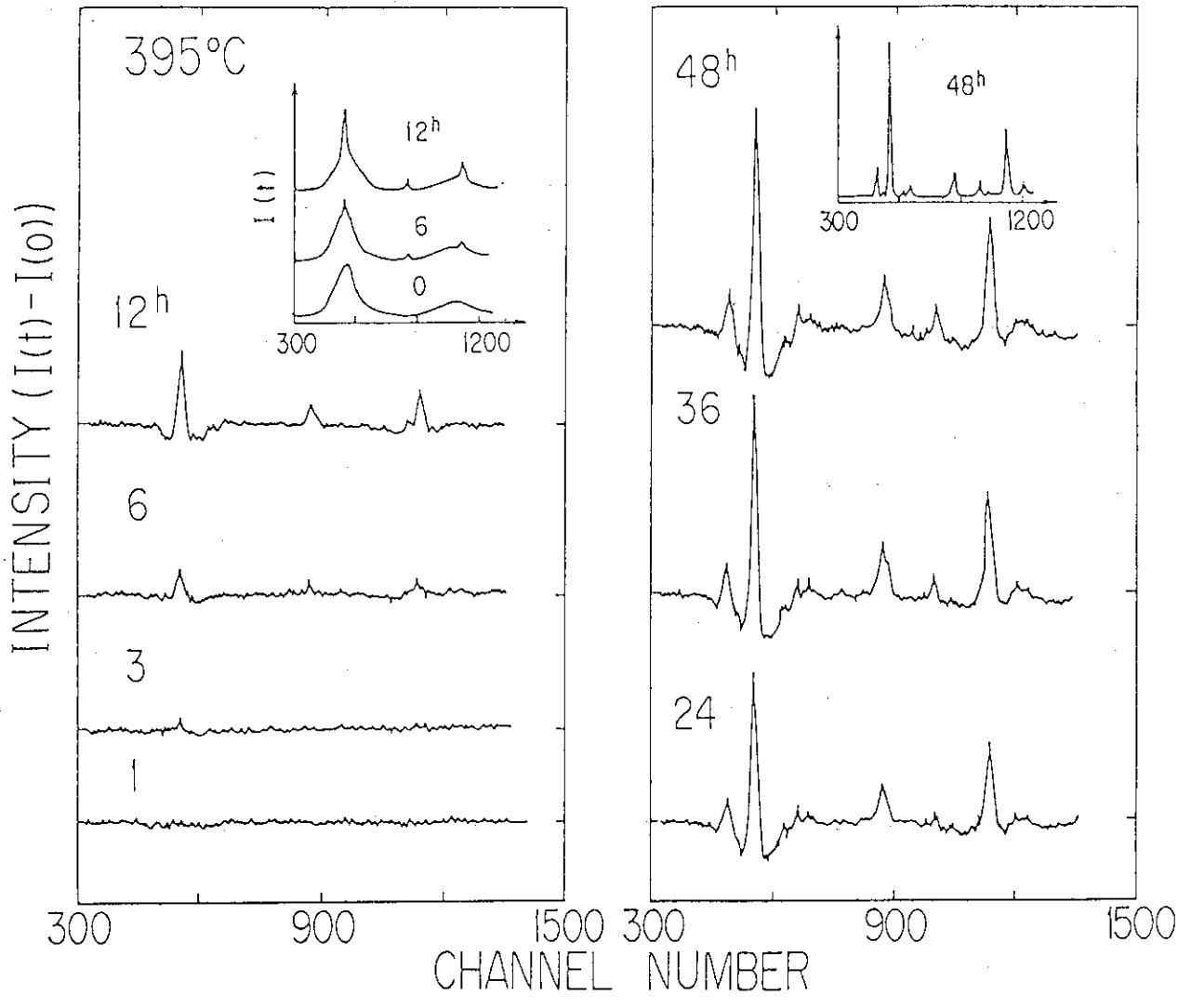

Fig. 1 Time evolution of the diffraction pattern annealed at 395°C. In order to clarify small changes in the diffraction pattern, the difference between the diffraction patterns at various time and that of the amorphous state is plotted. The insert indicates the measured pattern, which shows a superposition of the amorphous and crystalline state.

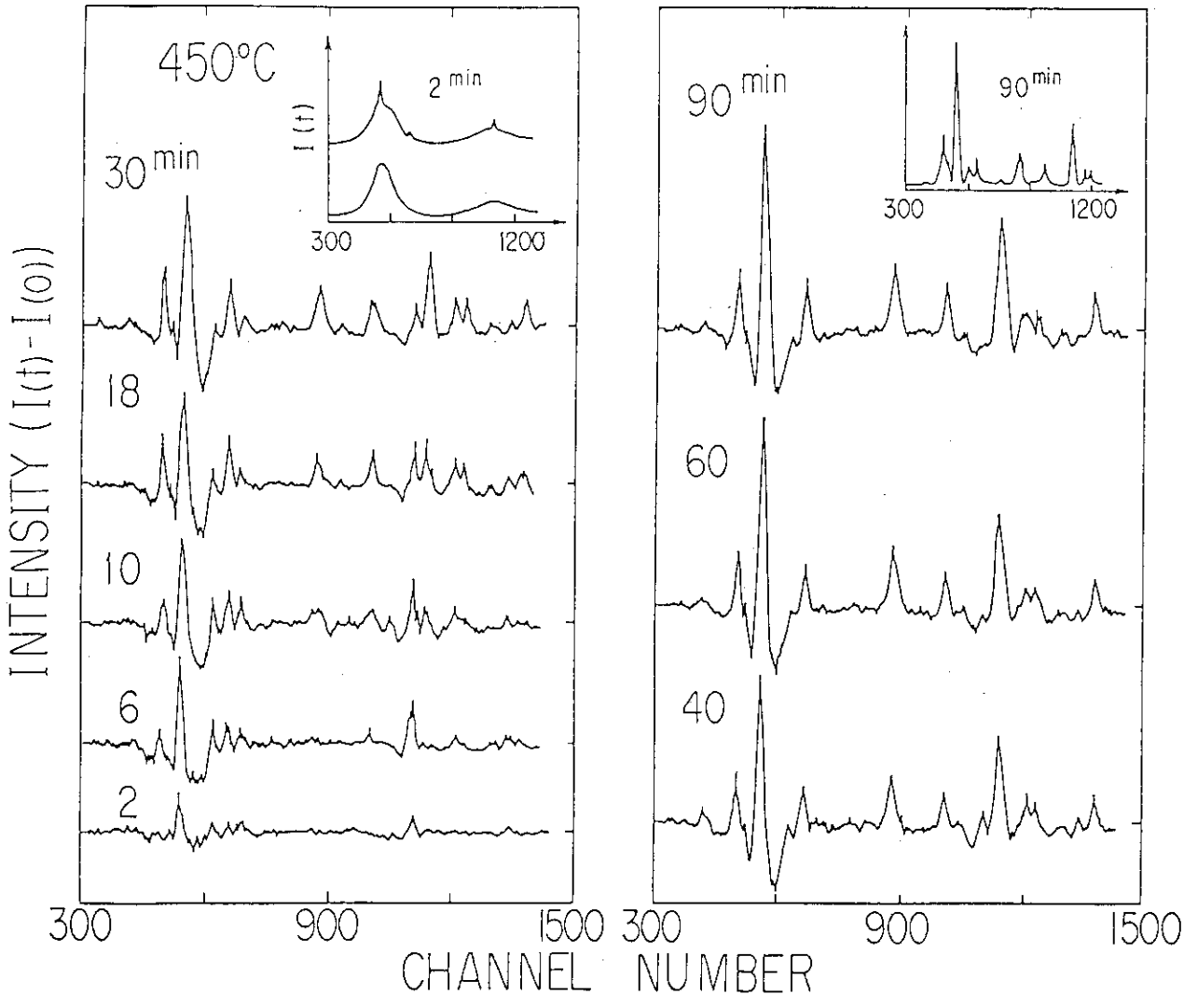

Fig. 2 Time evolution of the diffraction pattern annealed at 450°C.

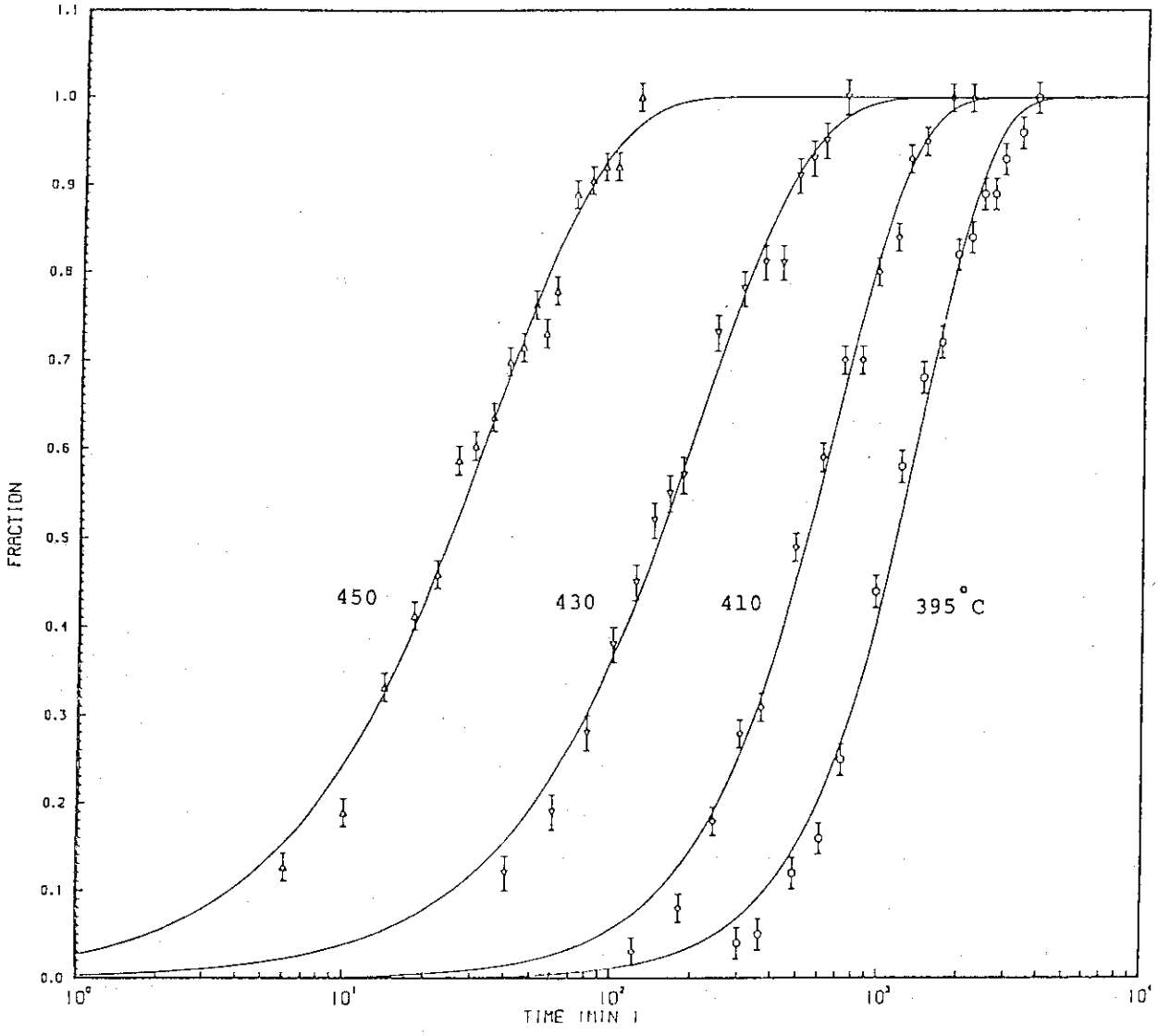

Fig. 3 Time evolution of the fraction of the crystalline FeSi.

7. Phase Stability of Metastable Tetragonal Zirconia Powder
I. Isothermal Transformation

H.Ohno, Y.Morii, H.Murakami, T.Nagasaki, H.Katsuta, M.Iizumi, H.R.Child and R.M.Nicklow

1. Introduction

Pure zirconia(ZrO_2) has three polymorphic phases. The high-temperature cubic phase with the fluorite structure is stable from the melting point 2680°C to 2370°C. Between 2370°C and 1170°C, a tetragonal disatorted fluorite structure is stable. Below 1170°C a further distortion to monoclinic symmetry occurs.

Cubic zirconia stabilized with CaO, Y_2O_3 or Yb_2O_3 additives has been proposed to the special applications in nuclear reactor systems. Ohno et al. have proposed a solid oxide electrolysis cell, which make use of the oxygen ionic conductivity of cubic stabilized zirconia for the decomposition of tritiated water in the deuterium-tritium(D-T) fusion reactor system[1-3]. This cell has almost no tritium inventory and little fear of radiation damage from tritium, produces no solid waste, and decomposes water vapor in gas system continuously,

On the other hand, yittria-containing tetragonal ZrO_2 poly-crystals (Y-TZP) have currently received special attention primarily of its high strength and high resistance in fracture. Y-TZP has also enough oxygen ionic conductivities and is able to be applied as solid electrolyte for the decomposition of the tritiated water[4].

It is well known, however, that the strength and fracture toughness of Y-TZP are greatly decreased by low temperature aging(200 to 300°C)[5]. This strength degradation results from transformation from the tetragonal phase to monoclinic phase. Many experimental results of this transformation from tetragoanal to monoclinic phase indicate the martensitic transformation accompanied by lattice invariant shear deformation, which is

enhanced by applied stress. A few results, however,shosws the oxygen diffusion transformation.

A few papers appears in which kinetics and mechanism of metastable tetragonal to stable monoclinic phase transformation in pure ZrO_2 are observed by x-ray diffraction analysis [6] and DTA /TGA analysis [7].

Whitney has measured the isothermal transition curves of metastable ZrO_2 prepared via the thermal decomposition of zirconyl chloride tetrahydrates at $\sim$ 500°C . The observed temperatures were in the range 522-650°C and the conversion curves in all cases exhibited no indication of an induction period. The results have also indicated that the transition rate was particularly rapid at above 580°C and the kinetic data did not comply with either the first- or second-order rate equation but could be fitted reasonably well by Avrami equation (Fig. 1). On the other hand, Osendi et al.[7] has analyzed the phase stability of metastable tetragonal ZrO_2 gel and ZrO_2 obtained by thermal decomposition of zirconyl accetate by DTA/TGA methods. The results were much different with those of Whitney[6].

In this work, the time-dependency of the isothermal transition of pure metastable tetragonal ZrO_2 with fine crystallite size less than 150A was investigated by means of wide-angle neutron diffraction and x-ray diffraction techniques in the range 650°-950°C.

2. Experimentals

Pure metastable tetragonal zirconia(ZrO_2) was prepared by the thermal decomposition of zirconyl chloride octahydrate $ZrOCl_2 \cdot 8H_2O$ at 450°C in oxygen gas flow for about half a day.

The neutron diffraction experiments were performed by wide-angle neutron diffractometer(WAND) with the wave length of 1.5367A. A few grams(1-3g) samples of metastable tetragonal zirconia were dropped into 10mm OD fused silica tube situated in a high temperature furnace with circular infrared-lamps for rapid

heating and high pressure gas-blows for rapid cooling. The heating rate of the sample from room temperature to 450°C was 100°C/min. The sample was kept at 450°C for 5 minutes and the temperature was increased rapidly with heating rate of 400°C/min to the observed temperatures. Temperatures were measured with two alumero-cromel couples attached to the bottom and center of the sample. Recorded temperatures were accurate to ±0.1°C for long term experiment up to 10^4 minutes. All the measurements were done in air.

X-ray diffraction analysis was performed by θ-θ diffractometer with high temperature furnace up to 1500°C. CuKα(λ=1.5418A) was used for all the measurements. The powder sample(0.1-0.2g) was kept on the main heater of platinum+40% rhodium with additive small front heater which surrounds the sample. The temperatures were measured with platinum-platinum+13% rhodium couple and was controlled within ±2°C. The heating and cooling rates were limited the maximum value to 80°C/min according to the capacity of the heater.

The relative content of tetragonal ZrO_2 has been determined by considering the intensity relationship;

$$f_T = I_T(111)/[I_T(111)+I_M(111)+I_M(11\text{-}1)] , \qquad (1)$$

where $I_T(111)$, $I_M(111)$ and $I_M(11\text{-}1)$ are the measured intensities of one tetragonal and two monoclinic peaks.

The crystallite size was calculated by using the $(111)_M$ and $(111)_T$ x-ray diffraction peaks from the Scherrer formula

$$D = 0.9\,\lambda\,(\beta\cos\theta)^{-1} , \qquad (2)$$

where D is the crystallite size, λ is the radiation wavelength, β is the corrected half-width, and θ is the diffraction peak angle

3. Results and discussion

The typical crystallite size of the starting materials used

for neutron and x-ray diffraction analysis calculated by Sheller method are summarized in Table 1. The processes of the sample preparation are also listed in Table 1.

The typical data of the change of diffraction patterns of metastable tetragonal ZrO_2 to monoclinic ZrO_2 with time measured by the time-slicing function of the wide-angle neutron diffractometer at 825°C are shown in Fig.2. The detail analysis of deconvolution of three peaks $(111)_M$, $(11\text{-}1)_M$ and $(111)_T$ at 825°C are shown in Fig.3 as typical example. The total intensities $I_T(111)$, $I_M(111)$ and $I_M(11\text{-}1)$ in equation (1) are obtained with the observed line width and peak height calculated by least square method. The tetragonal phase decreased gradually as increasing the annealing time and has almost diminished after 765 minutes. The measuring time in this case at 825°C was 1 minute. The counting time was changed with the observed temperatures and 5-10 minutes were applied at low temperature region.

The volume fraction f(t) transformed at time t is known to be expressed generally by Avrami equation.

$$f(t) = 1 - \exp[-(t/\tau_\theta)^n], \qquad (3)$$

where the relaxation time τ_θ depends both on the nucleation rate and the growth speed. The exponent n=4 was originally proposed by Avrami for the case where the nuclei are formed homogeneously and the nucleation rate is constant in time and further the growth takes place isotopically with a constant velocity.

The time dependence of the transformed fraction was fitted to equation (3) with the relaxation time and kinetic exponent as fitting parameters. Typical data with linear scale of time are shown in Fig.4(750°C), Fig.5(875°C) and Fig.6(950°C). Fraction in these figures is the volume fraction of monoclinic phase. Fig.7 shows the summary of the time dependence of conversion of metastable tetragonal ZrO_2 to monoclinic ZrO_2 at different temperatures from 650°C to 950°C by neutron diffraction experiments. The calculated parameters of Avrami equation by

least square method are listed in Table 2.

According to the results shown in Fig.7, the rate of transformation from metastable tetragonal ZrO_2 to monoclinic ZrO_2 at 700°C is nearly equal to that at 650°C. The results has important information to the growth of crystallite size which will be discussed later.

The Avrami type equation satisfies the scaling with respect to time, if the time is scaled by the relaxation time τ ($=t/\tau_\theta$). The kinetics follows the universal equation

$$f(\tau) = 1 - \exp(-\tau^n) \quad , \qquad (4)$$

irrespective of the final temperature. This means that in approaching to the equilibrium from the metastable state the system follows the same mechanism at any temperature. Fig.8 shows the scaling behavior of the conversion with respects to the time measured for the tetragonal to monoclinic phase transition in metastable pure ZrO_2. All the data are well fitted to the single line with n=0.87 in equation (4).

Fig.9 shows the Arrhenius plots of τ_θ in equation (3). τ_θ has the activation energy E=188KJ/mol, which is nearly equal to the activation energy E=167KJ/mol of self-diffusion of oxygen ion in tetragonal zirconia[8]. The results indicates apparently that the diffusion of oxygen in ZrO_2 will have some important effects on the phase transformation from tetragonal to monoclinic phase.

Another analysis with the same data were tried. Fig.10 shows the conversion of tetragonal to monoclinic phase by neutron diffraction as a function of temperatures at different time. As seen from the figure, the conversion is strongly dependent upon temperature and time. For short time region up to 10^2 minutes, there is no typical temperatures at which the rate of phase transformation increases abruptly. On the other hand, the rates of phase transformation for longer times the a few hundreds minutes have strong dependence on temperatures, particularly in the range 700-800°C.

The tailing-off of the curves to the left in Fig.10 is interesting. This shows the rate of transformation of metastable tetragonal ZrO_2 below 750°C is considerably slow. The slow rate of transformation of metastable tetragonal to monoclinic form in ZrO_2 over a period of months at room temperature has been observed by Weber et al.[9], who prepared metastable ZrO_2 from zirconyl chloride at 500°C.

Fig.11 shows a series of Arrhenius curves obtained by plotting values of log t_n against 1/T, where n has the values 0.2, 0.4, 0.6 0.8 and 1.0, indicating 20,40,60,80 and 100% conversion from tetragonal to monoclinic ZrO_2, respectively. t_n is the time necessary to achieve a certain fraction of transformation. From Fig.11 it is apparent that the activation energy for the transformation of tetragonal to monoclinic ZrO_2 is nearly constant,E= 176.4KJ/mol, for all rates of transformation. This activation energy in Fig.11 is nearly equal to that analyzed from τ_θ shown in Fig.9.

The results in this work are much different from those reported by Whitney [6]. His results show the activation enegy increases considerably with increasing temperature. For example ,the curve for n=0.4 has the activation energy E=75KJ/mol at low temperature portion, and E=580KJ/mol for high temperature region. The break in the curve occurs at approximately 572°C.

The same analysis on data obtained by x-ray diffrcation have been applied to the same samples used for the neutron diffraction. Figs.12 and 13 show the conversion of tetragonal to monoclinic phases in ZrO_2 as a function of time at different temperature. The solid lines are calculated one with Avrami equation by leat square method. The time dependences of the transformation obtained by x-ray diffraction analysis are essentially similar to those by neutron diffraction analysis with the exception of initial stage at time=0. As seen in Fig.12, large fraction of monoclinic phase was observed at the initial stage and the fraction increased with increasing the observed temperature from 700°C to 900°C. These phenomena have also been observed by

Whitney[6] as shown in Fig.1. Such a situation is indicative of a high nucleation rate, at least in the early stages of conversion.

The differences of the observed results between x-ray and neutron diffraction would be due to the difference of the penetration depth of the beam. Neutron diffraction could analyze the phase transformation of all the sample, but only a part of phase transformation, especially in the region near surface of the sample, could be observed by x-ray diffraction.

Comparing both x-ray and neutron diffraction data, the phase transformation in metastable tetragonal ZrO_2 is cleared to start initially on the surface of the particles in very short time and then gradually to proceed into the particles.

The calculated parameters τ_θ and n in equation (3) are also listed in Table 2 with those of neutron diffraction. Arrhenius plots of τ_θ are also shown in Fig.9. The accuracy of the least square calculation at temperatures below 750°C is not enough, because the fractions of the transformation from tetragonal to monoclinic forms are not sufficient for the experimental time 400 minutes. The activation energy τ_θ with data at temperatures above 775°C is nearly equal to that obtained by neutron diffraction.

The smaller values of τ_θ of x-ray diffraction than those by neutron diffraction could be due to the same origin mensioned above. That is to say, x-ray diffraction is limited to observe relatively small volume, such as surface area of the particle, and the apparent transformation will be compleated much faster than that of neutron diffraction.

According to the Avrami model, n will have a value of from 3 to 1 for a process in which nucleation takes place only at the beginning, followed by three-dimensional(n=3), two-dimensional (n=2) or one-dimensional(n=1) growth. For the system having the constant rate of nucleation, n will have a value 4.

The values of n obtained by neutron diffraction are nearly constant(0.8-1.0) and have no temperature dependence. The

results are quite different with those by Whitney[6] with x-ray diffraction. He has reported that the values of n varied between 0.40 and 0.14 over the temperature range 522-650°C and the value of n dropped rapidly at 586°C.

On the other hand, the results of the present work on x-ray diffraction have similar behavior with those of Whitney according to the temperature dependence. But the values of n are much larger than the former one and reaches $n \simeq 0.5$ at high temperatures. According to the analysis of the kinetic law exponent in Avrami equation by Turnbull[10], n would equal 0.5 if complete edgewise impingement of thin plates occured at an early stage of their precipitation.

The summary of the results by the isothermal transformation of metastable tetragonal ZrO_2 to monoclinic ZrO_2 with x-ray and neutron diffraction indicates that two stages will exist in the mechanism of the transformation. The differences of the results between present work and Whitney's one will be due to the difference of crystallite size. The crystallite size of metasable ZrO_2 sample used in his experiments is estimated to be much larger than those used in this work.

Further analysis on the phase stability of metastable tetragonal ZrO_2 such as mechanism of the crystallite growth in air and in vacuum with different heating and cooling rates, and thermodynamical calculation with parameters of crystallite sizes and temperatures have been continued.

References

[1] S.Konishi,H.Ohno,H.Yoshida and Y.Naruse,
Nuclear Technol./Fusion, 3(1983)195.

[2] S.Konishi,H.Ohno,H.Yoshida,H.Katsuta and Y.Naruse,
Proc.5th World Hydrogen Energy Conf.,Toront,Canada,
(15-20 July,1984) 537.

[3] S.Konishi,H.Yoshida,H.Ohno,T.Nagasaki and Y.Naruse,
Proc.Inter.Symp. on Fusion Reactor Blanket and
Fuel Cycle Technology,(27-29 Oct.,1986) 109.

[4] H.Ohno,T.Nagasaki,T.Ishiyama,Y.Katano and H.Katsuta,
J.Nucl.Materials,141-143(1986) 392.

[5] N.Matsui,T.Soma and I.Oda,
pp.371-81 in Advance in Ceramics,Vol.12, Science and
Technology of Zirconia II, Edited by N.Claussen,M.Ruhle
and A>H>Heuer, American Ceramic Society,Columbus,OH.(1984)

[6] E.D.Whitney, Trans.Faraday Soc.,61(1965)1991.

[7] M.I.Osendi,J.S.Moya,C.J.Serna and J.Soria,
J.Am.Ceramic Soc.,68(1985)135.

[8] R.W.Vest and N.M.Tallan,
J.Am.Ceramic Soc.,48(1965)472.

[9] Weber and Schwartz, Der.deut.Keram.Ges.,34(1957) 391.

[10] Turnbull, Solid State Physics,Vol.3,Seitz and Turnbull(ed.)
(Academic Press, Inc.,New York,1956) 225.

Table 1 Crystallite size of tetragonal phase of starting materials used for the neutron and x-ray diffraction analysis

Method of Preparation of Tetragonal ZrO_2			% Tetragonal Phase	Crystallite Size/ A
Time/h	Decomp.Temp.	Environment		
23.0	500° C	air flow	88	132
31.5	450	O_2 gas flow	77	133
16.8	450	air flow	96	138
16.0	450	O_2 gas flow	98	127
14.3	450	O_2 gas flow	95	145
16.7	450	O_2 gas flow	99	148

Table 2 Calculated parameters τ_θ and n by neutron and x-ray diffraction analysis

	Temperature /° C	/° K	τ_θ /min.	n
Neutron Diffraction	650	923	7242	0.88
	700	973	8879	0.80
	750	1023	724.1	0.95
	800	1073	309.3	0.97
	825	1098	260.5	0.76
	850	1123	116.4	1.04
	875	1148	42.0	0.76
	950	1223	18.6	0.80
X-ray Diffraction	700	973	1039	0.67
	750	1023	2062	0.71
	775	1048	92.5	0.78
	800	1073	117.2	0.53
	825	1098	44.0	0.66
	850	1123	23.6	0.58
	875	1148	10.9	0.75
	900	1173	20.9	0.51

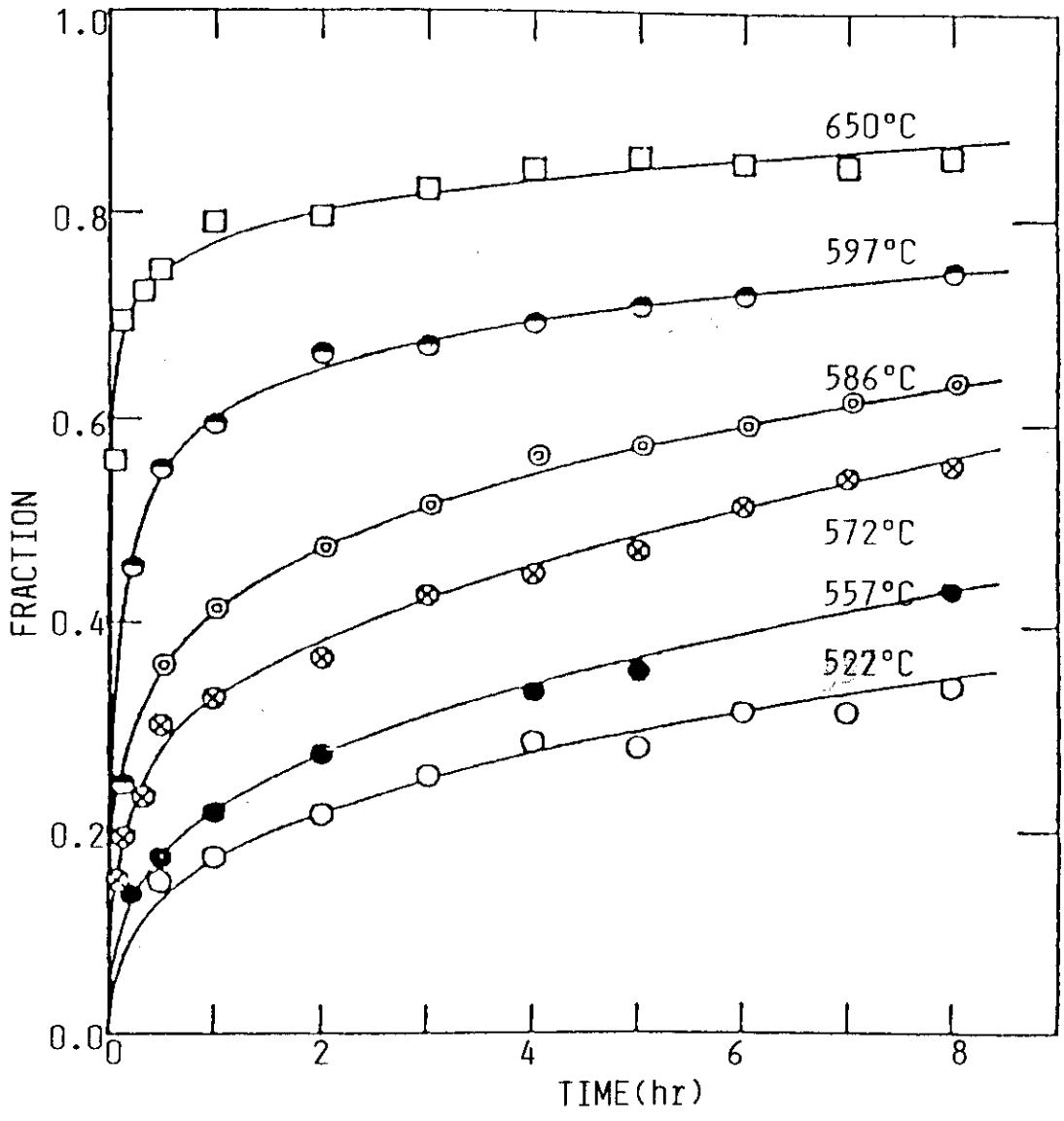

Fig.1 Conversion of tetragonal zirconia to monoclinic zirconia as a function of time and at different temperature by x-ray diffraction analysis [6].

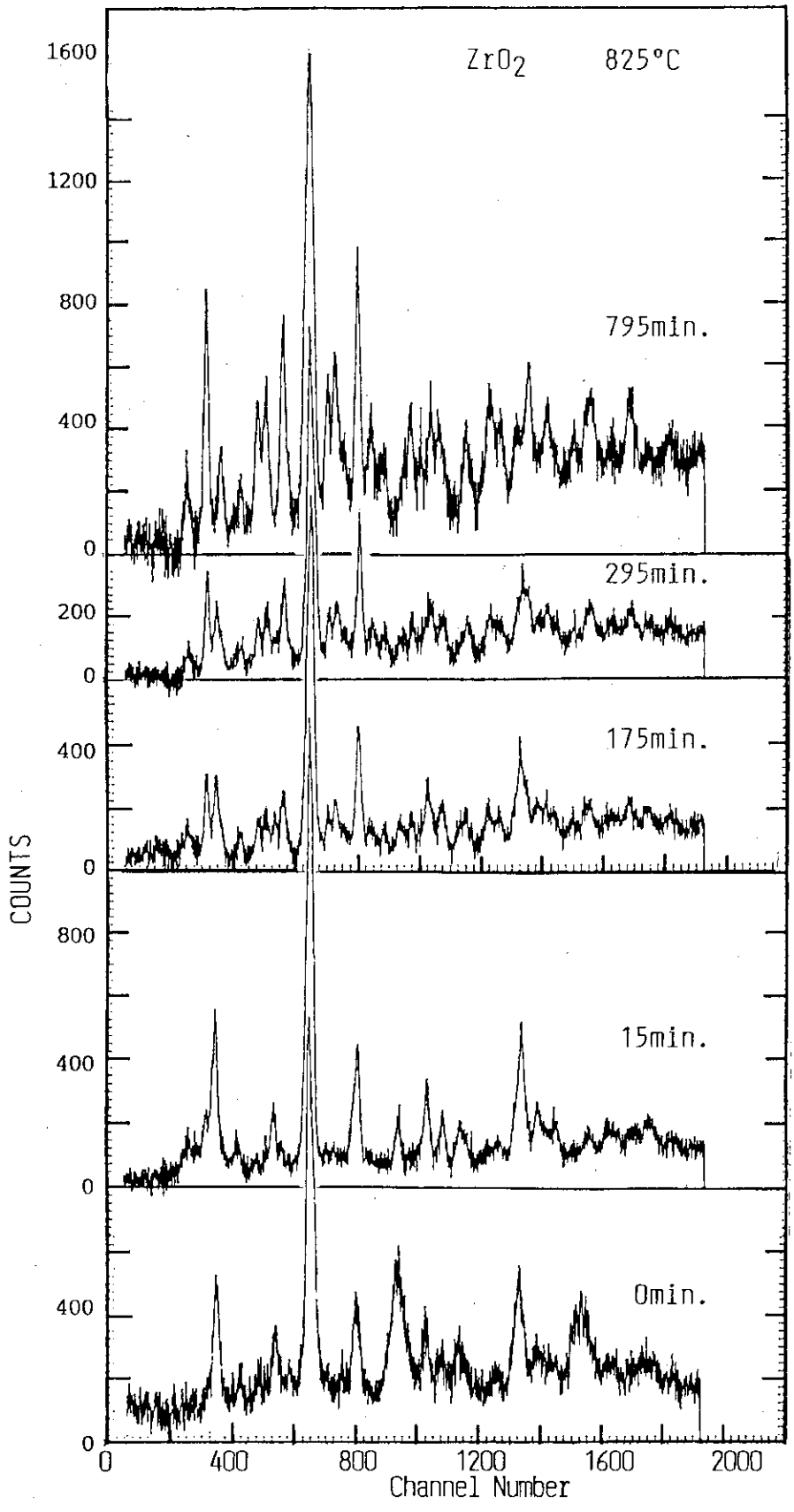

Fig.2 Change of diffraction patterns of metastable tetragonal ZrO_2 to monoclinic ZrO_2 with time measured by the time-slicing function of the wide-angle neutron diffractometer at 825°C.

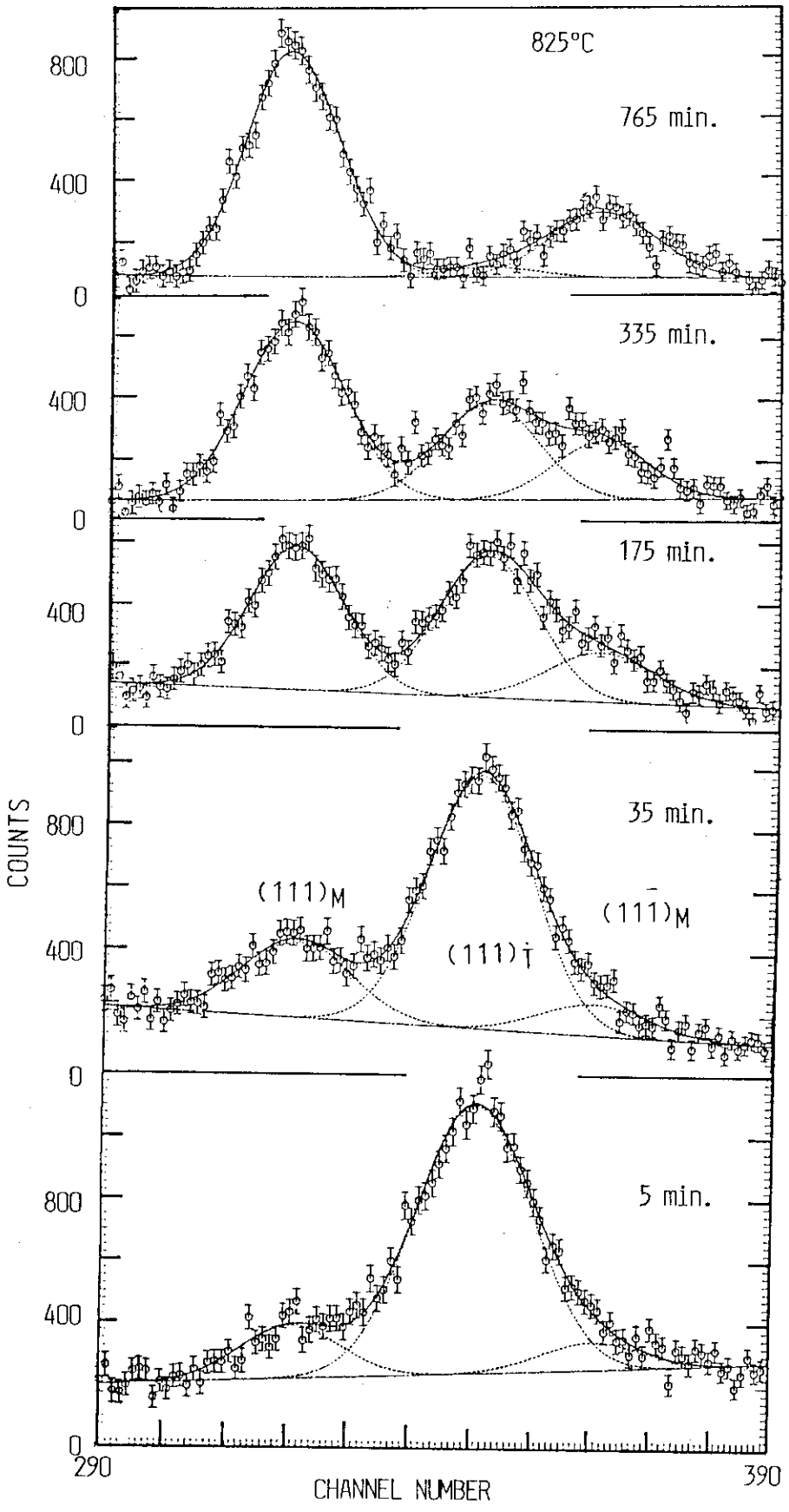

Fig.3 Deconvolution of diffraction patterns to tetragonal [$(111)_T$] and monoclinic [$(111)_M$,$(11\text{-}1)_M$] phases at different time at 825° C.

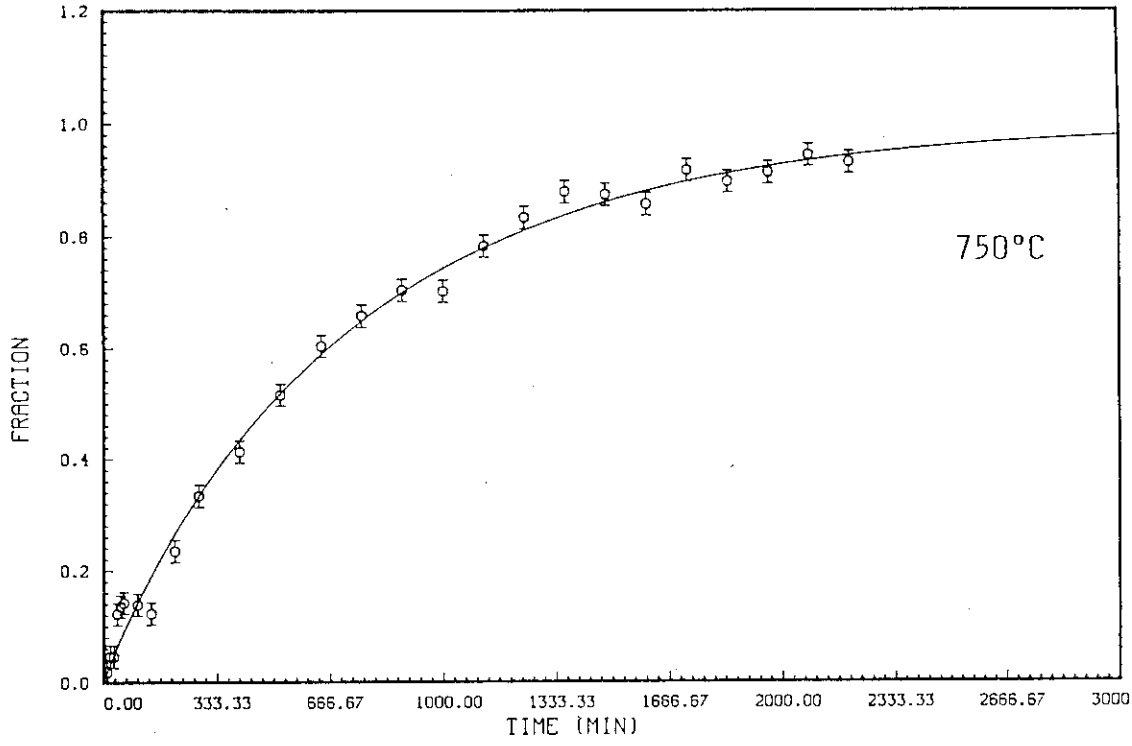

Fig.4 Conversion of tetragonal ZrO_2 to monoclinic ZrO_2 as a function of time at 750°C. Fraction is the ratio of the monoclinic phase.

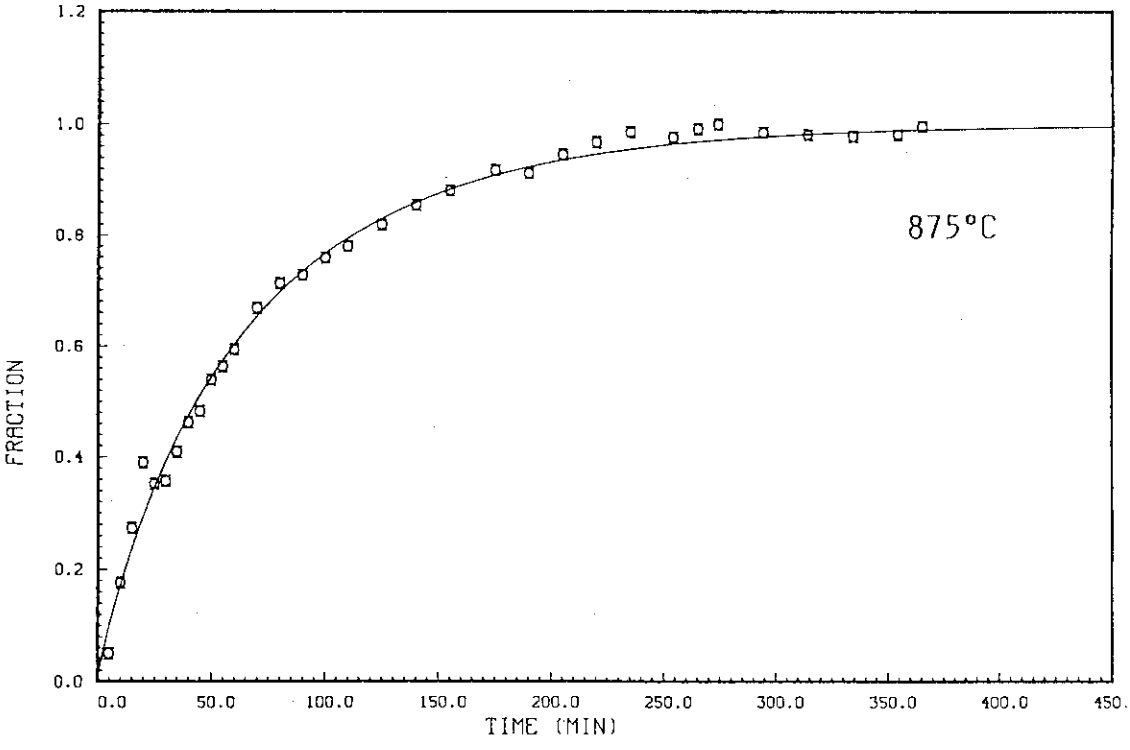

Fig.5 Conversion of tetragonal ZrO_2 to monoclinic ZrO_2 as a function of time at 875°C.

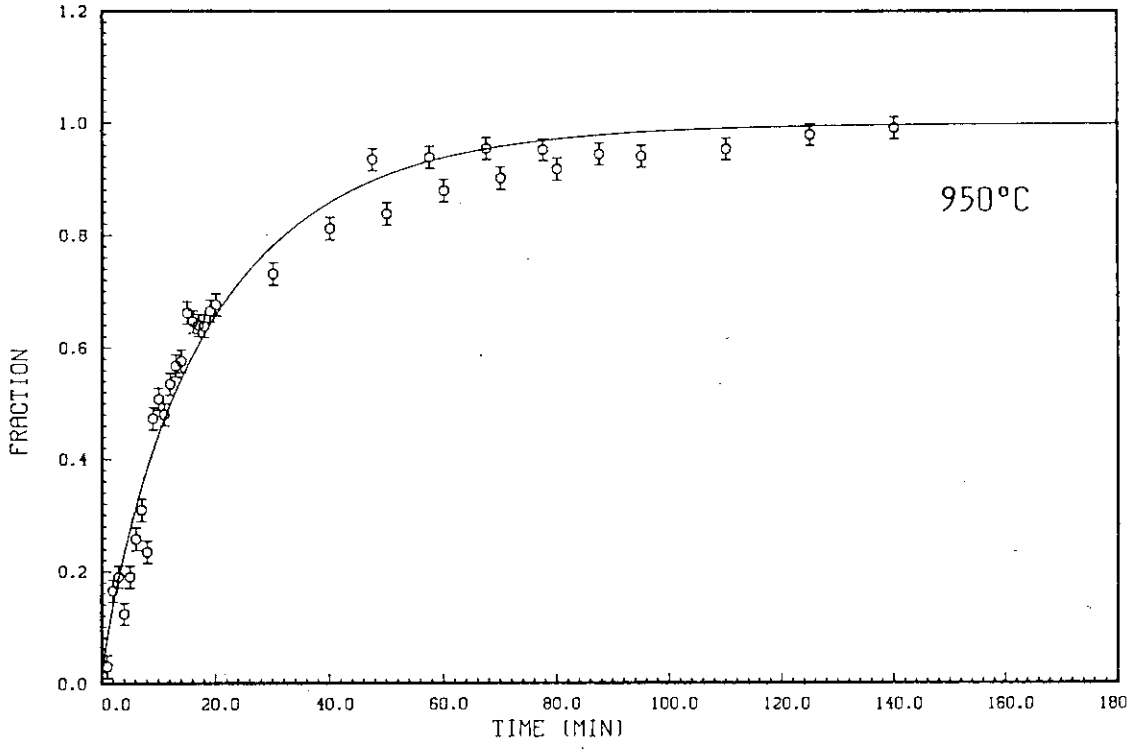

Fig.6 Conversion of tetragonal ZrO_2 to monoclinic ZrO_2 as a function of time at 950°C.

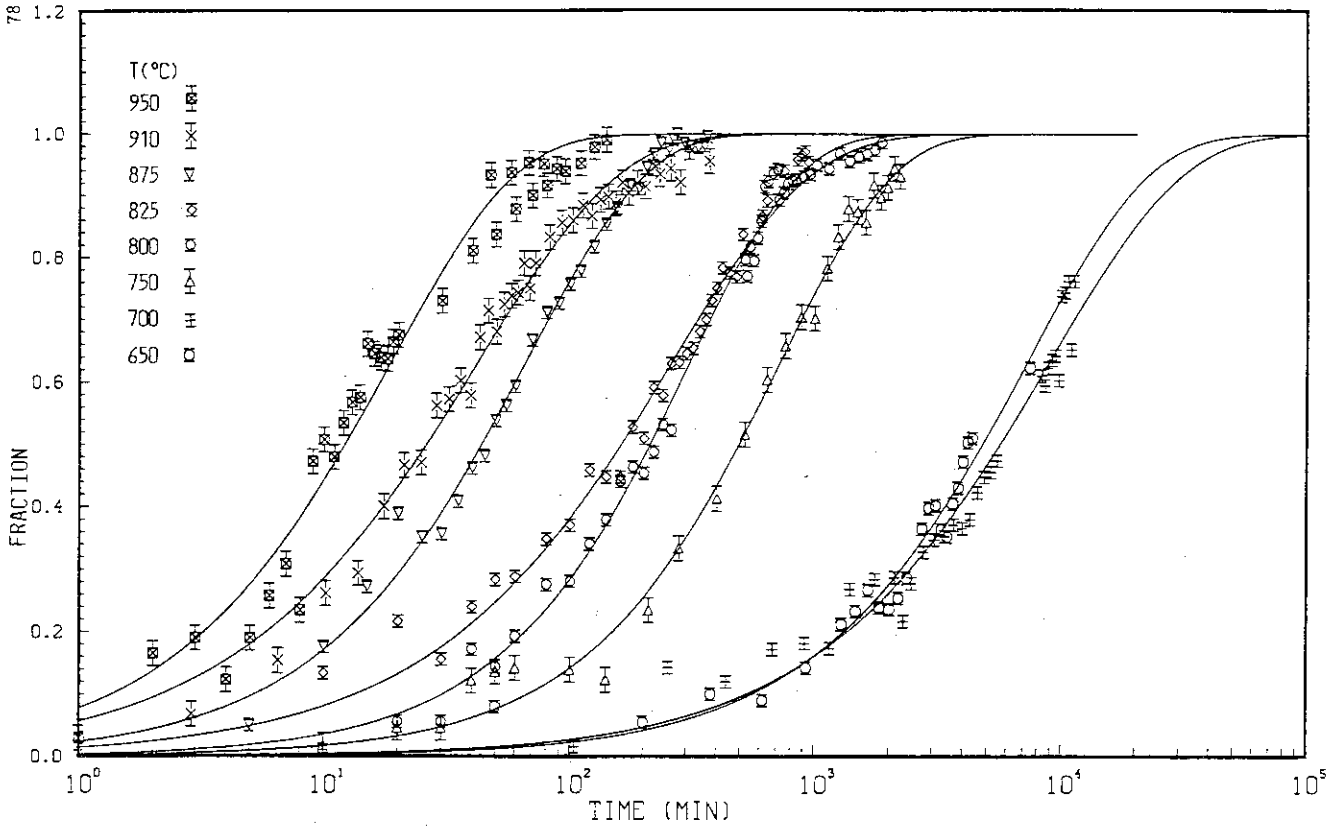

Fig.7 Time dependence of conversion of metastable tetragonal ZrO_2 to monoclinic ZrO_2 at different temperatures by neutron difraction.

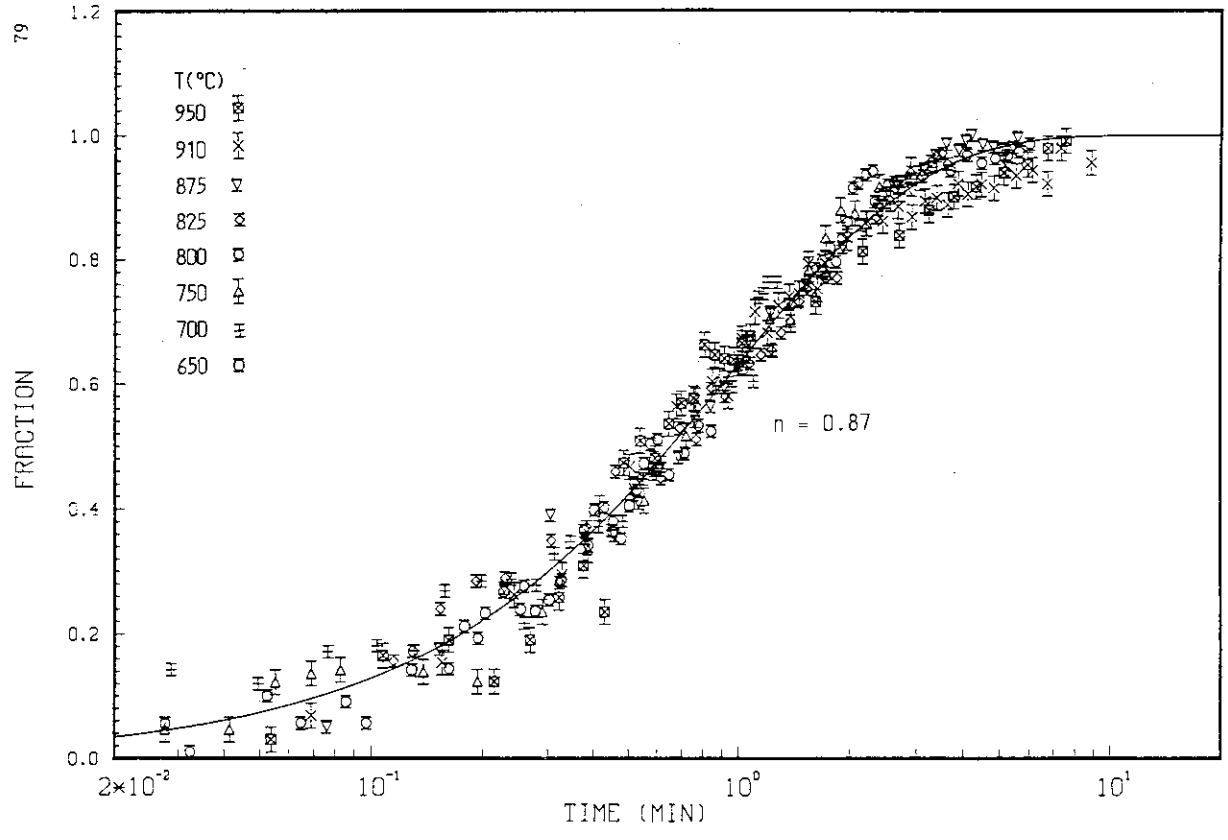

Fig.8 Scaling behaviour of the conversion with respects to time measured for the tetragonal to monoclinic phase transition in ZrO_2.

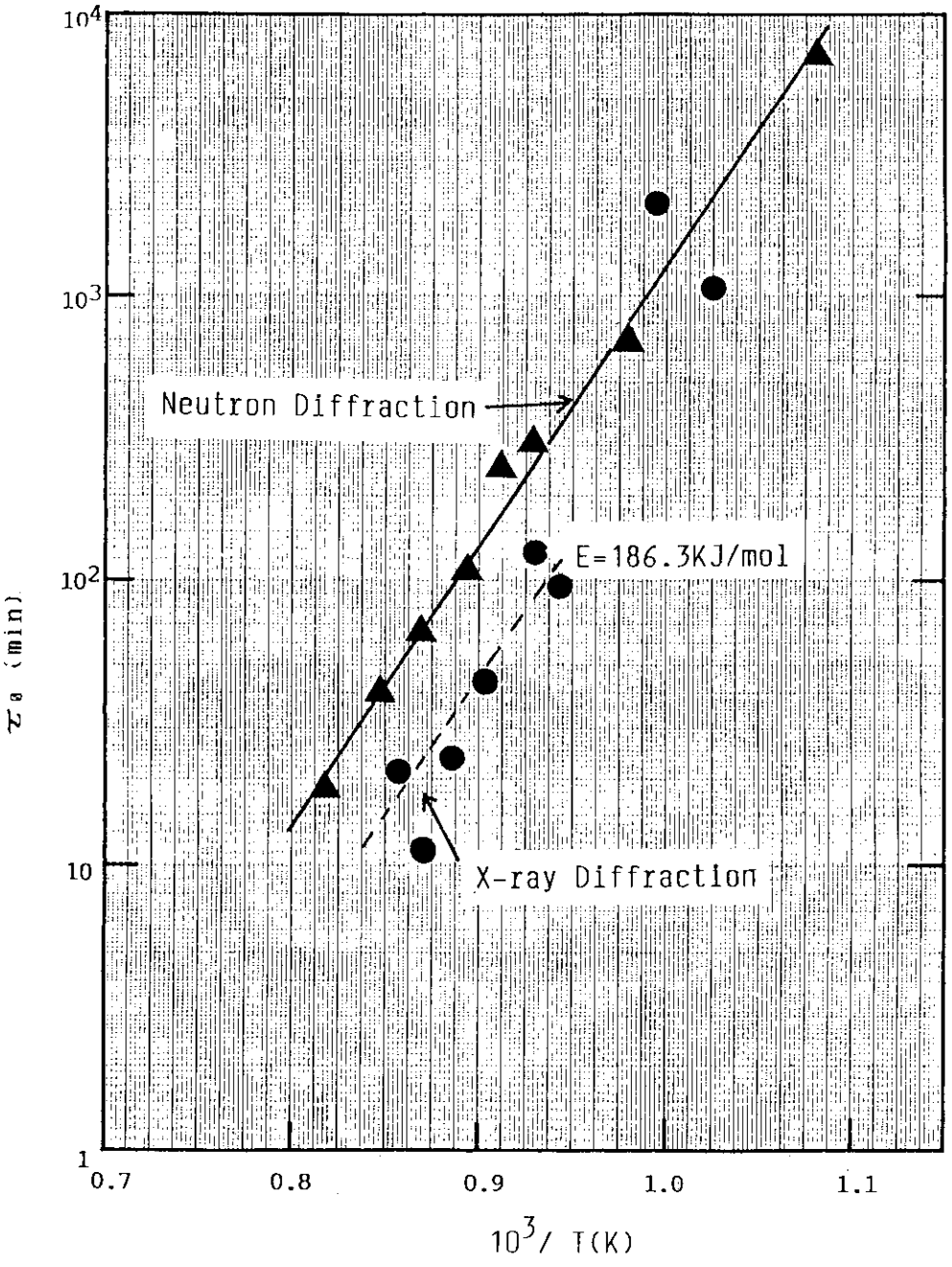

Fig.9 Arrhenius plots of τ_θ in Avrami equation.

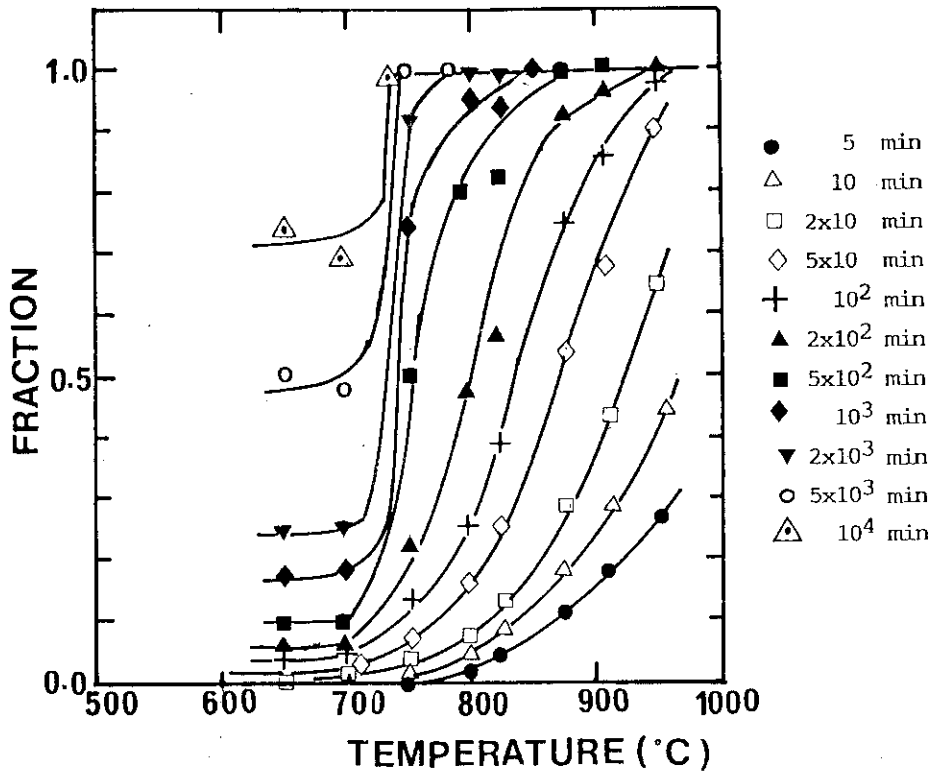

Fig.10 Conversion of tetragonal to monoclinic phase transition in ZrO_2 by neutron diffraction as a function of temperatures at different times.

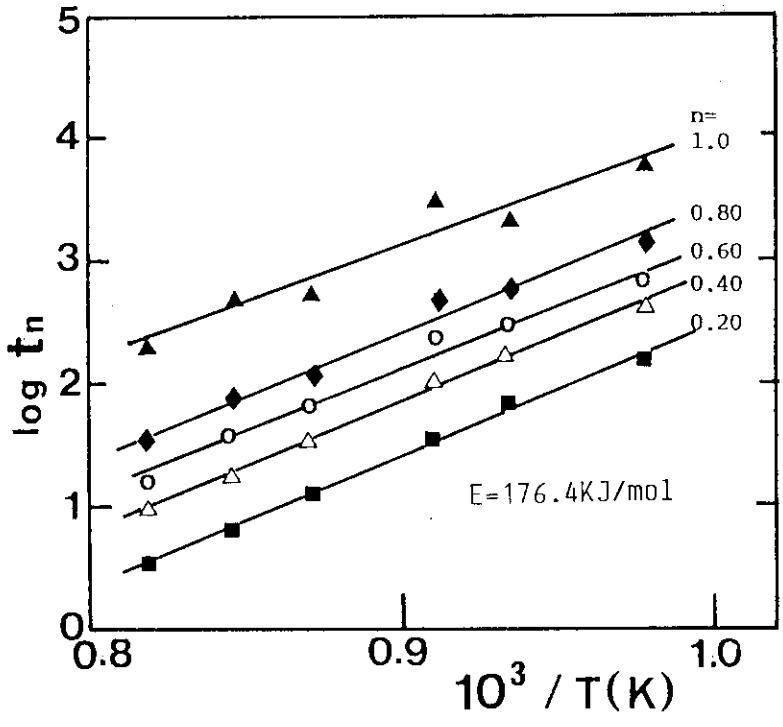

Fig.11 Arrenius plots of transformation data at different n values.

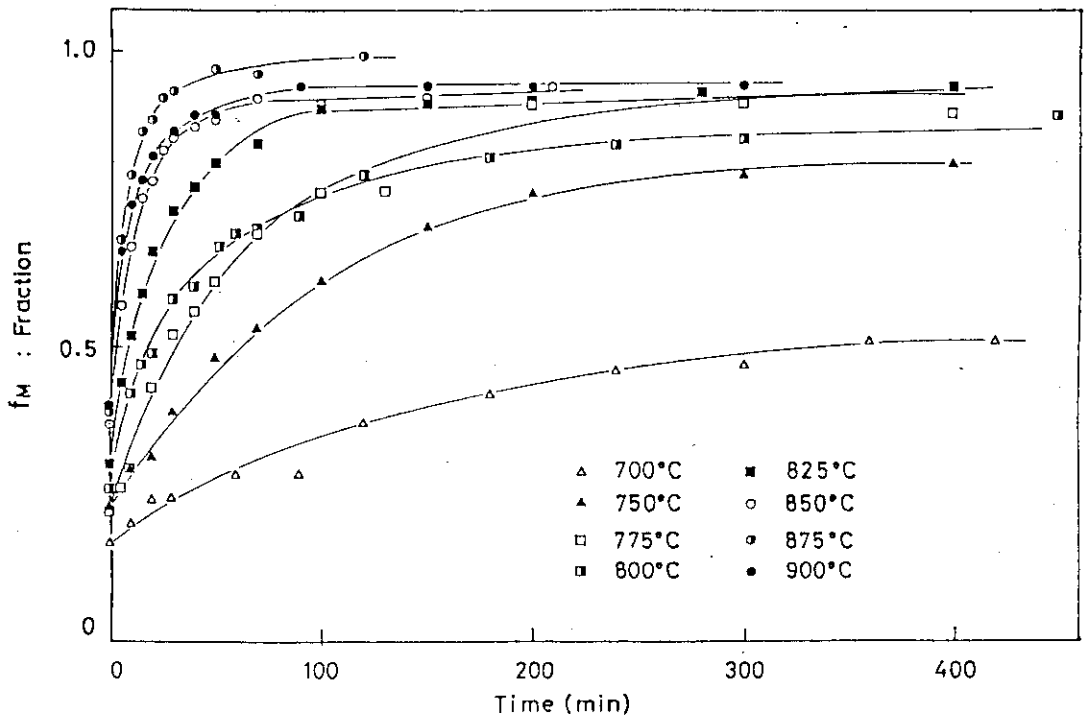

Fig.12 Conversion of tetragonal to monoclinic phase in ZrO_2 by x-ray diffraction as a function of time at different temperatures.

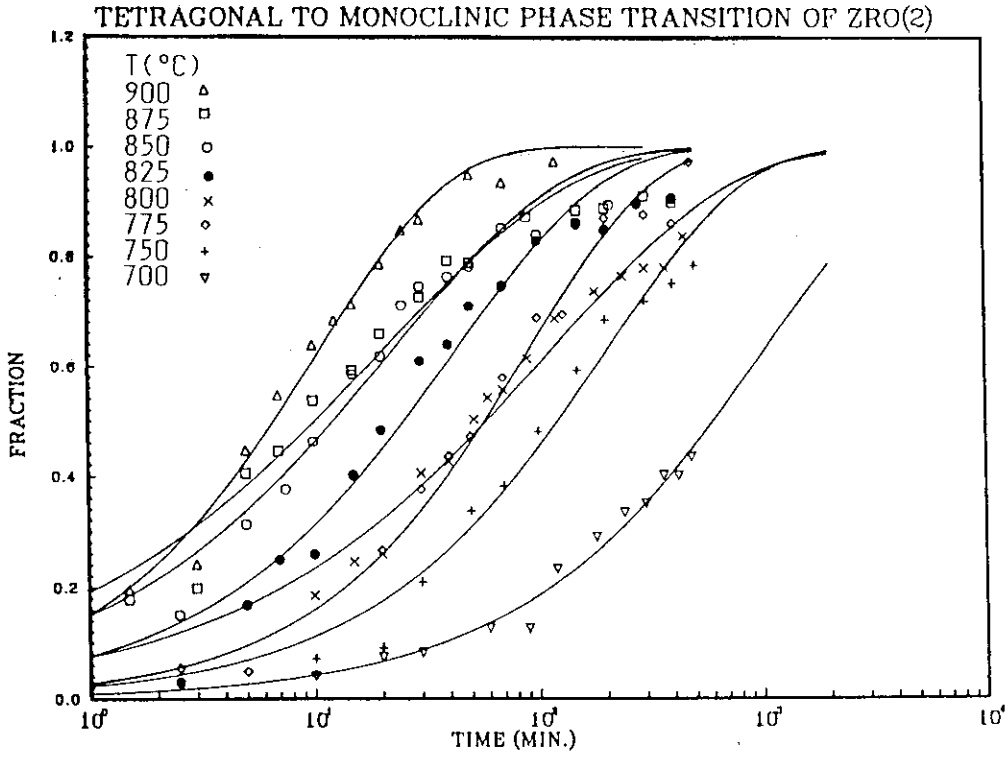

Fig.13 Time dependence of conversion of tetragonal to monoclinic phase in ZrO_2 by x-ray diffraction at different temperatures.

8. Magnetic Diffraction in Cr_2Te_3, $CsNiBr_3$ and Beta-Manganese

S.Funahashi, Y.Morii and H.R.Child

As reported in the earlier paper[1], the WAND machine has a useful capabilty of measuring two-dimensional diffraction patterns scanning reciprocal plane using single crystal samples. In the present experiment, measurements were performed on Cr_2Te_3, $CsNiBr_3$ and beta-manganese at various temperatures. In the case of beta-manganese, measurements were carried out to scan several parallel planes to collect three-dimensional information of diffuse scattering.

(1) Cr_2Te_3

Two-dimensional measurements to scan basal(ℓ=0) plane of hexagonal lattice were carried out at temperatures 295, 240, 200, 150, 100 and 13K each of which consisted of about 800 measurements. Below 240K, magnetic diffraction was observed at (1/3 1/3 0) and (2/3 2/3 0) reflecting antiferromagnetic ordering. It has been supposed from other experiments that a ferrimagnetic arrangement develops at lower temperature that magnetic moments are not necessarily equal on the crystallographically equivalent sites. In order to follow this problem quantitatively, a measurement of temperature dependence of some nuclear and magnetic intensity was carried out with a conventional triple-axis spectrometer in JAERI. Any two of the integrated intensities of (1/3 1/3 0), (2/3 2/3 0), (1 0 0), (1 1 0) and (2 0 0) were not found to be proportional to each other. This result suggests not only a different temperature dependence of the antiferromagnetic sublattice moments but also a temperature change of position parameter of the tellurium atoms.

(2)$CsNiBr_3$

This material is one of the typical examples of the hexagonal ABX_3 type magnetic materials showing a quasi one-dimensional magnetic character.[2] Two-dimensional measurements were performed at two different sample settings. One of the configuration was to measure

a*-c* plane and the other was to scan planes perpendicular to the c*-axis. In the latter case, most of the measurements were carried out to follow temperature dependence of the two-dimensional pattern of ℓ=1 plane between 9.6 and 22K. A noticeable diffuse magnetic scattering was observed to develop around the magnetic diffraction points above the ordering temperature as shown in Fig.1. On the other hand, any significant change was not observed below the Neel temperature(13.48K) down below the lower transition temperature(11.07K) observed in specific heat measurement.[2] Magnetic scattering was not observed in ℓ=0 plane reflecting the antiferromagnetic ordering along the c-axis.

(3)Beta-Manganese

Several years ago, we observed a remarkable diffuse magnetic scattering in polycrystalline beta-manganese below about 100K.[3] In order to investigate this problem more in detail, measurements were performed using two samples containing 15 and 30 percent cobalt. The samples were set on the WAND machine in the orientation to scan the $(0\bar{1}1)$ plane at zero inclination of the diffractometer table. Diffuse magnetic scattering was observed in two regions in the $(0\bar{1}1)$ reciprocal plane with both samples, one in a rectangle enclosed in 100, 111, 211 and 222 reciprocal points and another in a area between 022 and 033. As shown in Fig.2, numbers of two-dimensional scans were carried out with the both samples at different inclination angles to accumulate scans parallel to the $(0\bar{1}1)$ basal plane to cover one half of the periodicity in the reciprocal space, eventually to build three-dimensional data sets.

The authors would like to express their sincere thanks to Dr. Y.Nishihara, Prof. K.Nagata, Prof. T.Hori and Mr. N.Oyamatsu for supplying them single crystal samples of Cr_2Te_3, $CsNiBr_3$, beta-Mn(Co30%) and beta-Mn(Co15%), respectively.

REFERENCES

1)S.Funahashi, Y.Morii and H.R.Child, J.Appl.Phys.61,4114(1987).
2)R.Brener, E.Ehrenfreund, H.Shechter and J.Makovsky, J.Phys.Chem. Solids 38,1023(1977).
3)S.Funahashi and T.Kohara, J.Appl.Phys.55,2048(1984).

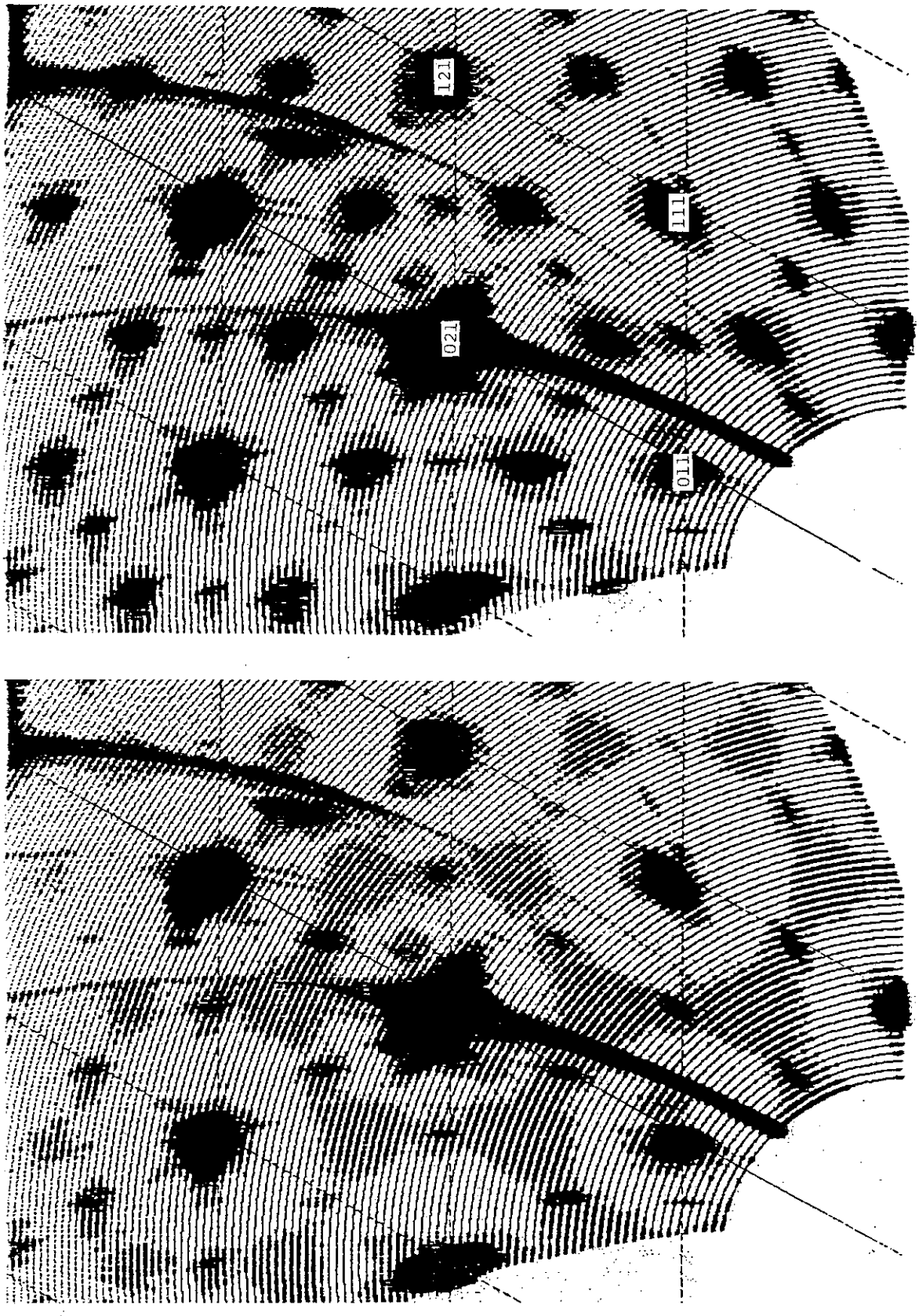

Fig.1 Two-dimensional diffraction patterns of $CsNiBr_3$ in hexagonal plane at ℓ=1. Diffuse scttering grows above T_N(13.48K) as shown in the left figure(17K). Below T_N, it concentrates into points as seen in the right figure(10K).

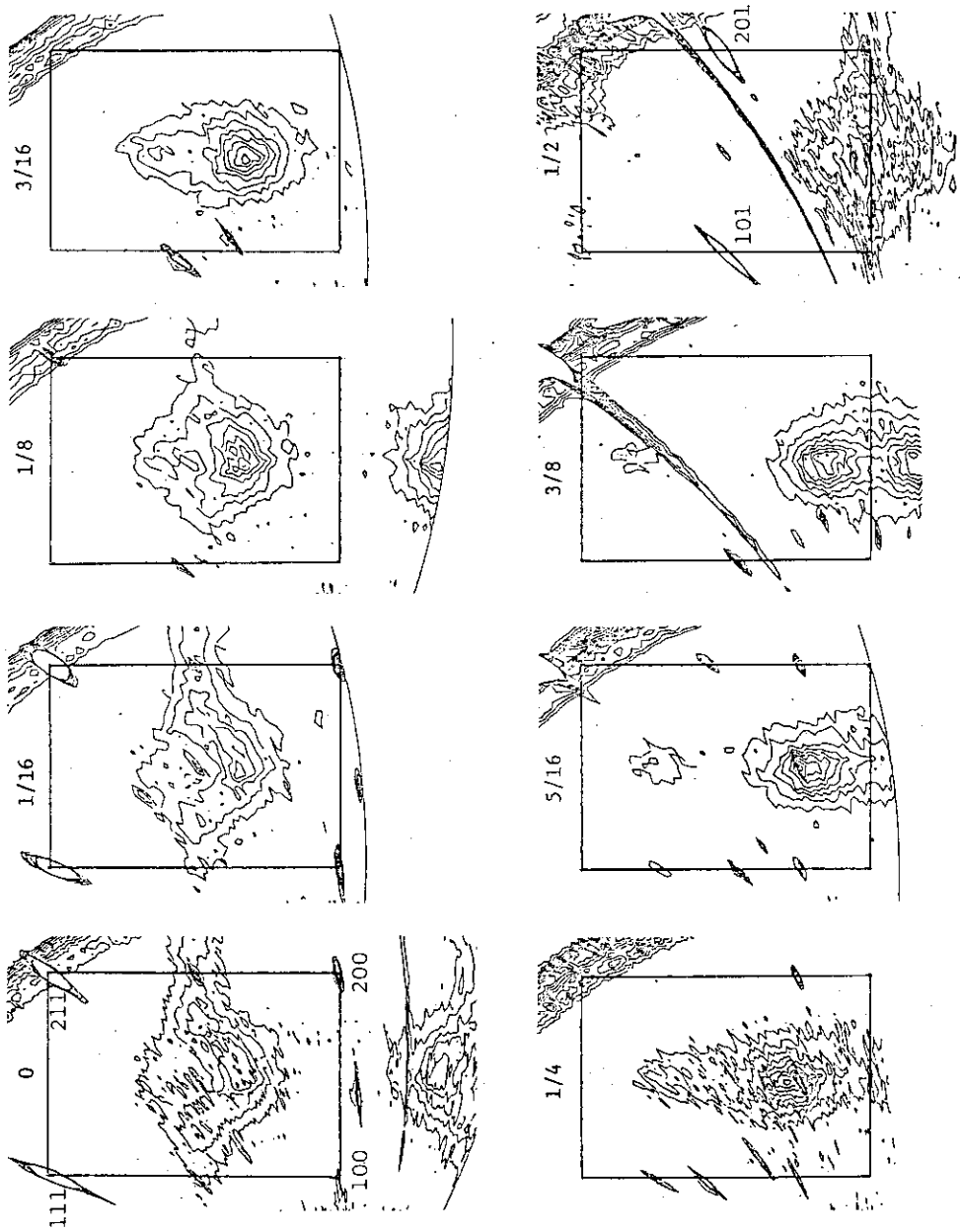

Fig.2 Contour map of diffuse magnetic scattering of beta-Mn(Co30%) at 10K. Upper leftmost figure shows the map in $(0\bar{1}1)$ plane where the rectangle shows a zone cornered with 100, 200, 211 and 111 reciprocal points. Other figures show maps of the planes parallel to the $(0\bar{1}1)$ plane. They are equally spaced successively. Numbers atop each rectangle indicate distance from the $(0\bar{1}1)$ plane in the unit of $|Q_{110}|=\sqrt{2}/a$. Lower rightmost map includes 101 and 201 reciprocal points.

9. The Kinetics of phase separation in $Mn_{0.67}Cu_{0.33}$

B. D. Gaulin and S. Spooner
Solid State Division
Oak Ridge National Laboratory
Oak Ridge, Tennessee 37831

and

Y. Morii
Physics Division
Japan Atomic Energy Research Institute
Tokai, Ibaraki, 391-11
Japan

ABSTRACT

We have examined the kinetics of phase separation in $Mn_{0.67}Cu_{0.33}$ using time resolved neutron scattering techniques. In an early time regime, the kinetics follow the Cahn-Hilliard-Cook linear theory of spinodal decomposition. There is an intermediate stage. Then, at a late time, dynamic scaling is obeyed. The time-dependence of the wave vector at maximum scattering intensity [which is inversely proportional to the average linear domain size] can be closely described over the entire range of observation by a modification of arguments recently put forward for earlier time corrections to the limitingly late time stages of phase separation.

PACS numbers: 61.50 Ks, 64.75 + g, 81.40 Cd

The kinetics of first order phase transitions[1] has been of prime interest due to its technological importance in materials science. More recently, the physics community has turned its attention to this field as part of a wider effort examining nonequilibrium phenomena, growth processes, and pattern formation. Most of this effort has been in theoretical or computer simulation studies of systems which undergo either phase separation (in which the order parameter is conserved) or order-disorder (in which the order parameter is not conserved) transitions. Only a few systems have been examined experimentally with techniques capable of measuring appropriate time dependence of spatial correlations. All of these studies have considered how a quenched system evolves towards an equilibrium state below an ordering temperature.

Understanding in this field is in transition. Two ideas are significant in the understanding of phase transition kinetics. First, spatial self-similarity and dynamic scaling are expected to describe the evolution of the structure at late times. A single length, the average linear domain size, would characterize the decomposing structure and the pattern of the structure at different times differs only in its scale. Second, the growth rate of the characteristic length at late times is believed to follow an asymptotic late time dependence. However, conflicting predictions have recently been put forward[2,3] concerning the form of this dependence.

Experimental studies on phase separating systems have examined metal alloys,[4] glasses,[5] liquids,[6] and polymer blends.[7] However, a definitive determination of the time-dependent phase separation behavior has not been made.[8] We have undertaken a time-resolved small-angle neutron scattering (SANS) study of $Mn_{0.67}Cu_{0.33}$ to examine the kinetics of phase separation

over early and late times with the purpose of establishing a comprehensive experimental description of the process.

The Cu-Mn alloy system is known to have a miscibility gap[9] in Mn-rich alloys. The variation of solid solution lattice parameters[10] in the range of phase separation compositions is small which leads to a minimal strain energy effect. Copper and Manganese possess neutron scattering lengths of opposite sign $\left(b_{(Mn)}/b_{(Cu)} = -.48\right)$. Consequently, at zero wave vector transfer, $Mn_{0.67}Cu_{0.33}$ shows approximately zero coherent scattering intensity. What is more, a disordered $Mn_{0.67}Cu_{0.33}$ sample displays approximately zero coherent neutron scattering at all wave vector transfers. Thus, this composition represents an experimental system where the coherent, intrinsic background scattering from the sample is kept to an absolute minimum. The $Mn_{0.67}Cu_{0.33}$ alloy lies near the center of the miscibility gap and at 450C the decomposition observation point is well within the classical spinodal instability regime.

The experiments were carried out on the 30 meter small-angle scattering machine of the National Center for Small-Angle Scattering Research at the Oak Ridge National Laboratory. Three sample-to-detector distances were employed in order to follow the time development of the structure function over a long time. Counting times were 30 seconds at 2.14 meters, 300 seconds at 4.73 meters, and 420 seconds at 12.75 meters. The wavelength was 4.75 A. The high purity polycrystalline sample was mounted in a specially designed rapid quench furnace.[11] The sample was solution treated at 800C for at least 45 minutes before quenching. The phase separation boundary for this alloy is 560C. Scattering data collection was started before the quench to 450C and temperature control was established in 30 seconds.

Data sets were stored at the above mentioned time intervals in the course of decomposition.

The structure function, S(Q), of the SANS experiment directly measures the equal time concentration correlation function. It displays a peaked form and the wave vector, Q_{max}, at which S(Q) is a maximum occurs such that, on average, the scattering lengths within each domain add up in phase. Therefore, Q_{max} is inversely proportional to the average domain size.

The measured intensity was corrected for detector sensitivity and background, where the background was taken to be the scattering measured at 800 C. S(Q) was thus determined for times from 65 seconds to 21109 seconds. These data were then reduced to one-dimensional data sets by circular averaging of the radially symmetric data. Each of these data sets was fit to a general form for the purpose of determining $Q_{max}(t)$. The excellent fits yielded values of $Q_{max}(t)$ which can be extracted from Fig. 1.

The linear theory of phase separation due to Cahn and Hilliard[12] was extended to include thermal fluctuations in the final quenched state by Cook.[13] The theories make a sharp distinction between unstable states (which evolve via spinodal decomposition) and metastable states (which evolve via nucleation and growth). For spinodal decomposition, the Cahn-Hilliard-Cook (CHC) structure function is

$$S(Q,t) = \tilde{S}(Q)\exp[RQ^2(Q_c^2-Q^2)t]$$

$$- \frac{\alpha T}{(Q_c^2-Q^2)} \{1-\exp[RQ^2(Q_c^2-Q^2)t]\} \quad ,$$

where T is the final state temperature, and R is related to the mobility of the system in the final state, as well as the position of this state on the phase diagram. Consequently, the function $\tilde{S}(Q)$ is amplified exponentially for wave vectors below some critical wave vector, Q_c, while the maximum amplification is at the time-independent value of $Q_c/\sqrt{2}$.

Figure 2 shows our early time data for times from 65 seconds to 597 seconds. Using an assumed form of $\tilde{S}(Q)$, our early time data could be very well represented by the CHC structure factor. The form of $\tilde{S}(Q)$ used to propagate the time evolving structure functions is shown at the bottom of Fig. 2 and has been divided by two for clarity of presentation. Our best description of these data used Q_c = .139 A^{-1}, R = 32 (A^4/sec) and αT = 2.8 in units of $\tilde{S}(Q)\cdot A^{-2}$. The solid lines through the data show the excellent description of our data by the theory for times less than 300 seconds. For greater times, the description becomes systematically worse as can be seen in upper panel of Fig. 2. It is clear that for these larger times, the peak in the measured S(Q,t) moves to lower wave vectors with time, while the peak intensity lags progressively farther behind it's predicted value. This failure of the CHC theory at later times is due to nonlinearity in the decomposition process which is not included in the theory. Recently, Carmesin and co-workers[14] have argued that features of CHC theory can be induced by the effects of finite quench rate. To examine this point we performed a quench from 800C, first to 575C where we waited for 30 seconds before quenching further to 450C. This different cooling history resulted in a relatively weak distribution of scattering characteristic of the structure at 575C in addition to the peak scattering obtained by a direct quench. Subtraction of the scattering characteristic of 575C left a scattering pattern that was essentially identical to that obtained by direct

quenching. It was thus demonstrated that quenching effects did not exert an important influence in the early scattering patterns. Thus, to the best of our knowledge, this is the first demonstration of the applicability of the CHC theory over any time regime for a system with non-long range interactions (excluding polymer blends).

Binder,[16] as well as Grant and co-workers,[17] has shown that the maximum time over which the CHC theory would apply is related to the range of the interactions in the system. Specifically, $t_{max} \sim \ln Rg$ where Rg is the range of the interactions.

A dimensionless relative range of interaction parameter Rg can be extracted using our measured t_{max} value, following the arguments set out by Grant et al.[17] We obtain $Rg \sim 3.0$ which should be compared with $Rg = 1$ for the nearest neighbor Ising model, and $Rg \sim 20$ for a typical polymer blend with a chain length of 400 monomer units. We conclude that the interaction between the atoms in $Mn_{0.67}Cu_{0.33}$ is of intermediate range, which might be expected for a metal alloy.

At late times a dynamic scaling of the time dependent structure is predicted. The expected form of the structure function is

$$S(Q,t) = (Q_{max}(t))^{-d} F(Q/Q_{max}(t)),$$

where d is the dimensionality of the system, while $F(Q/Q_{max}(t))$ is the universal scaling function. The validity of this dynamic scaling is usually checked by examining the time dependence of $S(Q_{max})$ and $Q_{max}(t)$. If $Q_{max} \alpha t^{-a}$, then $S(Q_{max}(t)) \alpha t^{da}$ if this scaling is obeyed. Although

several systems have shown this behavior, others have not and a consistent experimental picture does not exist.[15]

Fig. 3 shows our results for $(Q_{max})^3 S(Q)$, the expected form of the scaling function $F(Q/Q_{max}(t))$, at later time. Data sets of $F(Q/Q_{max}(t))$ for times from 5115 through 8429 seconds are shown in the top panel of Fig. 3. These data sets fall almost precisely on top of one another, as do later time data sets from 12582 through 21109 seconds (which are not shown in Fig. 3 as the absolute intensities at the 4.73 and 12.75 meter sample-detector distance settings are not normalized to each other). This indicates that at these late times, the dynamic scaling relation is followed exactly within the limits of the experimental error bars of the data. At earlier times, the data sets follow the scaling form to a systematically lesser and lesser extent, as can be seen in the bottom panel of Fig. 3. Hence, we can explicitly see the breakdown of the late time scaling for times less than 5000 seconds.

Of course, given that at early time CHC theory is obeyed, the late time dynamic scaling must fail at some point as CHC theory does not exhibit this scaling. We consequently divide the kinetic behavior into three regimes; an early time regime where CHC theory applies, a late time regime where dynamic scaling applies and a crossover stage connecting the early and late time regimes. These regimes are shown in Fig. 1 for $Mn_{0.67}Cu_{0.33}$. Dynamic scaling would be obscured if a significant part of the test data were in the crossover regime. We believe that this is the cause of inconsistent experimental findings on late time dynamic scaling.

The time dependence of the average linear domain size, R(t), is currently a controversial theoretical point. As $Q_{max}(t) \sim 1/R(t)$, the relevant arguments can be tested experimentally. Lifshitz and Slyozov[18] originally

argued $R(t) \sim t^{1/3}$ at late times for a system which initially evolves via nucleation and growth. Very recently Huse[2] has argued for the same result for a system which initially evolves via spinodal decomposition; however, he has also produced earlier time corrections to this behavior based on the existence of an enhanced interfacial atomic conductivity. The competing argument,[3] a zero-temperature renormalization group approach, predicts $R(t) \sim \ell nt$ and is valid at late times only. Our data for Q_{max} vs time is plotted in Fig. 1 in such a way as to test these two dependencies. A logarithmic time dependence is not observed over any convincing time range, while the power law we obtain in fitting our time data yields a power exponent slightly below $-1/3$; it is $-.37 \pm .03$. Theoretical arguments which include earlier time corrections must clearly be accounted for.

We have modified Huse's arguments in such a way as to make a relevant comparison with our data. His arguments implied the relation

$$\left(\frac{Q_{max}(t)}{Q_0}\right) = \left(\frac{t}{\tau}\right)^{-n} ,$$

holds, provided that

$$\left| \frac{1}{n} \frac{dn}{d \ln\left(\frac{t}{\tau}\right)} \ln\left(\frac{t}{\tau}\right) \right| \ll 1 ,$$

with

$$n = 1/3 - \frac{A}{\left(\frac{t}{\tau}\right)^{1/3} - A \ln\left(\frac{t}{\tau}\right)} ,$$

where we've employed an expansion of $(\frac{t}{\tau})^{(1/3-n)}$ in powers of $(^1/_3-n)$. We have fit this form of $Q_{max}(t)$ to our data with A, Q_0, and τ as adjustable parameters. The fitted expression is shown as the solid line in Fig. 1. Remarkably, *the fit is excellent over the entire time range*. As Q_{max} and t must be reduced, this description of the experiment is obtained with essentially a single adjustable parameter, A = .29. It should be noted that this form of $Q_{max}(t)$ allows for values of $\frac{d \ln Q_{max}}{d \ln (\frac{t}{\tau})}$ lesser than $-^1/_3$.

In conclusion, the kinetics of phase separation in $Mn_{0.67}Cu_{0.33}$ displays three time regimes. In the early time regime, the scattering is described by CHC theory. There is a crossover stage. In the late time regime, dynamic scaling applies. Arguments based on Huse's work permit us to describe the $Q_{max}(t)$ behavior over the entire time range of our experiment. In addition to demonstrating a consistent description of decomposition over a wide kinetic range, these findings underscore the importance of extending theoretical development from limitingly long times to earlier times.

This work has benefited from useful discussions with M. Grant and M. Hagen.

Research was carried out under U.S.-Japan Cooperative Program on Neutron Scattering, and was supported by U.S. DOE under contract DE-AC05-84OR21400 with Martin Marietta Energy Systems, Inc., and the NSF under Grant No. DMR 7724459. One of us (BDG) is the holder of a NSERC of Canada postdoctoral fellowship.

REFERENCES

1. J. D. Gunton, M. San Miguel, and P. S. Sahni in "Phase Transition and Critical Phenomena," C. Domb and J. L. Lebowitz (editors), Vol. 8, Academic Press, London, (1983).
2. D. A. Huse, Phys. Rev. B 74, 7845 (1986).
3. G. F. Mazenko, O. T. Valls, and F. C. Zhang, Phys. Rev. B 31, 4453 (1985); Phys. Rev. B 32, 5807 (1985); O. T. Valls and G. F. Mazenko (preprint).
4. For example: S. Katano and M. Iizumi, Phys. Rev. Lett. 52, 835 (1984); S. Komura, K. Osamura, H. Fujii, and T. Takeda, Phys. Rev. B (RC) 30, 2944 (1984).
5. A. F. Craievich, J. M. Sanchez, and C. E. Williams, Phys. Rev. B 34, 2762 (1986).
6. M. Takahashi, H. Horiuchi, S. Kinoshita, Y. Ohyama, and T. Nose, J. Phys. Soc. Jap. 55, 2687 (1986).
7. H. L. Snyder, P. Meakin, and S. Reich, J. Chem. Phys. 78, 3334 (1983).
8. Some of the experimental inconsistencies are discussed in: H. L. Snyder and P. Meakin, J. Chem. Phys. 79, 5588 (1983).
9. J. M. Vitek and H. Warlimont, Metal Science, 7, January (1976).
10. N. Cowlam, Metal Science, 483, October (1978).
11. S. Katano, H. Motohashi, and M. Iizumi, Rev. Sci. Intrum. 57, 1409 (1986).
12. References 4–6 investigate this point and provide both examples and counter-examples of this behavior.
13. H. E. Cook, Acta. Metall. 18, 297 (1970).
14. H. O. Carmesin, D. W. Heerman, and K. Binder (preprint).

15. J. W. Cahn and J. E. Hilliard, J. Chem. Phys. 28, 258 (1958).

16. K. Binder, Phys. Rev. A 29, 342 (1984).

17. M. Grant, M. San Miguel, J. Viñals, and J. D. Gunton, Phys. Rev. B 31, 3027 (1985).

18. I. M. Lifshitz and V. V. Slyozov, J. Phys. Chem. Solids 19, 35 (1961).

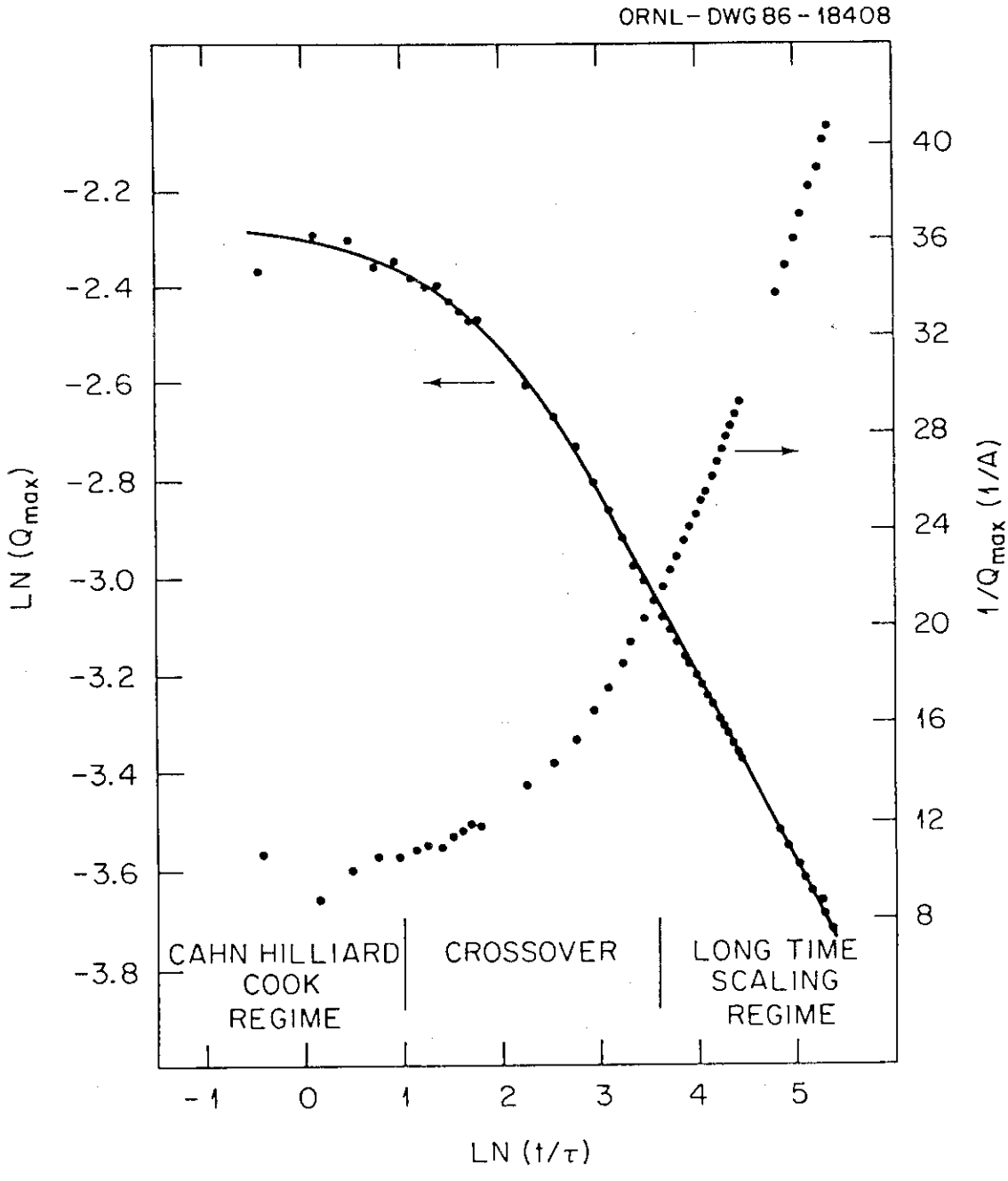

Fig.1 The measured values of Q_{max} (in inverse angstroms) are shown as a function of reduced time (τ = 100.22 sec). The kinetics can be characterized by three time regimes as described in the text. The solid line is the result of fitting a theoretical expression, based on Huse's arguments, to the data.

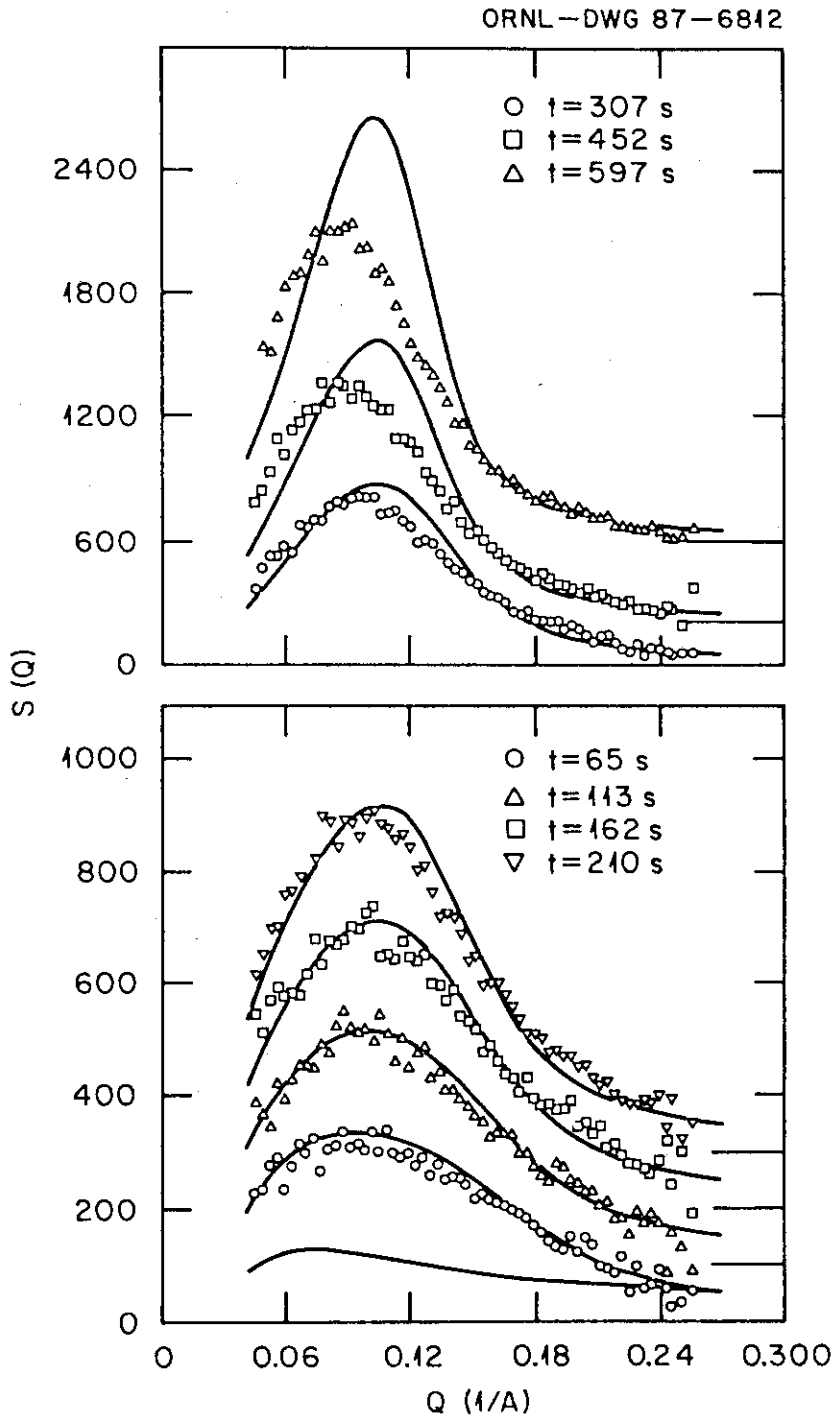

Fig.2 The S(Q,t) data sets at relatively early times are shown. The solid lines are the results of fitting CHC theory (using the $\frac{\tilde{S}(Q)}{2}$ base function shown at the bottom of the figure) to the data. Systematic discrepancies are clear for times longer than 300 seconds.
Data sets have zero S(Q) values set by the solid lines to the right of the panels for clarity of presentation.

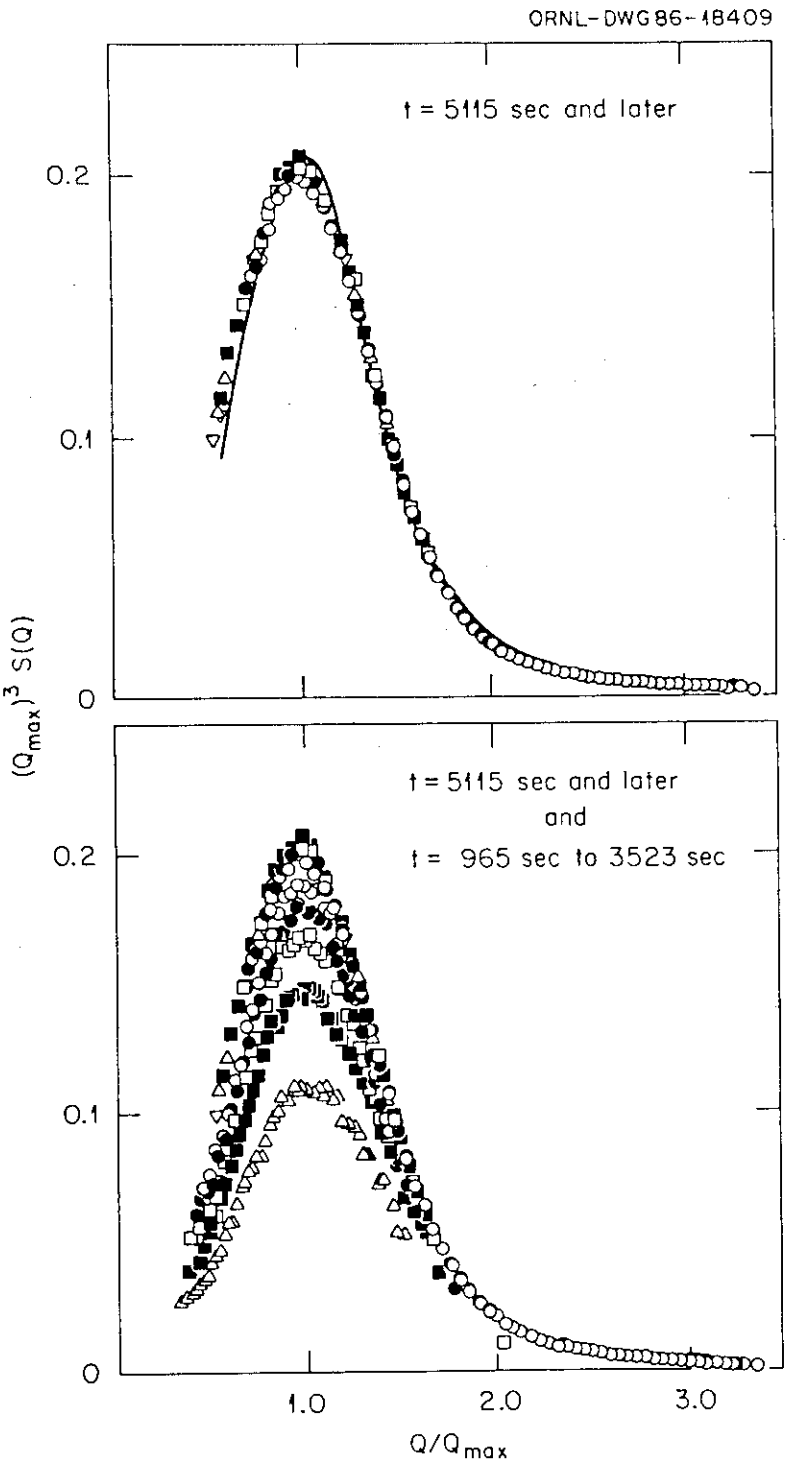

Fig.3 The scaling behavior of the data sets of $F(Q/Q_{max}) = Q_{max}^3 S(Q)$ for times exceeding 5000 seconds is shown in the top panel. The bottom panel shows the same data sets as the top panel, as well as five data sets at 965, 1602, 2239, 2886, and 3523 seconds. These earlier time data sets depart from the scaling relation to a systematically greater extent with decreasing time.

10. Kinetics of Verwey Transition of Magnetite

S. Katano, M. Iizumi, Y. Morii,
H. R. Child and R. M. Nicklow

Magnetite(Fe_3O_4) exhibits a first-order phase transition at about 120 K: the Verwey transition. This transition is caused by a charge ordering. The kinetics of this phase transition has been investigated by time resolved neutron diffraction technique.

A single crystal in the cylindrical shape of 5 mm diameter and 30 mm length was used. This sample was placed in a Displex cryostat. The appearance of new reflections due to the charge ordering shows that the transition temperature of this sample is 111 K, which is, however, considerably low compared with the value of previous reports. In order to study the kinetics, the temperature was abruptly decreased from 116 K to several temperatures across the transition temperature. The time evolution of the intensity of the reflection was measured using WAND (Wide-Angle Neutron Diffractometer).

Fig. 1 shows the diffraction pattern when the final temperature was set at 107 K. The pattern was measured every 6 sec. The peak at about 400 channel is the (4 4 1/2) reflection. (The peak around 600 channel is a fundamental reflection which does not change by the transition.) The intensity of the new reflection increases rapidly with time.

The time evolution of the intensity of this reflection is

shown in Fig. 2 for several final temperatures. This indicates that there is a delay time before the reflection appears, and that the transition proceeds with a relaxation time. Moreover, these characteristic time become longer when the final temperature approaches to the transition temperature. However, the rapid change of the temperature using a conventional cryostat is difficult; it takes more than 5 min to reach the final temperature. Hence, there may be ambiguity in the interpretation of the experimental result. Several improvements in the measurements and further studies are planned.

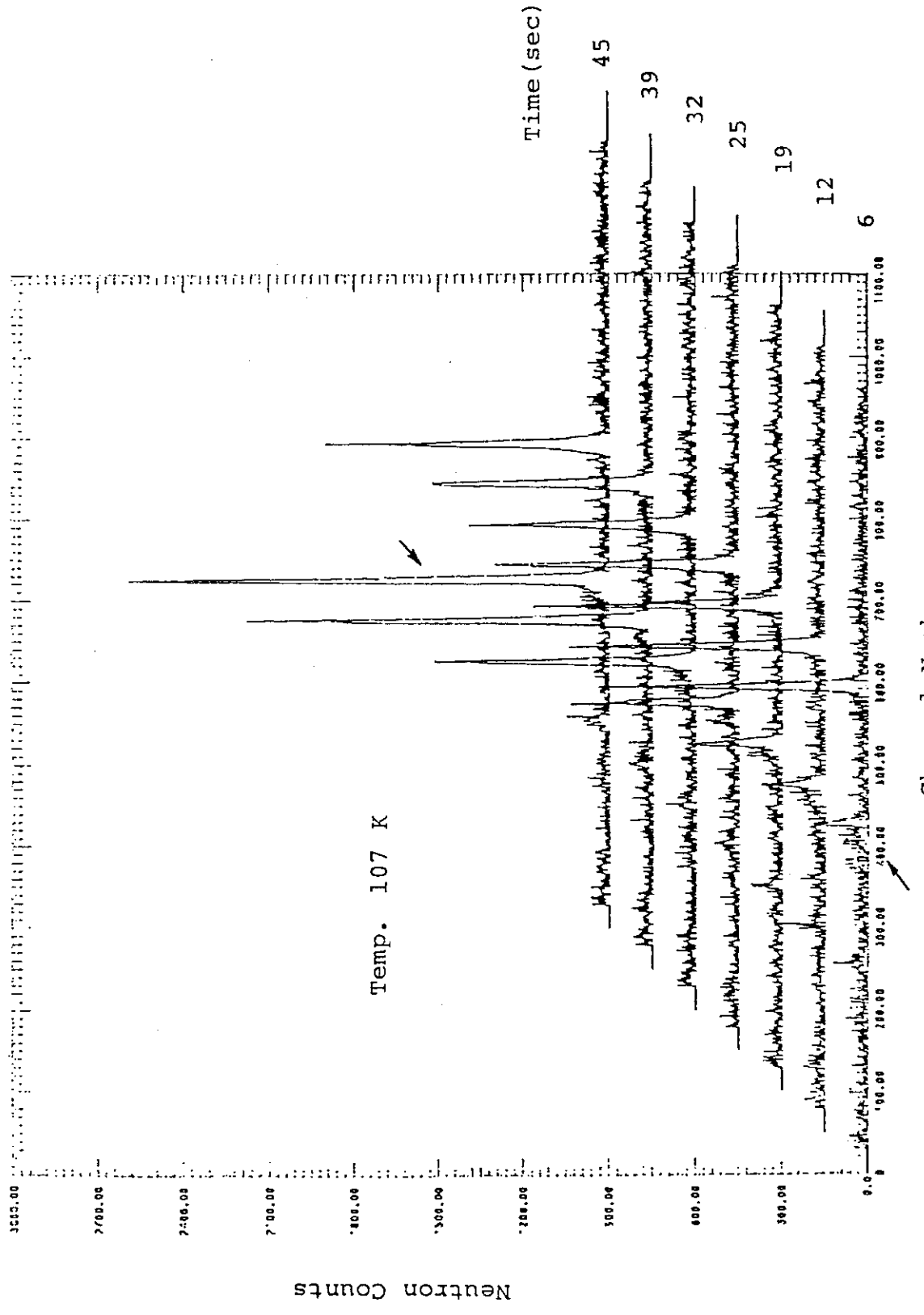

Fig. 1 Time evolution of the diffraction pattern when the final temperature was set at 107 K.

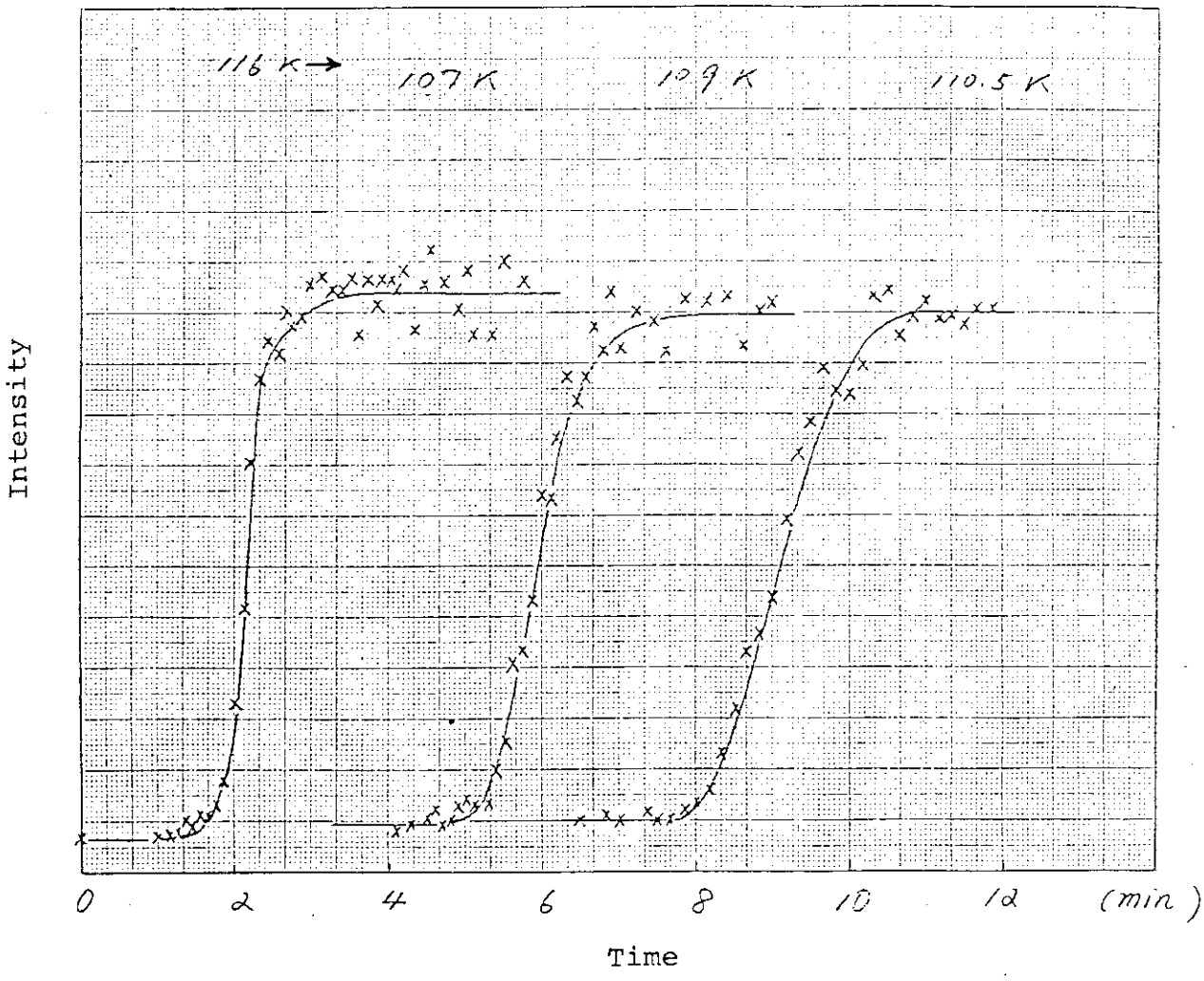

Fig. 2 Time evolution of the intensity of the (4 4 1/2) reflection for several final temperatures.

11. The Growth of Crystallites in the Phase Separation of $Mn_{67}Cu_{33}$

Y.Morii

Department of Physics, JAERI

S.Spooner and B.D.Gaulin

Solid State Division, ORNL

The kinetics of the crystallite growth in the phase separation of $Mn_{67}Cu_{33}$ was studied after in-situ rapid quenching from 800 C to 450 C with a specially designed furnace[1] by a time sliced measurements of the Bragg scattering from the precipitates with the Wide Angle Neutron Diffractometer (WAND).

The evolution of the Bragg peaks of the crystallites which is coherent scattering domain in the precipitates is shown in figure 1. No coherent scattering intensity was observed at 800 C since the ratio of the scattering amplitude of manganese to copper is a negative number, -0.48. Therefore the Bragg intensity is nearly zero at 1.78 minutes after quenching to 450 C.

The width of the Bragg peak is broad at the beginning due to the so called particle size broadening. The width B is related to the particle size L by

$$B=0.94\,\lambda\,/L\cos\theta \qquad (1)$$

where λ is the wavelength, θ the Bragg angle.

The observed Full Width at Half Maximum (FWHM), $B_{obs}(t)$, is composed of two parts[2]

$$B^2_{obs}(t)=B^2_{instr}+B^2_{p.s.}(t) \qquad (2)$$

where B_{instr} is the width due to standard sample of which size is big enough to eliminate the broadening. Therefore the width, B_{instr}, is instrumental and time independent in this study. While the width, $B_{p.s.}$, is due to small size of crystallites so that the width changes when the crystallites grow in the phase separation.

The evaluated $B^2_{p.s.}$ is plotted in figure 2. The width is constant in the early times (less than about 9 minutes). This is consistent with a constant average size of the new phase measured with a Small Angle Neutron Scattering (SANS) using the same specimen in the early time regime (less than 4.5 minutes) where Cahn-Hilliard-Cook (CHC) theory is obeyed.[3] From equation 1, a length, 26.1 A, is obtained for an average size of the crystallite L_{av} in the early time regime.

In the intermediate and late time regimes the width decreases with a power function of $B_{p.s.}=At^n$. The fitting power n is evaluated to be -0.236 for the data at 450 C and -0.251 for 500 C. Therefore one can say that the average size of the crystallites increases with a power function of $t^{1/4}$ until about 365 minutes. The average size of crystallite was 64.2 A at 365 minutes. While it is found from SANS experiment that the average size of the new phase changed from 26 A at CHC regime to 106 A at 365 minutes in the scaling regime where Furukawa's scaling function[4] is obeyed. The particle sizes of crystallites (WAND experiments) and the precipitates (SANS experiments) are shown in figure 3.

The power of 1/4 may be indicating that the thermal force and the surface mobility dominate in the formation of crystallite in the present system.

The integrated intensity of the Bragg peak increases with a power function of $t^{0.363}$ in the CHC and intermediate time regimes and with $t^{0.123}$ in the

scaling regime. Figure 4 shows the fitted line only in the late times. The cross over time, 64 minutes, between the two power laws is in very good agreement with the starting time of the scaling regime (about 72 minutes). Assumed that the volume of the crystallites is proportional to that of the precipitates of the new phase, the volume of the new phase increases slowly even in the scaling regime.

References

1. S.Katano, H.Motohashi, and M.Iizumi, Rev. Sci. Instrum. 57, 1409 (1986).

2. See for example B.E.Warren "X-ray Diffraction" Addison-Wesley.

3. B.D.Gaulin, S.Spooner, and Y.Morii, submitted to Phys. Rev. Lett..

See page 95 of this report.

4. H.Furukawa, Adv. in Phys., 34, 703 (1986).

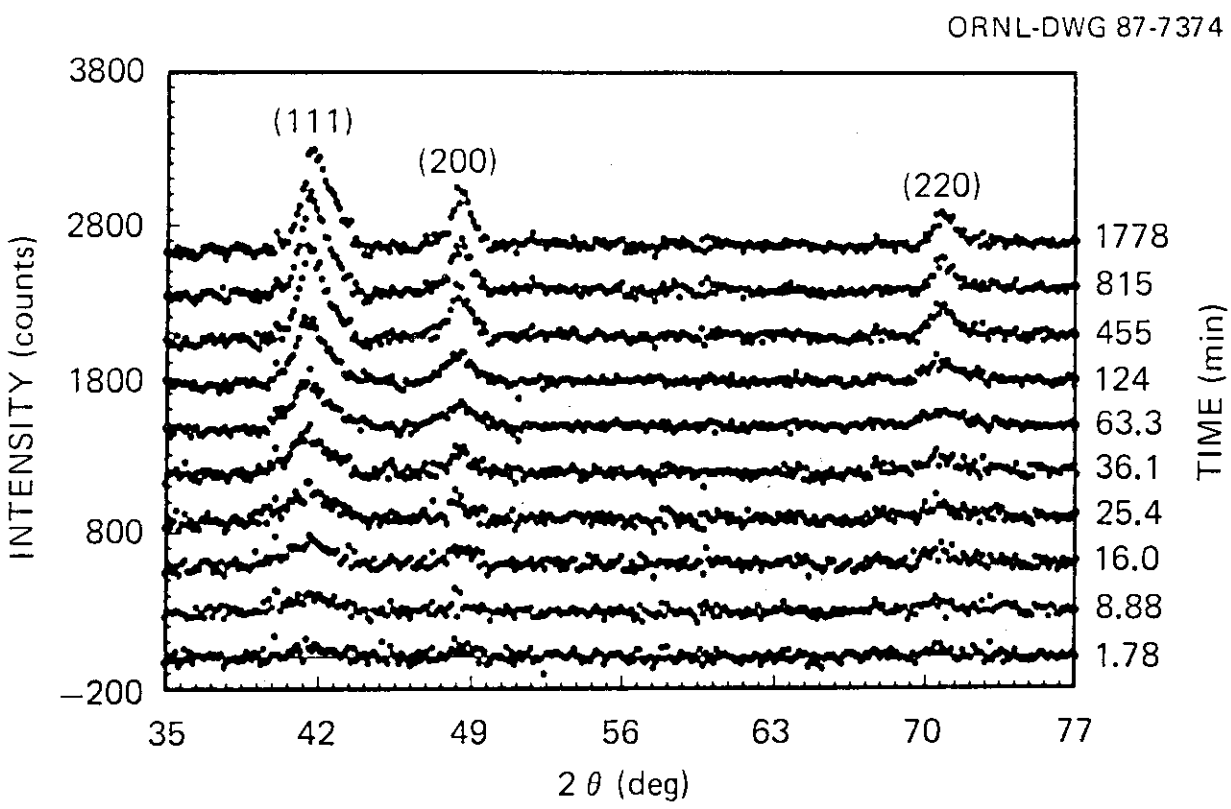

Fig.1 The evolution of the Bragg peaks of the crystallites in the phase separation of $Mn_{67}Cu_{33}$ after rapid quenching from 800 C to 450 C.

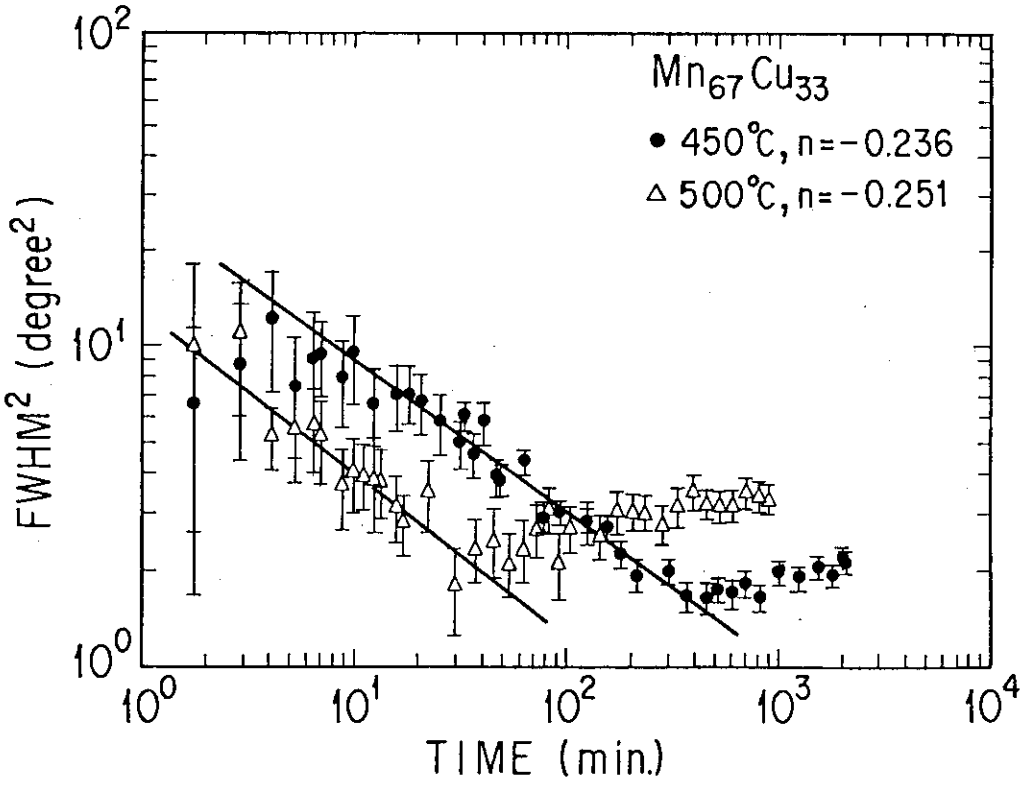

Fig.2 The Full Width at Half Maximum (FWHM) of the (111) Bragg peak of $Mn_{67}Cu_{33}$ is fitted with a power function of t^n in the phase separation at 450 C and 500 C. The obtained numbers n are close to 1/4 as shown in the figure.

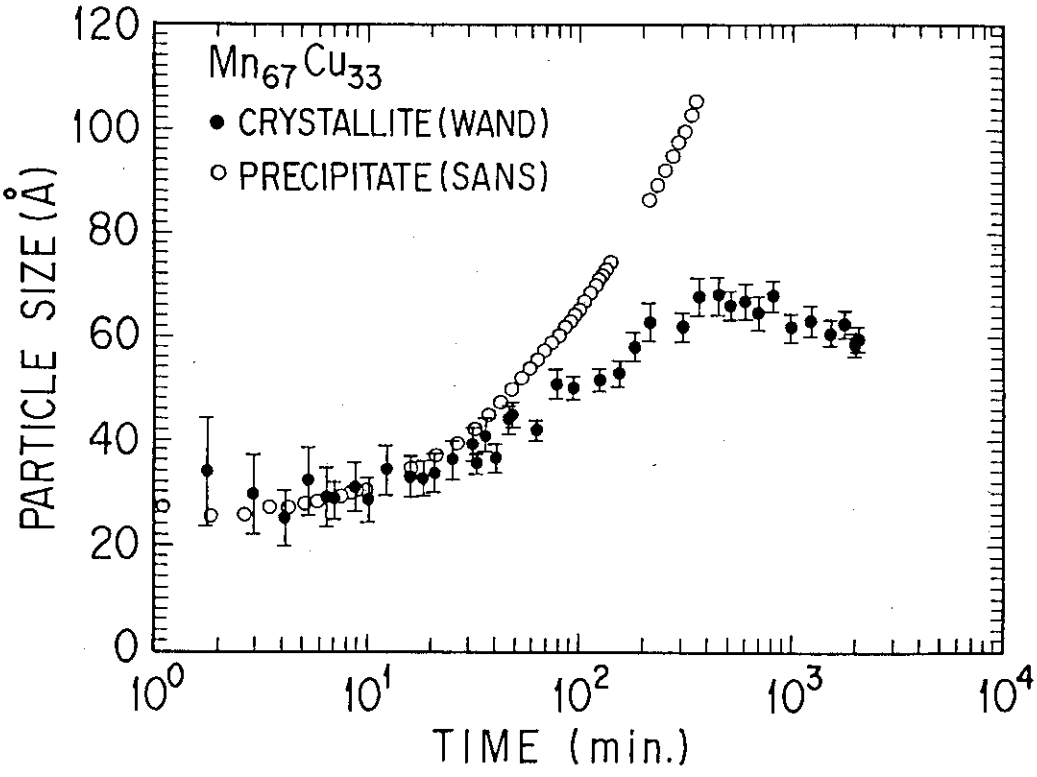

Fig.3 The particle size of the crystallites obtained from WAND and the precipitates of the new phase obtained from SANS in the phase separation of $MN_{67}Cu_{33}$ at 450 C.

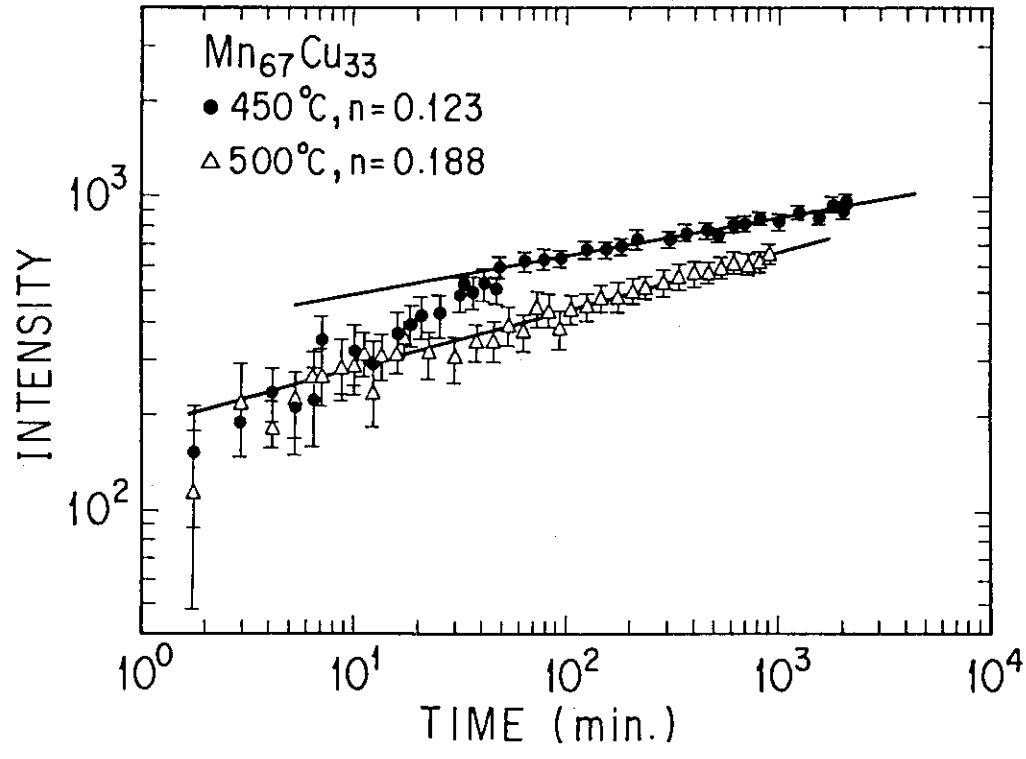

Fig.4 The integrated Bragg intensity is fitted to a power function of time. In the scaling regime (after 64 minutes), power of 0.123 is obtained for the phase separation at 450 C.

APPENDIX

List of JAERI personnel visiting ORNL in JFY 1985 and 1986

N. Minakawa	April	1985
M. Watanabe	July	1985
M. Iizumi	Aug.	1985
	Dec.	1985
S. Funahashi	Sep.	1985
	July - Sep.	1986
	March	1987
S. Katano	Jan. - Feb.	1986
	Oct.	1986
H. Ohno	March - April	1986
Y. Morii	March 1985 -	
	- March	1987